MAGYAR ÁLLAMI
EÖTVÖS LORÁND
GEOFIZIKAI INTÉZET

EÖTVÖS LORÁND
GEOPHYSICAL INSTITUTE
OF HUNGARY

GEOFIZIKAI KÖZLEMÉNYEK

GEOPHYSICAL TRANSACTIONS

ВЕНГЕРСКИЙ
ГЕОФИЗИЧЕСКИЙ
ИНСТИТУТ
ИМ Л. ЭТВЕША

ГЕОФИЗИЧЕСКИЙ
БЮЛЛЕТЕНЬ

CONTENTS

VOL. 32. NO. 4. APR. 1987. (ISSN 0016–7177)

BUDAPEST

TARTALOMJEGYZÉK

СОДЕРЖАНИЕ

GEOPHYSICAL TRANSACTIONS 1987
Vol. 32. No. 4. pp. 277–289

A FRESH LOOK AT CAUSALITY IN WAVE PROPAGATION

Peter HUBRAL* and Martin TYGEL**

Causality is a fundamental physical principle in wave propagation. As is well known, it means that there can be no response before an excitation. "Mathematical causality" on the other hand, implies that a mathematical solution describing the physical reality should have no contribution for all times before the source excitation. Unlike physical causality, mathematical causality need not, however, be adhered to. Mathematically causal are, for instance, all solutions that describe the response of a layered medium to a transient causal source formulated with the Sommerfeld or the Weyl integral. It is well known that the resulting solution integrals then have an infinite integration limit. However, this can simply be changed to a finite integration limit by relaxing the mathematical causality requirement and looking for noncausal solutions that are symmetric in time with respect to the instant of source excitation, after which they agree with the causal response. Therefore, time-symmetry gives wave propagation a certain completeness that has not previously been achieved. In this paper a time-symmetric broad-band transmission response of a point source near the planar interface separating two homogeneous acoustic half spaces of distinct constant velocities is formulated. It offers a nice example on how to use time-symmetry considerations to obtain simpler expressions in a direct way that are fairly easy to analyse. When tunnelling can be observed (i.e., when the source is close to the interface in the medium of higher velocity), the broad-band transmission response can be simulated as a superposition of homogeneous plane waves only. From a straightforward inspection of the solution integral, the phenomenon of tunnelling is easily inferred and a so-called quasi-spherical P^*-wave can be extracted.

Keywords: acoustical waves, point source, homogeneous half-space, wave propagation, velocity

1. Introduction

When studying the response of a point source from one or more planar interfaces, one usually considers the Sommerfeld or Weyl integrals as the starting point for formulating the solutions. These, as is well known, are (mathematically) causal and exhibit an infinite integration limit. The limit can be changed to a finite one by applying the so-called Causality Trick [TYGEL and HUBRAL 1985; HUBRAL and TYGEL 1986]. This provides a finite-range integral solution that can be evaluated more exactly.

A certain number of recent publications in the literature of seismic exploration have demonstrated revived interest in the phenomenon of tunnelling [TSVANKIN 1982; BORTFELD and FERTIG 1983; KUHN 1985; KIM and BEHRENS 1986]. This phenomenon is, in principle, well understood [BREKHOVSKIKH 1980; DALEY and HRON 1983], so any further investigation may appear unnecessary.

* Bundesanstalt für Geowissenschaften und Rohstoffe, 3 Hannover 51, BRD
** Instituto de Mathemática e Computação Cientifica, 13100 Campinas, S.P., Brasil
Paper presented at the 47th meeting of the EAEG, 4–7 June, 1985, Budapest, Hungary

However, we believe that the following analysis of this phenomenon is particularly simple and for that matter interesting. It serves as an example to demonstrate the value of transforming a mathematically causal solution integral into a noncausal one. This may then—as is the case with the solution studied here—be more easily analysed.

2. Transient Weyl integral for a broad-band point source

As shown previously in our paper [TYGEL and HUBRAL 1984], one can represent the acoustic broad-band potential for a point source at point S (*Fig. 1*) as a superposition of homogeneous and inhomogeneous plane waves as follows

$$\delta(t-\bar{R}/c_1)/\bar{R} = \mathrm{Re}\,\{\Phi_{1nc}(r, z, t)\} \tag{1a}$$

where

$$\Phi_{1nc}(r, z, t) = \frac{-1}{2\pi c_1} \int_0^{\pi/2+i\infty} \mathrm{d}\theta \sin\theta \int_0^{2\pi} \mathrm{d}\varphi\, \Phi_1(x, y, z, t), \tag{1b}$$

$$\Phi_1(x, y, z, t) = \Delta'(t - h\cos\theta/c_1 - \mathbf{n}\cdot\mathbf{R}/c_1), \tag{1c}$$

$$= \Delta'(t - (z+h)\cos\theta/c_1 - \eta\sin\theta/c_1), \tag{1d}$$

$$\mathbf{n}\cdot\mathbf{R} = \eta\sin\theta + z\cos\theta, \tag{1e}$$

$$\eta = x\cos\varphi + y\sin\varphi, \tag{1f}$$

$$\bar{R} = \sqrt{r^2 + (z+h)^2} \tag{1g}$$

and

$$r^2 = x^2 + y^2. \tag{1h}$$

δ denotes the Dirac delta function; $'$ signifies the derivative with respect to the argument; c_1 and ϱ_1 are the velocity and density of the upper medium (medium 1) and c_2 and ϱ_2 of the lower one (medium 2); φ (with $0 \le \varphi \le 2\pi$) is the azimuth angle and $(0 \le \theta \le \pi/2) \cup (\theta = \pi/2 + i\tau,\ 0 < \tau < \infty)$ is the "incidence angle" of the so-called analytic transient plane (ATP) wave $\Phi_1(x, y, z, t)$ that is defined with the help of the following analytic Δ-function

$$\Delta(\xi) = \int_0^{\infty} \exp(i\omega\xi) = \begin{cases} \delta(\xi) + i/\pi\xi & \text{if } \xi \text{ is real} \\ i/\pi\xi & \text{if } \mathrm{Im}\,\xi > 0 \end{cases} \tag{2}$$

As also shown in [TYGEL and HUBRAL 1984] Eq. (1a) can be utilized to construct the complete causal broad-band transient reflection/transmission response from a planar acoustic interface (Fig. 1) by strictly superposing the reflected/transmitted ATP waves that accompany those, which simulate the lower half of the spherical broad-band source $\delta(t-\bar{R}/c_1)/\bar{R}$ for $z > -h$.

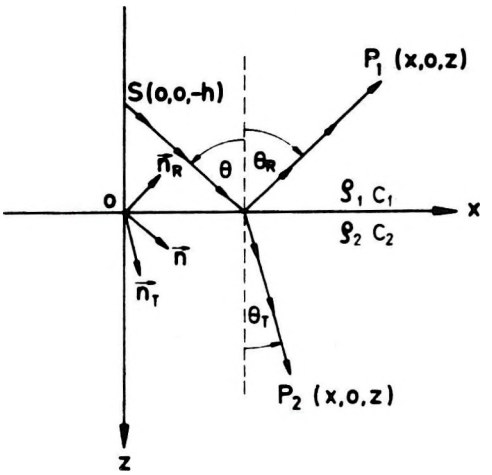

Fig. 1. Acoustic media (ϱ_1, c_1) and (ϱ_2, c_2) separated by a planar interface
S — source; P_1 and P_2 — observation points. A 2-D model

1. ábra. Sík határfelület által elválasztott akusztikus közegek (ϱ_1, c_1) és (ϱ_2, c_2)
S — forrás, P_1 és P_2 — észlelési pontok. Kétdimenziós modell

Рис. 1. Акустические среды (ϱ_1, c_1) и (ϱ_2, c_2), разделяемые плоским разделом
S — источник, P_1 и P_2 — точки наблюдения. Дбухмерная модель

3. Transient causal transmission response

In the following, we will investigate the transmission potential only. It has the form (see Eq. (55b) in [TYGEL and HUBRAL 1984])

$$\varphi_T(r, z, t) = \mathrm{Re}\{\Phi_T(r, z, t)\} \tag{3a}$$

where

$$\Phi_T(r, z, t) = \frac{-1}{2\pi c_1} \int_0^{\pi/2 + i\infty} \mathrm{d}\theta \sin\theta\, D(\theta) \int_0^{2\pi} \mathrm{d}\varphi\, A'(t - h\cos\theta/c_1 - \mathbf{n}_T \cdot \mathbf{R}/c_2), \tag{3b}$$

$$\mathbf{n}_T \cdot \mathbf{R} = \frac{c_2}{c_1}[\eta \sin\theta - zM(\theta)] \tag{3c}$$

and

$$M(\theta) = \sqrt{(c_1/c_2)^2 - \sin^2\theta}. \tag{3d}$$

The plane wave transmission coefficient is

$$D(\theta) = 2\varrho_1 \cos\theta/[\varrho_2 \cos\theta + \varrho_1 M(\theta)] \tag{3e}$$

where the square root is defined as

$$\sqrt{\alpha} = \begin{cases} |\alpha|^{\frac{1}{2}} & \text{if} \quad \alpha > 0, \\ -i|\alpha|^{\frac{1}{2}} & \text{if} \quad \alpha < 0. \end{cases} \tag{3f}$$

The potential (3a) is causal (i.e., it can be shown to have no contribution to $t < 0$).

As shown in [HUBRAL and TYGEL 1986], the infinite integration limit in formula (3a) can easily be removed by applying the so-called Causality Trick. One readily obtains then a simple geometrically transparent time-symmetric finite-range integral expression for the transmission response, which (see Section 5) is, of course, noncausal. This however does not matter because it still perfectly describes the desired causal broad-band response (Green's function) given by formula (3a) for $t>0$, i.e., for the time of actual interest after the explosion.

4. Applying the Causality Trick to the incident potential

Prior to applying the Causality Trick to the transmission response (3a), let us use it in connection with the incident potential (1b). The Causality Trick implies then the following operation

$$ {}_N\varphi_{Inc}(r, z, t) = \mathrm{Re}\left\{\Phi_{Inc}(r, z, t) - \overline{\Phi_{Inc}(r, z, -t)}\right\}. \tag{4a}$$

The bar denotes complex conjugate. It is obvious that the right-hand side of formula (4a) is identical to that of formula (1b) for $t>0$ as $\mathrm{Re}\,\Phi_{Inc}(r, z, -t)$ has no contribution to $t>0$.

Expression (4a) can be shown [HUBRAL and TYGEL 1985] to correspond to

$$ {}_N\varphi_{Inc}(r, z, t) = \mathrm{Re}\left\{{}_N\Phi^{II}_{Inc} + {}_N\Phi^{I}_{Inc}\right\}, \tag{4b}$$

where

$$ {}_N\Phi^{II}_{Inc} = \frac{-1}{2\pi c_1}\int_0^{\pi} \mathrm{d}\theta \sin\theta \int_0^{2\pi} \mathrm{d}\varphi\, \Delta'(t - h\cos\theta/c_1 - \mathbf{n}\cdot\mathbf{R}/c_1) \tag{4c}$$

$$ = \Delta(t - \bar{R}/c_1)/\bar{R} - \Delta(t + \bar{R}/c_1)/\bar{R} \tag{4d}$$

and

$$ {}_N\Phi^{I}_{Inc} = 0 \tag{4e}$$

Potential (4a) is not causal, but describes, as Eq. (4d) indicates, a so-called time-symmetric point source. This agrees however with the causal point source potential (1a) for $t>0$ and $z>-h$, i.e., $\varphi_{Inc} = \delta(t-\bar{R}/c_1)/\bar{R}$ for $t>0$.

5. Applying the Causality Trick to the transmission response

As indicated in [HUBRAL and TYGEL 1985], the application of the Causality Trick to the transient causal transmission response (3a) provides the so-called "time-symmetric transmission potential"

$$ \varphi_T = \mathrm{Re}\left\{\Phi_T(\tau_0, r, z, t) - \overline{\Phi_T(\tau_0, r, z, -t)}\right\} \tag{5a}$$

where

$$\Phi_T(\tau_0, r, z, t) =$$

$$\frac{-1}{2\pi c_1} \int_0^{\pi/2+i\tau_0} \mathrm{d}\theta \sin\theta\, D(\theta) \int_0^{2\pi} \mathrm{d}\varphi\, \Delta'(t - h\cos\theta/c_1 - \eta\sin\theta/c_2 - zM(\theta)) \qquad (5b)$$

with $\tau_0 = \cosh^{-1}(c_1/c_2)$ if $c_1 > c_2$ and $\tau_0 = 0$ if $c_1 < c_2$.

Like the time-symmetric source, solution (5a) is of physical interest only for $t > 0$. It can further be simplified by analytically performing the φ-integration as shown in the Appendix (see Eq. A.2). We will not, however, perform this integration as our objective here is to bring solution (5a) into a geometrically more transparent form that will make it immediately possible to infer the so-called P^*-wave and some of its features. In the following we now assume that $c_1 > c_2$. The P^*-wave is then a spherical wave in the lower medium that appears to originate at $t = 0$ at point O (Fig. 1).

Now that we have reviewed the essential steps that lead to the time-symmetric transmission potential (5a), we will reformulate the response and begin with its analysis.

6. Transmission response in terms of up- and downgoing homogeneous plane waves

The transmission response (5a) can be rewritten as a superposition integral of homogeneous (down- and upgoing) ATP waves only. This will simplify the interpretation of this response as a surface integral since one will no longer have to pay any attention to the inhomogeneous ATP waves, which have, for instance, their presence in the causal solution integral (3a).

Let us start by writing the potential (5b) in the form

$$\Phi_{Tr}(\tau_0, r, z, t) = \frac{-1}{2\pi c_1} \int_0^{\pi/2} \mathrm{d}\theta \sin\theta\, D(\theta) \int_0^{2\pi} \mathrm{d}\varphi\, \Delta'(t - h\cos\theta/c_1 - \mathbf{n}_T \cdot \mathbf{R}/c_2)$$

$$- \frac{1}{2\pi c_1} \int_{\pi/2}^{\pi/2+i\tau_0} \mathrm{d}\theta \sin\theta\, D(\theta) \int_0^{2\pi} \mathrm{d}\varphi\, \Delta'(t - h\cos\theta/c_1 - \mathbf{n}_T \cdot \mathbf{R}/c_2) \qquad (6a)$$

In the second term of Eq. (6a) we consider the natural change of coordinates $\sin\theta/c_1 = \sin\gamma/c_2$, which is suggested by Snell's law and transforms the vertical imaginary path $\theta = \pi/2 + i\tau$ $(0 \le \tau \le \tau_0)$ into the horizontal real one $\gamma_c \le \gamma \le \pi/2$, where $\gamma_c = \sin^{-1}(c_2/c_1)$ is the critical angle. Recall that $c_1 > c_2$.

Calling the second term in formula (6a) $\Phi^*(\tau_0, r, z, t)$, we can write

$$\Phi^*(\tau_0, r, z, t) = \frac{-1}{2\pi c_2} \int_{\gamma_c}^{\pi/2} \mathrm{d}\gamma \sin\gamma\, \tilde{D}(\gamma) \int_0^{2\pi} \mathrm{d}\varphi\, \Delta'(t + ih\tilde{M}(\gamma)/c_2 - \mathbf{m}\cdot\mathbf{R}/c_2) \quad (6b)$$

where

$$\mathbf{m}\cdot\mathbf{R} = \eta \sin\gamma + z\cos\gamma \quad (6c)$$

and

$$\tilde{M}(\gamma) = \sqrt{\sin^2\gamma - (c_2/c_1)^2}\,. \quad (6d)$$

Note that $\tilde{M}(\gamma)$ in Eq. (6d) is always positive in the range $\gamma_c \le \gamma \le \frac{\pi}{2}$.

Also,

$$\tilde{D}(\gamma) = 2\varrho_1 \cos\gamma/[\varrho_1 \cos\gamma - i\varrho_2\tilde{M}(\gamma)] \quad (7)$$

Transforming in a similar way as in [HUBRAL and TYGEL 1985] the second expression $\overline{\Phi_T(r, z, -t)}$ on the right-hand side of formula (5a) and combining it with the first leads to

$$\varphi_T = \mathrm{Re}\{{}_N\Phi_T\} = \frac{-1}{2\pi c_1} \int_0^{\pi} \mathrm{d}\theta \sin\theta\, D(\theta) \int_0^{2\pi} \mathrm{d}\varphi\, \delta'(t - h\cos\theta/c_1 - \mathbf{n}_T\cdot\mathbf{R}/c_2)$$

$$+ \mathrm{Re}\left\{\frac{-1}{2\pi c_2} \int_{\gamma_c}^{\pi-\gamma_c} \mathrm{d}\gamma \sin\gamma\, \tilde{D}(\gamma) \int_0^{2\pi} \mathrm{d}\varphi\, \Delta'(t + ih\tilde{M}(\gamma)/c_2 - \mathbf{m}\cdot\mathbf{R}/c_2)\right\}. \quad (8)$$

Here the φ-integration in both terms can readily be performed. Doing this however destroys the immediate geometrical appeal which formula (8) provides as a surface integral over transient homogeneous plane waves only. Let us now analyse expression (8). We base the analysis on a comparison with formulae (4).

It is quite plausible to expect that if the integration variable θ in formula (4c) would only cover the smaller angular range $\theta_L < \theta < \theta_H$, the resulting plane wave superposition will still approximate the spherical potential (1a) for $t > 0$ within the angular range $\theta_L < \theta < \theta_H$. Likewise, it is equally reasonable to expect that if the homogeneous ATP waves in formula (4c) would have in addition a slowly varying θ-dependent amplitude and/or pulse shape, one could still observe a quasi-spherical wave field radiating away from S for $t > 0$.

As we will note below, the second term of Eq. (8) has a great similarity with the representation (4c). This similarity turns out very useful as a means of understanding the P^*-wave.

7. Detection of the P^*-wave

The first term on the right-hand side of Eq. (8) can be clearly recognized as a superposition of down- and upgoing homogeneous plane waves of identical δ'-pulse waveshape and ϑ-dependent amplitude. These δ'-pulse plane waves radiate at $t=0$ through point S and are responsible for the direct transmitted wave (see example in Section 8).

We now pay attention to the second term in Eq. (8). This is responsible for the so-called P^*-wave (see example in Section 8). The second term can be recognized as a superposition integral of homogeneous ATP waves of varying amplitude and wave shape. Each ATP wave can be expressed as

$$\tilde{D}(\gamma)\Delta'(t+ih\tilde{M}(\gamma)/c_2-\mathbf{m}\cdot\mathbf{R}/c_2) = \tilde{D}(\gamma)b(t,-ih\tilde{M}(\gamma)/c_2) * \Delta'(t-\mathbf{m}\cdot\mathbf{R}/c_2) \quad (9)$$

where

$$b(t,\alpha) = \operatorname{Re}\{\Delta(t-\alpha)\} = \begin{cases} \delta(t-\alpha) & \text{if } \alpha \text{ is real} \\ \dfrac{-\operatorname{Im}\alpha}{\pi[(t-\operatorname{Re}\alpha)^2+(\operatorname{Im}\alpha)^2} & \text{if } \operatorname{Im}\alpha > 0 \end{cases} \quad (10)$$

The symbol * denotes convolution over t. On account of expression (9) we can very clearly see that all ATP waves used in the second term of Eq. (8) pass simultaneously at $t=0$ through the epicentre 0 (and not through point S as the δ'-waves in the first term of Eq. (8)). The directional unit vectors of propagation cover the limited angular range $\gamma_c < \gamma < \pi-\gamma_c$; $0 \le \varphi \le 2\pi$ upon the unit sphere centred at 0.

The second term thus gives already directly by inspection a clear indication that the spherical P^*-wave exists in the vicinity of the wavefront $t = R/c_2$ ($R^2 = r^2+z^2$) within the angular range $\gamma_c < \gamma < \pi/2$ of the unit sphere centred at O. This hint comes a) straight from the mathematical formulation of the transmission response (8) in terms of a superposition of homogeneous ATP waves and b) from a comparison with the time-symmetric source representation integral (4c). No need exists to employ any more involved mathematical analysis in order to detect and extract this particular event. (In fact let us remark that the P^*-wave cannot be associated with a distinct singularity of the integrand in Eq. (3b).)

8. Example

To get a better appreciation of the significance of the P^*-wave within the total response, we evaluated integral (8) at the fixed time $t=0.06$ s for different values of r and z. The reflection response was likewise computed with the solution integral described by HUBRAL and TYGEL [1986]. In other words, we computed what is in general called a snapshot. The model was defined by the following parameters; $\varrho_1=\varrho_2=1$ g/cm^3, $c_1=3000$ m/s, $c_2=1500$ m/s and $h=10$ m. The

frame was specified within the range $-1000\text{ m} < z < 1000\text{ m}$ and $-1000\text{ m} < r < 1000\text{ m}$. Instead of using the incident point-source potential $\mathrm{Re}\, \Delta(t - \bar{R}/c_1)$, we computed the response for the incident potential $\mathrm{Re}\, \Delta(t + i\varepsilon - \bar{R}/c_1)/\bar{R}$ with $\varepsilon = 0.004$. Displayed in *Figure 2* is the total pressure field in the form of an isometric plot. The critical angle is $\gamma_c = 30°$. In the upper medium one clearly recognizes the superposition of the upgoing direct and reflected wave (both events cannot be separated). In the lower medium we observe the downgoing transmitted wave and the P^*-wave.

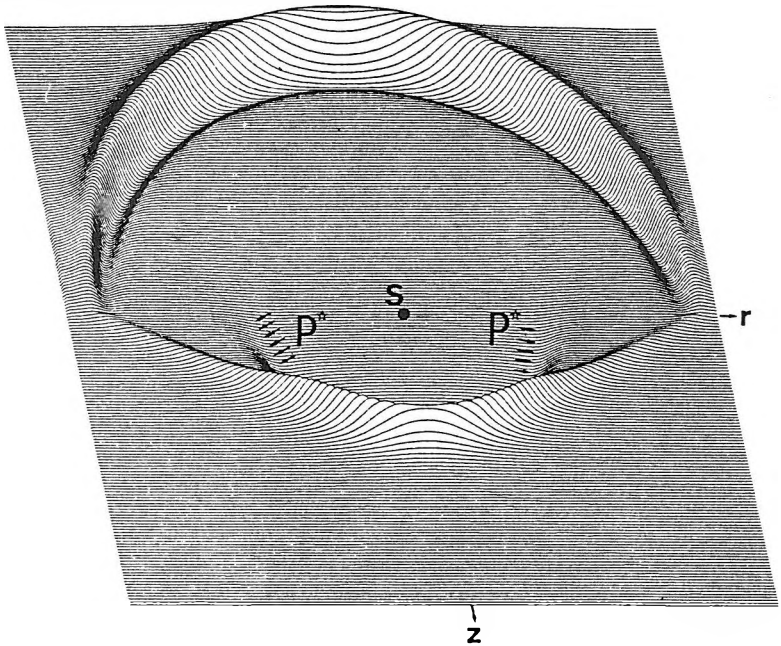

Fig. 2. Snapshot of the pressure wavefield in the r–z plane of the model described in the example

2. ábra. A példában ismertetett modell r–z síkjában kialakult nyomáshullámtér pillanatfelvétele

Рис. 2. Снимок поля волн сжатия по плоскости r–z модели, описанной в примере

9. Simplified expression of the P^*-wave

Above we observed the P^*-wave as a spherical concentration of energy in the transmitted wavefield provided that $c_1 > c_2$. In the Appendix we will show that for $t \cong R/c_2$, $R \gg h$ and $r = R \sin\gamma'$; $z = R\cos\gamma'$ ($\gamma_c < \gamma' < \pi/2$) it can be approximated as

$$\varphi^*(\tau_0, r, z, t) = \mathrm{Re}\left\{D(\gamma')b(t, -ih\tilde{M}(\gamma')/c_2) * \Delta(t - R/c_2)/R\right\} \tag{11}$$

where $R^2 = r^2 + z^2$.

Formula (11) completely agrees with the transient (high-frequency approximation) potential one obtains from Brekhovskikh's formula [1980, p. 282, Eq. (32.11)], where the second term is ignored.

10. Conclusion

The Causality Trick provides a simple means of transforming infinite-range to finite-range solution integrals. For this reason it may lead to a simpler analysis of the solution integrals and a better detection or understanding of the events that make up the total response. This paper demonstrates that a fairly simple representation integral can be obtained for the transmission response from a planar acoustic interface for the case $c_1 > c_2$. It is expressed in two terms that have the form of a surface integral. The superposition involves homogeneous ATP waves only that pass at $t = 0$ either through point S or point 0. The P^*-wave can directly be inferred from Eq. (8) as the second term. It has a similar structure to the time-symmetric point source (see Eq. (4c)).

An approximate transient expression of the P^*-wave has been extracted. It agrees with the time-harmonic equivalent expression for this wave given by Brekhovskikh [1980, p. 282, Eq. (32.11)].

We believe that the easy detectability of the P^*-wave and the insight that the time-symmetric formulation (8) of the transmission response for $c_1 > c_2$ offers, are clear indications of the value of the Causality Trick in analysing a solution in order to better understand higher-order wave propagation phenomena.

Acknowledgements

This research was partly done during our stay at the Programa de Pesquisa e Pos Graduacao em Geofisica (PPPG/UFBa) in Salvador, Bahia. We thank the coordinator of the Program Dr. C. Dias as well as Petrobras/CNPq/FINEP/UFBa/BGR for the encouragement and support.

Appendix

We consider the second (complex) term in Eq. (8). Namely

$$\Phi_T^*(\tau_0, r, z, t) = \frac{\mathrm{d}}{\mathrm{d}t}\left\{\frac{-1}{2\pi c_2}\int_{\gamma_e}^{\pi-\gamma_e} \mathrm{d}\gamma \sin\gamma\, \tilde{D}(\gamma) \int_0^{2\pi} \mathrm{d}\varphi\, \Delta(\tilde{t}(\gamma) - \mathbf{m}\cdot\mathbf{R}/c_2)\right\} \quad \text{(A.1)}$$

where

$$\tilde{t}(\gamma) = t + ih\tilde{M}(\gamma)/c_2.$$

We suppose that $R \gg h$ and $t \cong R/c_2$. We know that [see TYGEL and HUBRAL 1984]

$$\int_0^{2\pi} \mathrm{d}\varphi \, \Delta(\tilde{t}(\gamma) - \mathbf{m} \cdot \mathbf{R}/c_2) = 2[r^2 \sin^2 \gamma/c_2^2 - (\tilde{t}(\gamma) - z \cos \gamma/c_2)^2]^{-1/2} \tag{A.2}$$

where the square root is of the form $\sqrt{b^2 - a^2}$ ($b > 0$, $\operatorname{Im} a > 0$) and satisfies

$$\operatorname{Re} \sqrt{b^2 - a^2} > 0 \quad \text{if} \quad \operatorname{Im} a > 0,$$

and

$$\sqrt{b^2 - a^2} = \begin{cases} |b^2 - a^2|^{\frac{1}{2}} & \text{if } a^2 < b^2 \\ -i \operatorname{sgn}(a) \, |b^2 - a^2|^{\frac{1}{2}} & \text{if } b^2 < a^2 \end{cases} \tag{A.3}$$

Introducing Eq. (A.2) into Eq. (A.1) we obtain

$$\Phi_T^*(\tau_0, r, z, t) = \frac{\mathrm{d}}{\mathrm{d}t} \left\{ \frac{-1}{2\pi c_2} \int_{\gamma_c}^{\pi - \gamma_c} \mathrm{d}\gamma \sin \gamma \, \tilde{D}(\gamma) \times \right.$$

$$\left. \times [r^2 \sin^2 \gamma/c_2^2 - (\tilde{t}(\gamma) - z \cos \gamma/c_2)^2]^{-\frac{1}{2}} \right\} =$$

$$= \frac{-1}{2\pi c_2} \int_{\gamma_c}^{\pi - \gamma_c} \mathrm{d}\gamma \sin \gamma \, \tilde{D}(\gamma) \frac{\mathrm{d}}{\mathrm{d}t} [r^2 \sin^2 \gamma/c_2^2 - (\tilde{t}(\gamma) - z \cos \gamma/c_2)^2]^{-\frac{1}{2}} =$$

$$= \frac{-1}{2\pi c_2} \int_{\gamma_c}^{\pi - \gamma_c} \mathrm{d}\gamma \sin \gamma \, \tilde{D}(\gamma) \, (\tilde{t}(\gamma) - z \cos \gamma/c_2) \times$$

$$\times [r^2 \sin^2 \gamma/c_2^2 - (\tilde{t}(\gamma) - z \cos \gamma/c_2)^2]^{-\frac{3}{2}} \tag{A.4}$$

Let us investigate this potential upon the ray specified by the angles ($0 \leq \varphi \leq 2\pi$) and γ' ($\gamma_c < \gamma' < \pi/2$), where the angle γ' is such that $\cos \gamma' = z/R$; $\sin \gamma' = r/R$.

We can write Eq. (A.4) as

$$\Phi_T^*(\tau_0, r, z, t) = \frac{-c_2}{\pi R} \int_{\gamma_c}^{\pi - \gamma_c} \mathrm{d}\gamma \sin \gamma \, \tilde{D}(\gamma) \, (c_2 \tilde{t}(\gamma)/R - \cos \gamma \cos \gamma') \times$$

$$[-(\cos \gamma - c_2 \tilde{t}(\gamma) \cos \gamma'/R)^2 + \sin^2 \gamma' (1 - c_2^2 \tilde{t}^2(\gamma)/R^2)]^{-\frac{3}{2}} \tag{A.5}$$

If $t \cong R/c_2$ and $R \gg h$, then for all γ ($\gamma_c \leq \gamma \leq \pi - \gamma_c$)

$$\tilde{t}(\gamma) \cong R/c_2 + ih\tilde{M}(\gamma)/c_2 \cong \tilde{t}(\gamma') = R/c_2 + ih\tilde{M}(\gamma')/c_2, \tag{A.6}$$

this being the case since

$$|ih\tilde{M}(\gamma')/c_2| = h|\tilde{M}(\gamma')|/c_2 \leq h/c_2 \ll R/c_2 \quad \text{and} \quad |\tilde{M}(\gamma')| \leq 1.$$

Hence for $t \cong R/c_2$ and $R \gg h$, we have $\tilde{t}(\gamma) \cong \tilde{t}(\gamma') = \tilde{t}$ for all γ. In this case we write

$$\Phi_T(\tau_0, r, z, t) \cong \frac{-c_2}{\pi R^2} \int_{\gamma_c}^{\pi-\gamma_c} \mathrm{d}\gamma \sin\gamma\, \tilde{D}(\gamma)\,(c_2\tilde{t}/R - \cos\gamma' \cos\gamma) \times$$

$$\times [-(\cos\gamma - c_2\tilde{t}\cos\gamma'/R)^2 + \sin^2\gamma'(1 - c_2^2\tilde{t}^{\,2}/R^2)]^{-\frac{3}{2}} \tag{A.7}$$

Moreover, at $\tilde{t} \cong R/c_2$, the integrand in Eq. (A.7) possesses a singularity at $\gamma = \gamma'$. Namely, if $\tilde{t} \cong R/c_2$ that integrand reduces to

$$\sin\gamma\, \tilde{D}(\gamma)\,(1 - \cos\gamma' \cos\gamma)\,[-(\cos\gamma - \cos\gamma')^2]^{-\frac{3}{2}} =$$

$$= \sin\gamma\, \tilde{D}(\gamma)\,(1 - \cos\gamma\cos\gamma')\left\{\frac{1}{-i|\cos\gamma - \cos\gamma'|}\right\}^3 = \frac{-i\sin\gamma\, \tilde{D}(\gamma)}{|\cos\gamma - \cos\gamma'|^3} \tag{A.8}$$

where the sign convention for the square root was used.

More specifically we have at $\tilde{t} = R/c_2$

$$a = \tilde{t} - z\cos\gamma/c_2 = R(c_2\tilde{t}/R - \cos\gamma'\cos\gamma)/c_2 = R(1 - \cos\gamma'\cos\gamma)/c_2 > 0$$

so that

$$\sqrt{b^2 - a^2} = -i\,\mathrm{sgn}\,(a)\,|b^2 - a^2|^{\frac{1}{2}} = -i\,|(\cos\gamma - \cos\gamma')^2|^{\frac{1}{2}} = -i\,|\cos\gamma - \cos\gamma'|.$$

Therefore

$$(b^2 - a^2)^{-\frac{3}{2}} = \left(\sqrt{b^2 - a^2}\right)^{-3} = (-i\,|b^2 - a^2|)^{-3} =$$

$$= \left\{\frac{1}{-i\,|\cos\gamma - \cos\gamma'|}\right\}^3 = \frac{-i}{|\cos\gamma - \cos\gamma'|^3}$$

It follows that most of the weight of the integral (A.7) is concentrated in the neighbourhood of $\gamma = \gamma'$.

In the light of this observation we draw the following conclusions:

a) The integral (A.7) should not change significantly if we change the integration limits from $[\gamma_c, \pi - \gamma_c]$ to $[0, \pi]$.

b) The integral (A.7) should also not vary significantly if we replace $\tilde{D}(\gamma)$ by its value at $\gamma = \gamma'$, $\tilde{D}(\gamma')$ as what matters happens in the vicinity of $\gamma = \gamma'$.

In this case we get

$$\Phi_T^*(\tau_0, r, z, t) \cong \frac{c_2}{\pi R^2}\,\tilde{D}(\gamma') \int_0^{\pi} \mathrm{d}\gamma \sin\gamma\,(c_2\tilde{t}/R - \cos\gamma'\cos\gamma) \times$$

$$\times [-(\cos\gamma - c_2\tilde{t}\cos\gamma'/R)^2 + \sin^2\gamma'\,(1 - c_2\tilde{t}^{\,2}/R^2)]^{-\frac{3}{2}} =$$

$$= \tilde{D}(\gamma')\frac{\mathrm{d}}{\mathrm{d}t}\int_0^{\pi} \mathrm{d}\gamma \sin\gamma\,[-(\cos\gamma - c_2\tilde{t}\cos\gamma'/R)^2 + \sin^2\gamma'\,(1 - c_2\tilde{t}^{\,2}/R^2)]^{-\frac{1}{2}} =$$

$$= \tilde{D}(\gamma')\Delta(\tilde{t} - R/c_2)/R = \tilde{D}(\gamma')\Delta(\tilde{t} + ih\tilde{M}(\gamma')/c_2 - R/c_2)/R =$$

$$= \tilde{D}(\gamma')b(t, -ih\tilde{M}(\gamma')/c_2) * \Delta(t - R/c_2)/R \qquad \text{(A.9)}$$

REFERENCES

Bortfeld R. K. and Fertig J. 1983: On the importance of the shear wave S^* for seismic prospecting (in German). Erdöl und Erdgas, Heft 4, pp. 127–133

Brekhovskikh L. M. 1980: Waves in layered media. Academic Press, New York

Daley P. F. and Hron F. 1983: Non-geometric arrivals due to highly concentrated sources adjacent to plane interfaces. BSSA, 73, pp. 1655–1671

Hubral P. and Tygel M. 1985: Transient response from a planar acoustic interface by a new point-source decomposition into plane waves. Geophysics **50,** 5, pp. 766–774

Hubral P. and Tygel M. 1986: Transient finite integral point source response from a planar acoustic interface: The causality approach. Geophys. Prosp. **34,** 1, pp. 1–10

Kim J. Y. and Behrens J. 1986: Experimental evidence of the S^*-wave. Geophys. Prosp. **34,** 1, pp. 100–108

Kuhn M. J. 1985: A numerical study of Lamb's problem. Geophys. Prosp. **33,** 8, pp. 1103–1137

Tsvankin I. D. 1982: Effect of heterogeneous waves on the field of a refracted spherical wave. Vestnik Moskovskogo Universiteta, Geologiya **37,** pp. 80–86. (Allerton Press, Inc)

Tygel M. and Hubral P. 1984: Transient representation of the Sommerfeld–Weyl integral with application to the point source response from a planar acoustic interface. Geophysics **49,** 9, pp. 1495–1505

A HULLÁMTERJEDÉSBEN MEGNYILVÁNULÓ OKSÁGI ÖSSZEFÜGGÉSEK ÚJ MEGVILÁGÍTÁSBAN

Peter HUBRAL és Martin TYGEL

Az okság alapvető fizikai elv a hullámterjedésben. Mint ismeretes, az okság azt jelenti, hogy gerjesztés előtt nem lehet átvitel. A „matematikai okság" viszont azt jelenti, hogy a fizikai valóságot leíró matematikai megoldás nem terjedhet ki a forrás gerjesztése előtti időre. Azonban a fizikai ok–okozati viszonytól eltérően, a matematikai okság elvéhez nem kell ragaszkodni. Matematikai okság például minden olyan megoldás, mely leírja a rétegzett közeg válaszát a Sommerfeld- vagy Weyl-integrállal leírható átmeneti okszerű forrásra. Jól ismert, hogy ekkor az eredő megoldási integrálok végtelen integrálási határral rendelkeznek. Ez azonban egyszerűen átváltoztatható véges integrálási határral a matematikai oksági követelmény enyhítése útján és olyan nem-oksági megoldások keresése útján, melyek időben szimmetrikusak a forrás gerjesztésének pillanatára vonatkoztatva, minekutána megegyeznek az okszerű átvitellel. Így az időbeli szimmetria a hullámterjedésnek bizonyos teljességet ad, mely korábban nem volt elérhető. Ebben a cikkben megfogalmazzuk két

eltérő, állandó sebességgel bíró homogén akusztikus félteret elválasztó sík határfelület közelében elhelyezkedő pontszerű forrás időben szimmetrikus, szélessávú átviteli függvényét. Ez szép példáját nyújtja annak, hogy hogyan használhatjuk fel az időbeli szimmetriára vonatkozó megfontolásainkat olyan egyszerűbb kifejezések közvetlen úton történő előállítására, melyek viszonylag könnyen elemezhetők. Amikor alagút-hatás figyelhető meg (vagyis amikor a forrás a nagyobb sebességű közegben közel van a határfelülethez), akkor a szélessávú átviteli függvény csupán a homogén síkhullámok szuperponálásával szimulálható. A megoldási integrál közvetlen megfigyeléséből az alagút-hatás jelenségére könnyen lehet következtetni és egy úgynevezett kvázi-szferikus P^*-hullám vezethető le.

НОВЫЙ ВЗГЛЯД НА ПРИНЦИП ПРИЧИННОСТИ В РАСПРОСТРАНЕНИИ ВОЛН

Петер ХУБРАЛ и Мартин ТЫГЕЛ

Причинность является основным физическим принципом в распространении волн. Как известно, она означает, что не может быть передачи до возбуждения. «Математическая причинность» внушает, с другой стороны, что описывающее физическую реальность математическое решение не должно охватывать все времена до возбуждения источника. В отличии от причинности в физике, математическая причинность не обязательно должна соблюдаться. Математическая причинность, например, представлена всеми решениями, описывающими поведение слоистой среды под влиянием переходного причинного источника, описываемого интегралами Зомерфельда или Вейла. Известно, что результирующие интегралы решения при этом обладают бесконечным пределом интегрирования. Однако, он может быть просто преобразован в конечный предел интегрирования путем ослабления требования математической причинности и отыскания непричинных решений, которые являются симметричными во времени по отношению к моменту возбуждения источника, после чего они совпадают с причинным ответом. Поэтому симметрия во времени дает распространению волн некоторую полноту, которая оказалась раньше недосягаемой. В настоящей работе формулируется симметричная во времени широкополосная характеристика передачи точечного источника, находящегося вблизи плоского раздела между двумя однородными акустическими полупространствами с явными постоянными скоростями. Это является хорошим примером применения соображений по симметрии во времени для получения прямым путем более простых выражений, которые относительно легко подвергаются анализу. При наличии туннельного эффекта (т. е. при хаождении источника вблизи раздела в среде повышенной скорости) широкополосная характеристика передачи симулируется наложением только однородных плоских волн. По непосредственному наблюдению интеграла решения легко сделать заключение о наличии туннельного явления и можно вывести т. н. квази-сферическую волну P^*.

GEOPHYSICAL TRANSACTIONS 1987
Vol. 32. No. 4. pp. 291–306

REMOVAL OF MEDIUM AND LONG-WAVELENGTH STATICS ANOMALY FROM VELOCITY GATHERS (A 2-D MODEL STUDY)

Ernest F. PAAL*

The anomalies associated with the weathered layer can affect the seismic data in different ways. They can change or completely remove the relief from structures with small closure. They can distort the shape of the reflection hyperbolae on velocity gathers. But their most obvious effect is the lowering of the signal-to-noise ratio together with causing a deterioration in the resolution of reflected events on the stacked seismic traces.

Among the three types of anomalies: long, medium and short, the medium and the long-wavelength ones are the most difficult to determine. The medium-wavelength anomaly is the one which distorts the shape of the reflection time–distance curves on velocity gathers and, therefore, the subsequent velocity analysis that scans these distorted, higher order curves hyperbolically results in erroneously defined VNMO velocities with decreased coherency values.

A 2-D model study example is used to demonstrate how the medium-wavelength anomaly distorts the normally hyperbolically shaped reflected arrivals. As a solution to the problem an iterative processing stream is presented where the combined effects of long-wavelength refraction and short-wavelength reflection static procedures are required. The removal of the medium-wavelength component is mainly required for accurate VNMO velocity determinations not so much for the sake of good normal-moveout corrections but rather to obtain correct migration velocities and more importantly reliable Dix interval velocities for time-to-depth conversion.

Keywords: seismic methods, reflection methods, low-velocity zone, signal-to-noise ratio, static correction

1. Introduction

Static anomalies associated with the weathered or low-velocity layer (LVL) can affect seismic data in different ways. They can change or completely remove the relief from structures with small closure. They can distort the shape of the reflection hyperbolae on velocity gathers. But their most obvious effect is the lowering of the signal-to-noise ratio together with adversely affecting the resolution of reflected events on the stacked seismic traces.

Among the three types of anomalies: long, medium and short, the medium and the long wavelength ones are the most difficult to determine. In this discussion wavelength defines the length or lateral extent of the anomaly with respect to the maximum source-to-receiver distance or spread length. Therefore, one spread length is equivalent to one wavelength. Our characterization and

* Exxon Production Research Company, P. O. Box 2189, Houston, Texas 77252-2189, USA
Paper presented at the 47th meeting of the EAEG, 4–7 June, 1985, Budapest, Hungary

separation of the LVL anomaly spectrum into these three components are the result of the three different types of effects these anomalies have on the various forms of the seismic data. In this work we assume the following approximate separation for these three components of the LVL-anomaly spectrum. The lateral extent of the short-wavelength anomaly is from the existing receiver interval to about one quarter of a spread length. For the medium-wavelength anomaly this extent is from one quarter to three-quarters of a spread length. And finally the long-wavelength anomaly extends from three-quarters of a wavelength to the extent of the entire seismic line.

We want to emphasize in this discussion, by showing the results of this model-study, that the complete removal of the medium wavelength anomaly requires the use of both residual reflection and surface consistent refraction static correction methods. The medium-wavelength anomaly is the one which distorts the shape of the reflection time–distance curves on velocity gathers and, therefore, the subsequent velocity determination routine that scans these distorted, higher than second order curves hyperbolically results in erroneously defined VNMO-velocities with decreased coherency values. We will follow-through a 2-D model study example to demonstrate how the medium-wavelength anomaly distorts the normally hyperbolically shaped reflected arrivals. As a solution to this problem an iterative processing stream will be presented where the combined application of long-wavelength refraction and short-wavelength reflection static procedures are required. As a result of this special processing flow the gained accuracy of VNMO-velocities is not primarily important for the sake of better normal-moveout corrections but rather to obtain reliable Dix interval velocities for time-to-depth conversions.

2. Discussion

In an idealized way *Fig. 1.* describes the problem caused by medium-wavelength LVL components on a source gather collected above a rather simple 2-D model (even the Snell's-law effects were ignored). The hyperbolic time–distance curve (dashed line) represents the shape of the reflected arrival from a single, flat reflector when there is no LVL, but only one single homogeneous layer.

The heavy, distorted curve with the "X"-es represents the time–distance curve with the medium-wavelength LVL distortion resulting from a weathered layer situated just below the surface. The other, hyperbolic curves represent some possible hyperbolic-scan functions which might sweep this gather in order to find the best fit to this distorted curve. There are several curves where some similarity can be found, none of which will correctly represent the actual VNMO velocity from the surface down to the reflector. The obtained coherency values as a measure of how well a scanning function matches the actual data, will be relatively small also in this case on the time–velocity plot associated with this gather.

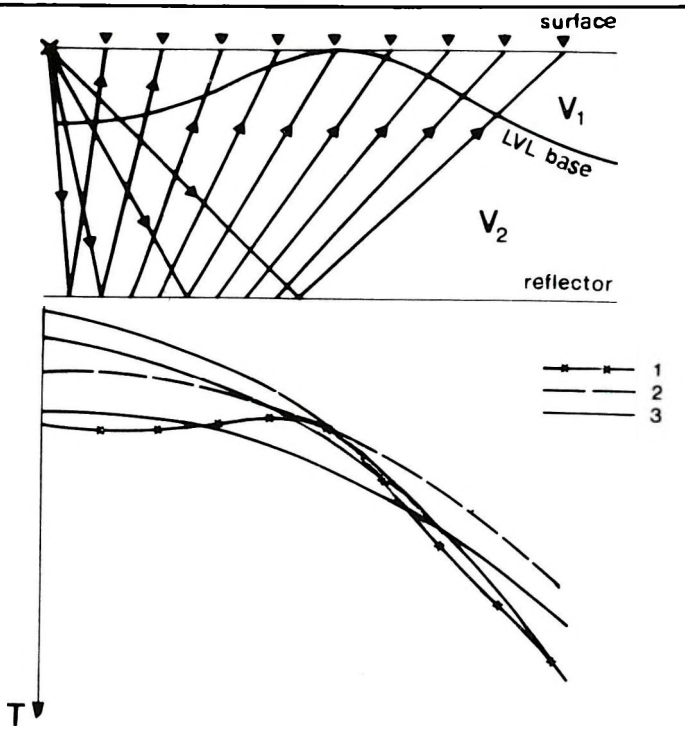

Fig. 1. Simplistic model to demonstrate the effect of the medium-wavelength LVL-anomaly on a source gather
1 — time–distance curve with medium-wavelength LVL distortion; 2 — hyperbolic time–distance curve; 3 — possible hyperbolic scan functions

1. ábra. Egyszerűsített modell a közepes hullámhosszúságú lazaréteg-anomália hatásának szemléltetésére robbantópont szerinti csatornagyűjtésre
1 — út–idő görbe közepes hullámhosszúságú lazaréteg torzítással; 2 — hiperbolikus út–idő görbe; 3 — lehetséges hiperbolikus modell függvények

Рис. 1. Упрощенная модель для иллюстрации влияния аномалии ЗМС, вызванной волнами средних длин, на отобранные сейсмические трассы
1 — годограф с искажением ЗМС, вызванным волнами средних длин;
2 — гиперболический годограф; 3 — возможные функции гиперболического обслеживания

To look into this problem in more detail and with a more quantitative scrutiny next we will discuss our 2-D model. The upper part of *Figure 2* represents the near-surface portion of the model. This part comprises topographic undulations up to approximately 55 meters maximum, which are in the medium and long wavelength range in relation to the almost 3000 meter spread length. The actual LVL-thickness varies with all three components of the anomaly spectrum, and it reaches a maximum value around 60 meters. The LVL-velocity is 915 m/s and the first subweathering layer velocity is 2285 m/s, their ratio being exactly 0.4. This value is found to hold surprisingly well in many places around the world.

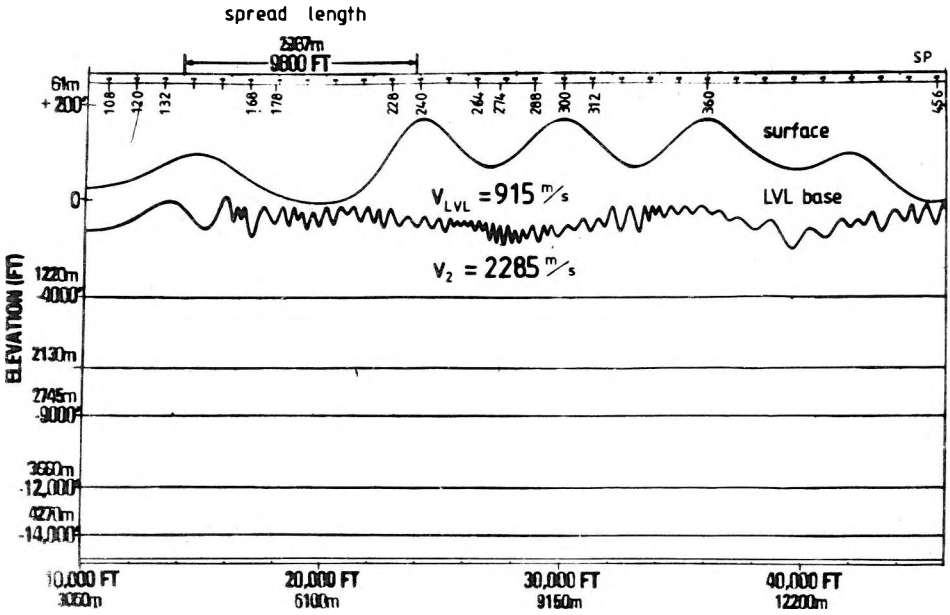

Fig. 2. Model providing the synthetic data by non-zero-offset ray tracing

2. ábra. A vizsgálat céljára használt modell

Рис. 2. Модель, за расчетов

Below the weathered layer, we placed 5 flat reflectors with depths indicated on the left hand side of the model. The synthetic traces from the model were generated by non-zero offset ray tracing. The data represent 48-channel offset recording resulting in 24 fold CDP coverage with 61 meters station and shot interval.

The model is a very close replica of an actual seismic line. *Figure 3* is the "stack" of the near trace in each stacking bin without any LVL or elevation static corrections. It verifies our contention that the model represents all three components of the LVL-anomaly spectrum as far as the LVL-thickness variation is concerned. This is especially a correct statement as far as the reflection from the base of the LVL is concerned. It does not have any topographic effects, but only the effects due to LVL-thickness changes.

On the Model two CDP-gathers are selected for more detailed analysis. One is extracted at a place on the model where the topography and the LVL-thickness change is the greatest (SP 274). This gather will only serve to dramatize how bad this distortion can become in extreme cases due to the medium-wavelength anomalies.

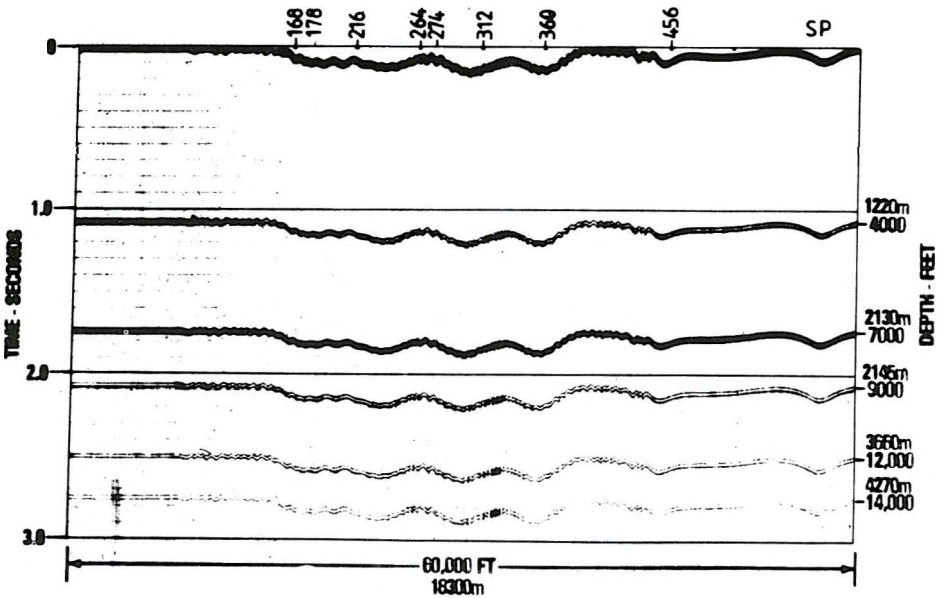

Fig. 3. Time section obtained after stacking the near-trace without the application of any elevation or LVL corrections

3. ábra. A robbantópont-közeli csatornák összegzésével nyert időszelvény, topografikus- és lazaréteg-korrekció nélkül

Рис. 3. Временной разрез, полученный в результате накопления близкой трассы без поправки за высоту или ЗМС

The location for the second gather (SP 178) was selected where these variations (topography & LVL) are the mildest on the model. This example will serve as a reminder that even at the most unexpected location there can be enough inherent nonhyperbolic distortion due to the medium-wavelength component that the error in velocity determination will exceed the error normally acceptable for depth conversion in this type of geological setting. (Small amounts of nonhyperbolic distortion cannot necessarily be detected with the naked eye as we will see on our second velocity gather).

Several of the CDP gathers are displayed in *Fig. 4;* these gathers were extracted along the line at a certain, constant distance interval. Each gather represents the refracted first arrival and five reflected time–distance curves on which the medium-wavelength distortions are obvious.

In *Fig. 5* we display the gather which is extracted from the model at the most complex topographic and LVL variations (SP 274). We normally combine two stacking bins (2 × 24 traces) to form these velocity gathers. The reason is to increase the multiplicity of offsets for better velocity definition. In spite of the removal of the distortion caused by the topographic effect (residual elevation statics applied), a large amount of medium-wavelength distortion is still present

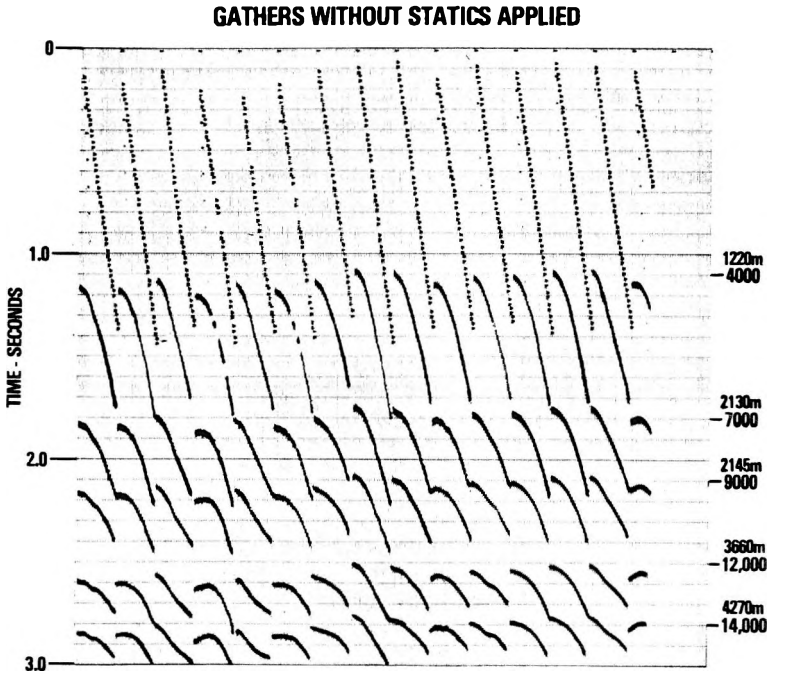

Fig. 4. 15 CDP gathers evenly distributed along the surface of the model, showing the distorted time–distance curves due to the medium-wavelength anomalies

4. ábra. 15 egyenközü közös mélységpontos csatornagyüjtés közepes hullámhosszúságú anomáliák torzító hatásának szemléltetésére

Рис. 4. Отбор сейсмических трасс по 15-и ОГТ, распределенных равномерно по поверхности модели, которые показывают искаженные годографы, связанные с аномалиями волн средних длин

on the time–distance curves. Multiple velocity picks with the same coherency values can be seen. The maximum velocity difference between picks representing the same reflector reaches as much as 3500 ft/s = 1066 m/s.

The non-hyperbolic distortion is clearly visible on the uncorrected gather. The corrected gather traces with the designated "correct" VNMO-function are displayed to the right of the uncorrected gather. After the application of this hyperbolic, second order correction to these gather traces did not transform the reflected events to the desired flat disposition. This can be looked at as further proof that the pre-NMO time–distance curves are higher than second order.

Figure 6 displays this same gather after the removal of the residual value of all static anomalies from the gather. The reason behind the removal only of the residual static effects vs. of their total values is that we want to maintain the reference of these velocities to a plane surface, near to the actual topographic surface. The applied residual corrections (refraction, reflection and elevation) reduce both source and receiver time values to this plane.

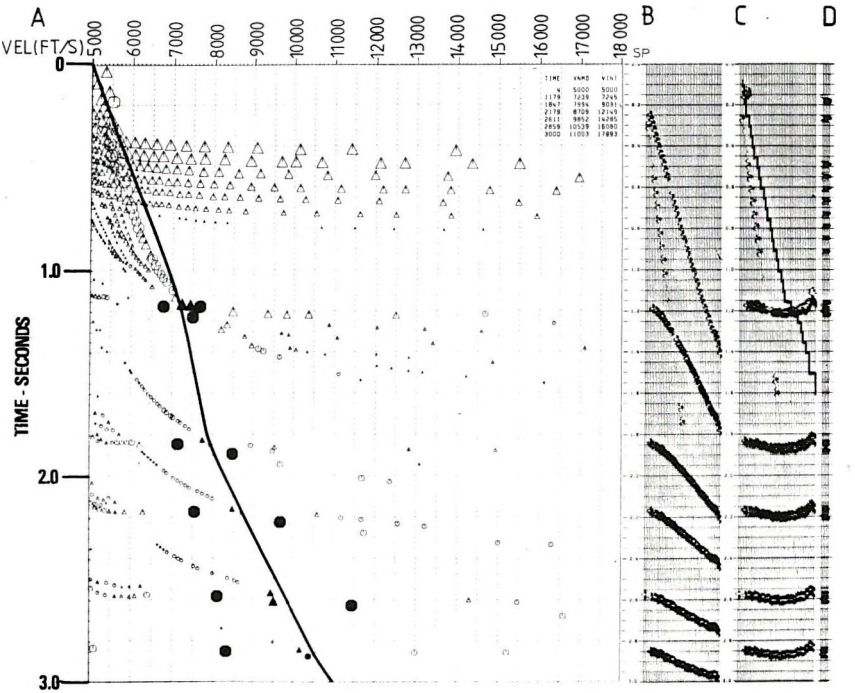

Fig. 5. Noiseless gather and time–velocity event display with only residual elevation statics applied for SP 274

A — the result of the hyerbolic scanning for two stacking bins (coherency peaks triangles and circles, size proportional with measure of coherency); B — the uncorrected (raw) gather traces; C — NMO-corrected gather-traces; D — sum of NMO-corrected gather displayed 5 times

5. ábra. Zajmentes csatornagyűjtés és idő–sebesség függvény a 274-es robbantópontra, maradék topografikus statikus korrekció alkalmazása után

A — két közös mélységpont hiperbolikus sebességvizsgálatának eredménye (a koherenciacsúcsokat háromszögek és körök ábrázolják, méretük arányos a koherencia mértékével); B — korrigálatlan (nyers) csatornagyűjtések; C — csatornagyűjtések NMO korrekció után; D — a korrigált csatornák összege, ötször egymás után kiíratva

Рис. 5. Отбор сейсмических трасс без шума и график зависимости времени от скорости для ПВ 274 с применением только остаточной статической поправки

A — результат гиперболического обследования двух совокупностей накопления (пики когерентности изображены треугольниками и кружками, размер их пропорционален величине когерентности); B — отбор неисправленных трасс; C — отбор трасс после введения кинематической поправки; D — сумма сейсмических трасс после введения кинематической поправки, вычерченная 5 раз

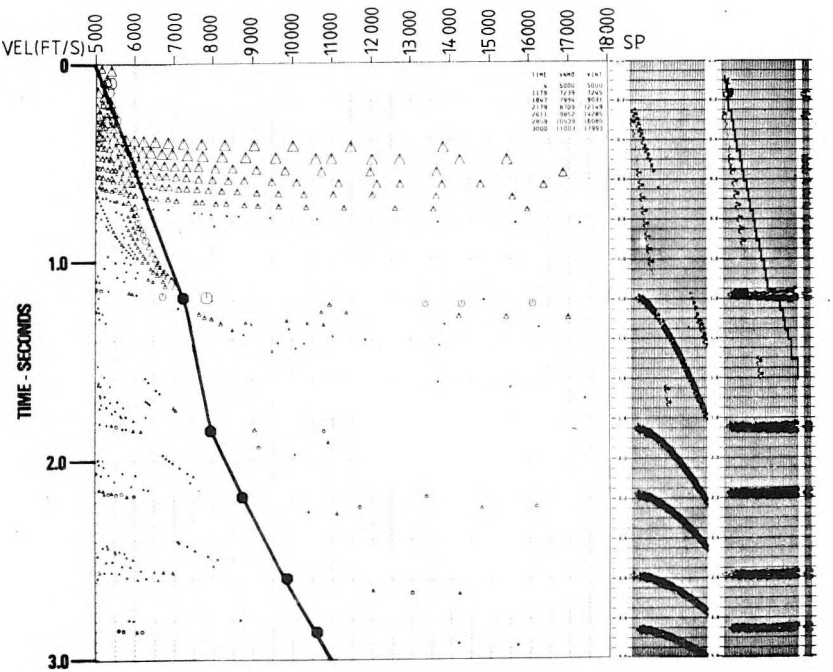

Fig. 6. Noiseless gather with all LVL-anomalies removed by refraction, reflection and elevation static correction procedures

6. ábra. Zajmentes csatornagyűjtés és idő–sebesség függvény lazaréteg korrekció (refrakciós, reflexiós és topografikus) után

Рис. 6. Отбор сейсмических трасс без шума и график зависимости времени от скорости с устранением всех аномалий ЗМС путем введения статических поправок ОВ, ПВ и за высоту

The formula used for this residual static correction calculation is the following:

$$\mathrm{RESID}_i = \mathrm{TOTAL}_i - \frac{1}{N}\sum_{i=1}^{N} \mathrm{TOTAL}_i$$

where i = trace no. in the gather
N = max. trace no. in the gather

RESID_i = Residual correction for trace i
TOTAL_i = the sum of all LVL and elevation corrections with their total values reducing each trace to the datum plane.

Figure 6 of the corrected gather provides the proof that the previously distorted reflections were fully restored to their proper shapes, and the velocity determination process (hyperbolic scanning) could find only one matching hyperbola to 4 out of 5 of these reflections with large coherency values.

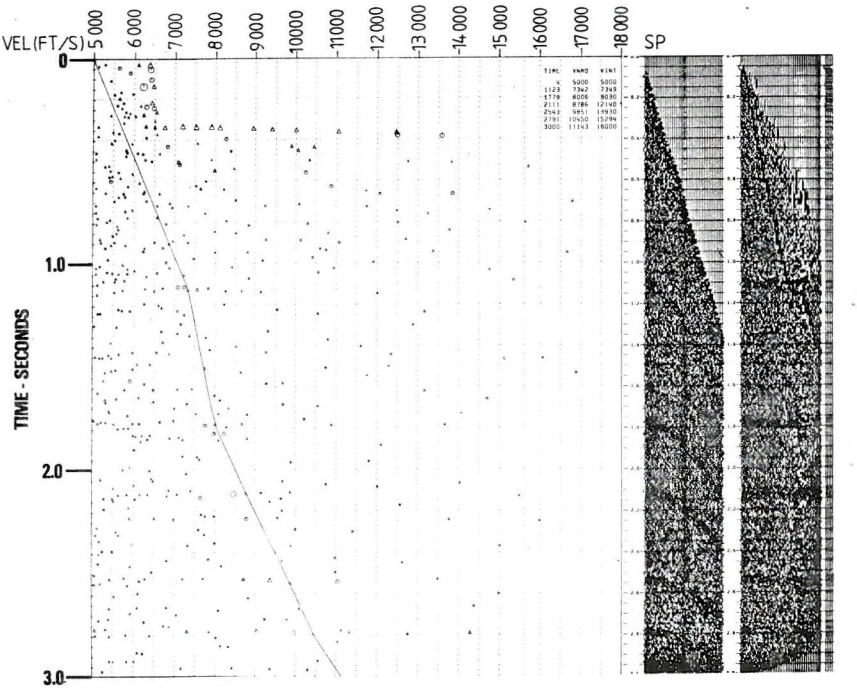

Fig. 7. CDP-gather and time–velocity event display for SP 178 where random noise was added to the signal and only residual elevation static corrections were applied

7. ábra. Közös mélységpontos csatornagyűjtés és idő–sebesség függvény a 178-as robbantópontra, véletlen zaj hozzáadásával, maradék topografikus korrekció alkalmazása után

Рис. 7. Отбор сейсмических трасс с ОГТ и график зависимости времени от скорости для ПВ 178, где к сигналу был добавлен случайный шум, а применялась только остаточная статическая поправка за высоту

Now we will move to the other, somewhat less distorted gather on the model (SP 178). Here, to simulate real data gathering conditions more closely we added random noise with a 1.5 to 1 signal-to-noise ratio to corrupt our gather traces. While the noise on *Figs 7 and 8* looks overwhelming, in actuality this will not impede to any considerable degree the cross correlation routine, which is used in all residual reflection static procedures, to find the short and the low to medium-wavelength anomaly components of the LVL [WIGGINS et al. 1976, FARREL and EUWEMA 1984].

The addition of random noise to pure synthetic signals, unfortunately does not quite simulate real data. In real data we encounter, besides additive, random noises variations in source energy and in source and geophone coupling. In addition direct and hyperbolically arriving noises are being added and convolved with the signal. Some other factors are the various loss mechanisms due to

geometric divergence, inelastic attenuation, conversion losses and energy scattering in the near surface. Due to these further degradation takes place in our signal amplitude spectrum and to the trace to trace similarity of the reflected pulse. Under these conditions we have found that the need for both static correction procedures (refraction and reflection) is highly desirable. As far as the result of this model study is concerned the above message was portrayed only qualitatively because we fell somewhat short of simulating real data conditions. In Fig. 7 it is very difficult to see the coherent reflection events on both the corrected and uncorrected displays. If we look at the "sum traces", which are the stacked gather traces repeated five times on the right side of the corrected gather they immediately tell the story. The amplitudes of the 5 events on these traces are practically zero. On the left side, on the time–velocity event display no coherency peaks with any acceptable size or any pattern can be detected in the clutter of the randomly distributed low value event picks. Obviously the short-wavelength component which was not affected by the residual elevation correction values plus the random noise caused this degradation in S/N ratio.

Figure 8 displays the same gather which, in addition to the residual elevation statics, was processed by a residual reflection static process also. Significant improvements can be detected in S/N ratio on both gather displays and in the coherency values of the reflected arrivals on the time–velocity plot. What is even more noticeable, which is the main message of this discussion, is the fact that in spite of the considerable improvement the velocity picks as a result of the hyperbolic scans are still incorrectly positioned in respect to the correct values. These are 50–75 m/s off from the solid line of the VNMO curve. Also interesting is that there are only singular values displayed, which might indicate to the casual observer that everything is in order and all the medium-wavelength distortion was removed. This false assumption can also be adopted by examining the corrected and uncorrected gathers. By visual means there can be seen no distortion whatsoever on these gathers, indicating that the naked eye cannot detect this distortion until it is already too large. As far as the quality of these gathers is concerned, for NMO correction there are some errors for the higher frequency components. The centre frequency of this synthetic pulse is 25 Hz. Taking the reflection just below 2 seconds where the difference between the picked and the correct velocity is approximately 250 ft/s = 75 m/s the residual Δt is 15 ms, as the following calculation indicates.

$$\Delta T_{err} = \left[\left(\frac{X}{V_e}\right)^2 + T_0^2\right]^{\frac{1}{2}} - T_0 = \left[\left(\frac{9800}{8536}\right)^2 + (2.111)^2\right]^{\frac{1}{2}} - 2.111 = 0.2919$$

$$\Delta T_{corr} = \left[\left(\frac{X}{V_c}\right)^2 + T_0^2\right]^{\frac{1}{2}} - T_0 = \left[\left(\frac{9800}{8786}\right)^2 + (2.111)^2\right]^{\frac{1}{2}} - 2.111 = 0.2766$$

$$\Delta\Delta T = \Delta T_{err} - \Delta T_{corr} = 0.2919 - 0.2766 = 0.015 = 15 \text{ ms}$$

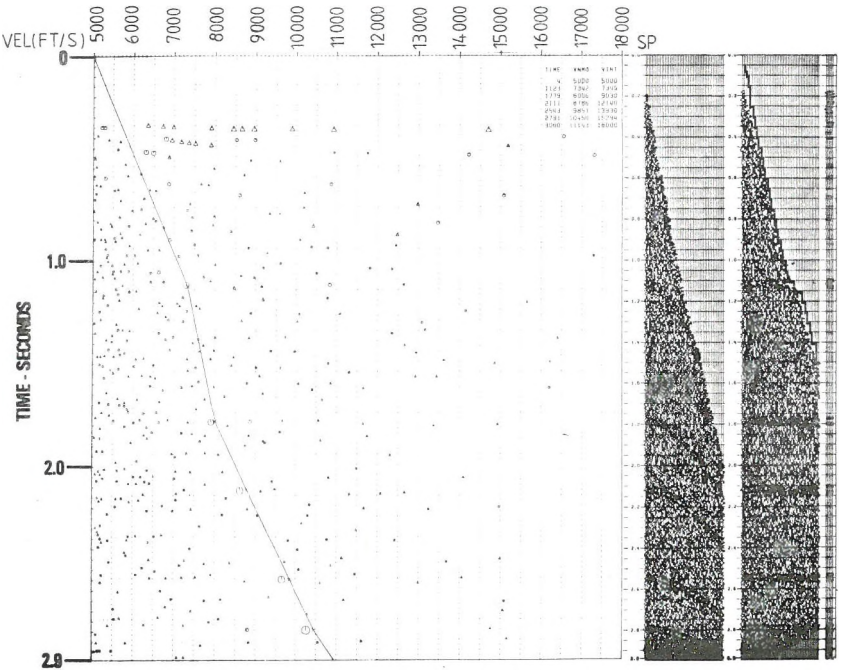

Fig. 8. The same as Fig. 7, after residual elevation and reflection statics application

8. ábra. Ugyanaz, mint a 7. ábra, maradék topografikus és reflexiós statikus korrekció után

Рис. 8. То же, что и на рис. 7, после введения поправки за остаточную высоту и статической поправки ОВ

This same 250 ft/s or 75 m/s error in velocity on the other hand in respect to the generally allowed not more than 1%–1.5% error in depth conversions is too large. The error here is 2.85%:

$$T_0 = 2.111 \text{ s} \qquad V_{\text{NMO}} = 8786 \text{ ft/s} \qquad \Delta V = 250 \text{ ft/s}$$

$$Z_{corr} = \frac{T_0 V_{\text{NMO}}}{2} = \frac{2.111 \cdot 8786}{2} = 9273.6 \text{ ft} = 2826.4 \text{ m}$$

$$Z_{err} = \frac{T_0 (V_{\text{NMO}} - \Delta V)}{2} = \frac{2.111(8786 - 250)}{2} = 9009.7 \text{ ft} = 2746.0 \text{ m}$$

$$\Delta Z = 80.4 \text{ m} = 263.9 \text{ ft}$$

$$\frac{\Delta Z}{Z_{corr}} \cdot 100 = 2.85\%.$$

The error in absolute depth due to not using Dix's converted interval velocities is 263.9 ft or 80.4 meters.

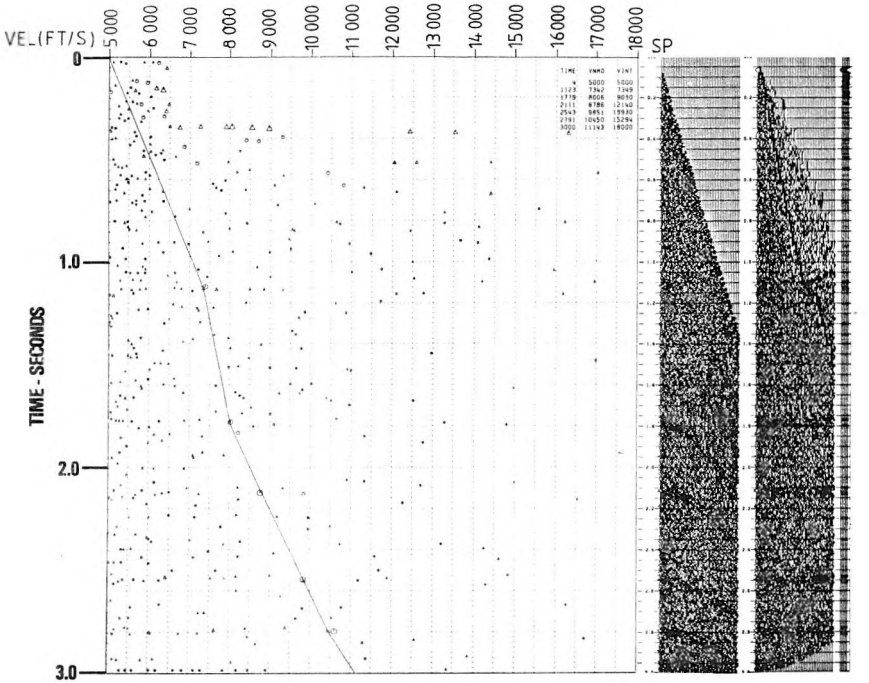

Fig. 9. The same as Fig. 7, after residual elevation and residual refraction statics application

9. ábra. Ugyanaz, mint a 7. ábra, maradék topografikus és maradék refrakciós statikus korrekció után

Рис. 9. То же, что и на рис. 7, после введения поправки за остаточную высоту и остаточной статической поправки ПВ

Figure 9 is the gather with residual elevation and refraction statics. The differences with Fig. 8 are immediately apparent. Since the refraction statics, even the surface consistent ones, are not as effective against the short-wavelength components as are the reflection static procedures, the coherency peaks on the plot are smaller in value. This can also be seen when we examine the corrected and uncorrected gathers and the 5 sum traces. All these show a reduction in signal-to-noise ratio which indicates that the alignment of the traces in the stacking bin has been disturbed by a laterally high frequency near-surface event. These are the negative aspects of this comparison between Figs. 8 and 9. The advantage of the refraction (Fig. 9) vs. reflection (Fig. 8) process is in the improvement of the velocities for 4 out of the 5 events. Three of these peaks were correctly positioned on the designated velocity curve.

When both refraction and reflection statics are applied in addition to residual elevation statics (*Fig. 10*), all three components of the LVL anomaly spectrum are removed. This can be verified by the accurately positioned velocity event picks which all lie on the correct velocity function, and by the improvement of the coherency or S/N ratio of the gather traces. The sum traces, just

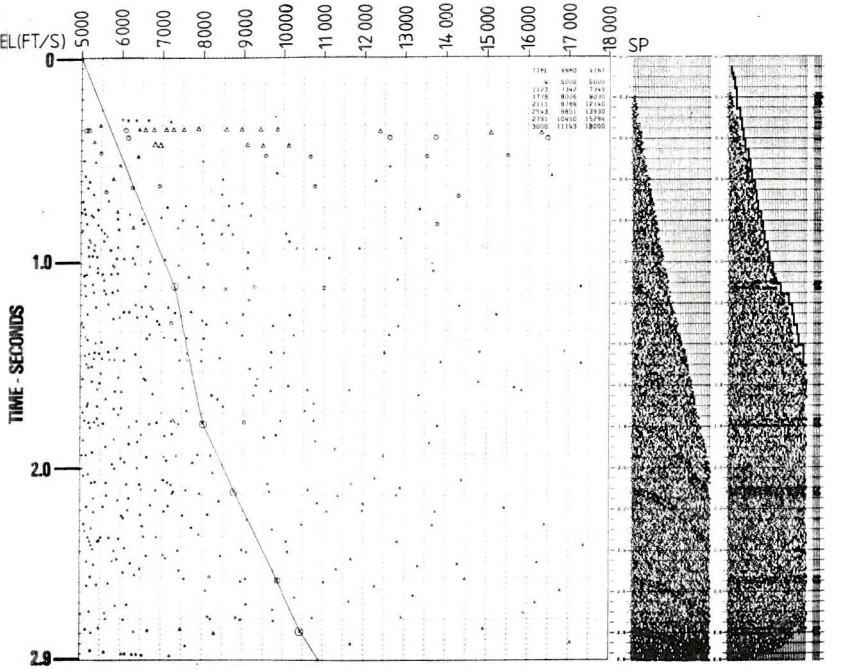

Fig. 10. The same as Fig. 7, after residual elevation, refraction and reflection statics application

10. ábra. Ugyanaz, mint a 7. ábra, maradék topografikus, refrakciós és reflexiós statikus korrekció után

Рис. 10. То же, что и на рис. 7, после введения остаточной поправки за высоту и статической поправки ПВ и ОВ

right from the corrected gather, will indicate both of these improvements. The summed wavelet amplitudes representing the five distinct reflections are the highest and the wavelets have shortest duration among all 4 displays we have analysed.

This figure portrays the fact that a definite improvement both in velocity picks and in the coherency values of the reflections can be realized by this combined process.

Our final display *(Fig. 11)* is a flow diagram which discusses the iterative process flow that was applied to these model traces and is being applied to all of our land data gathers where the initial analysis indicates medium-wavelength distortions on the reflected arrivals. The input tape to this process should be a gain recovered CDP ordered trace data set with the appropriate header records which carry information for further processing. The data might already have been subjected to some other processes either for first-arrival (refraction) or for reflection enhancement.

The first step is to determine the long-wavelength refraction statics which will be stored for later application in the trace headers. Parallel with the

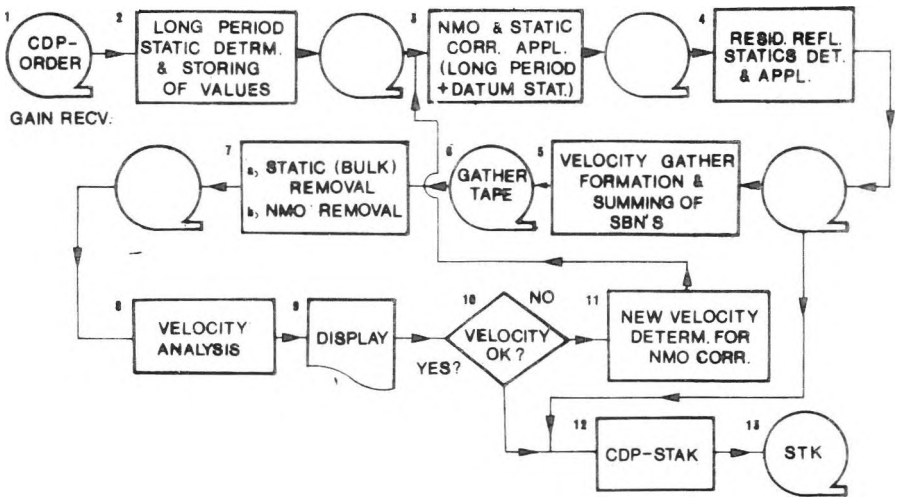

Fig. 11. Generalized data flow diagram illustrating the iterative application of the various static correction values with appropriate quality control checks inserted

11. ábra. Általánosított folyamatábra a különféle statikus korrekciós értékek iteratív alkalmazásának szemléltetésére, megfelelő minőség-ellenőrző vizsgálatok közbeiktatásával
1 — közös mélységpontos rendezés, erősítés helyreállítás; 2 — hosszú periódusú statikusok meghatározása és értékek tárolása; 3 — NMO és statikus korrekciók alkalmazása (hosszú periódusú + topografikus statikusok); 4 — maradék reflexiós statikusok meghatározása és alkalmazása; 5 — csatornaválogatás sebesség-meghatározásra és az SBN-ek összegzése; 6 — gyűjtőszalag; 7 — a) statikusok eltávolítása, b) NMO eltávolítása; 8 — sebességanalízis; 9 — kiírás; 10 — sebesség jó? 11 — új sebesség-meghatározás az NMO-korrekcióhoz; 12 — közös mélységpontos összegzés; 13 — összegszalag

Рис. 11. Обобщенная диаграмма обработки, иллюстрирующая итеративное применение разных значений статической поправки с включением соответствующих процедур проверки качества:
1 — отбор по ОГТ, восстановление усиления; 2 — определение и хранение значений длиноволновых поправок; 3 — применение кинематической и статических (длиноволновой + топографической) поправок; 4 — определение и применение остаточных статических поправок; 5 — отбор трасс для определения скорости и суммирование SBN; 6 — лента, на которую отбираются трассы; 7 — а) введение статических поправок, b) введение кинематических поправок; 8 — анализ скоростей; 9 — вывод на дисплей; 10 — скорость правильна? 11 — новое определение скорости для кинематической поправки; 12 — накопление ОГТ; 13 — накопительная лента

long-wavelength statics determination the analysis of the initial stacking velocities should also take place to optimize the processing time. Then the data will be NMO corrected and the elevation and long-wavelength statics will be applied. Next the residual reflection statics are determined and also applied to the data. At this point before we go any further it is advisable to see for quality control purposes how well we have done so far and stack the data. If they fulfil our expectation then we can proceed to form the velocity gathers. These gathers which are formed as a combination of more than one stacking bin are extracted

at certain intervals along the line and output to the so called "gather-tape" data set.

At this point processing the gathers are in the NMO and static corrected form, i.e. they are referenced to datum. For velocity analysis, as we know, the gathers should be referenced to the surface and must not be NMO corrected. Therefore, in the following step we remove that part of the static correction (bulk shift) which is the difference between the datum and the surface reference planes (in reverse order). This difference represents a bulk shift, in time, for all traces in the gather. Velocity analysis follows, the result of which will provide a better set of velocity values. We compare these with the previous set in order to make the correct decision: either to loop back with these better velocities to obtain a better NMO correction or, if satisfied after stacking for quality control, we can declare the gathers to be suitable for the next process.

The next process—generally when the data are intended for time-to-depth conversion—is a velocity smoothing process along horizons. The result will provide the required velocity quality (free from statistical and other local variations) for this final and crucial step. This iterative loop was used on our synthetic model-data set which we processed through this loop only once in order to come up with the correct velocities. Our experience with real data indicates that generally two iterations are necessary for the required data improvement.

3. Conclusion

This model study demonstrated that the removal of the medium-wavelength static anomalies required the combined use of refraction and reflection statics procedures. This message was portrayed in the result of this study only qualitatively. The reason is that the data we used for the study did not faithfully simulate real data. It is by no means adequate to simulate real data gathering conditions simply by adding random noise to pure synthetic signals.

From this study we learned that to obtain velocities which are accurate enough for time-to-depth conversions residual elevation and reflection statics alone under all possible LVL conditions, cannot resolve reliably the static anomalies quite up to a wavelength. Generally with fairly good quality data the resolution range of short-wavelength reflection and long-wavelength, surface consistent, refraction static procedures have a comfortable overlap just above the half wavelength range. As the data quality (S/N) deteriorates this overlap will shrink to a narrower zone.

REFERENCES

WIGGINS R. A., LARNER K. L., WISECUP R. D. 1976: Residual statics analysis as a general linear inverse problem. Geophysics **41**, 5, pp. 922–938

FARREL R. C., EUWEMA R. N. 1984: Refraction statics. Proceedings of the IEEE **72**, 10, pp. 1316–1329

KÖZEPES ÉS HOSSZÚ HULLÁMHOSSZÚSÁGÚ STATIKUS ANOMÁLIÁK ELTÁVOLÍTÁSA SEBESSÉGMEGHATÁROZÁSRA VÁLOGATOTT CSATORNÁKBÓL (2-D MODELLTANULMÁNY)

Ernest F. PAAL

A lazaréteggel kapcsolatos anomáliák különféleképpen befolyásolhatják a szeizmikus adatokat. Megváltoztathatják vagy teljesen eltüntethetik kis amplitúdójú szerkezetek domborzati formáit. Eltorzíthatják a közös mélységpontos csatornagyűjtés reflexiós hiperboláinak alakját. Legszembetűnőbb hatásuk a jel/zaj viszony csökkenése, amely rontja a reflexiós beérkezések felbontását az összegezett szeizmikus csatornákon.

A hosszú, közép és rövid hullámhosszúságú anomáliatípus közül a közép és hosszú hullámhosszú anomáliákat nehéz meghatározni. A közepes hullámhosszú anomália torzítja el a reflexiós út–idő görbék alakját a csatornagyűjtésekben, s ezért az ezt követő sebességanalízis, amely hiperbolikusan vizsgálja ezeket az eltorzított, magasabb rendű görbéket, hibásan meghatározott VNMO sebességeket eredményez, csökkentett koherenciaértékekkel. Egy 2-D modelltanulmány példáját használjuk fel annak bemutatására, hogy hogyan torzítja el a közepes hullamhosszú anomália a normálisan hiperbola formájú reflexiós beérkezéseket. A probléma megoldásaként bemutatunk egy iterációs feldolgozási folyamatot, ahol a hosszú hullámhosszú refrakciós és a rövid hullámhosszú reflexiós statikus eljárás kombinált hatására van szükség. A közepes hullámhosszú komponens eltávolítása főleg a pontos VNMO sebességmeghatározásokhoz szükséges, nem annyira a jó NMO korrekciók érdekében, hanem inkább helyes migrációs sebességek előállítása céljából, és ami még fontosabb: megbízható Dix intervallumsebességek előállítására az idő–mélység átalakításhoz.

УСТРАНЕНИЕ СТАТИЧЕСКИХ АНОМАЛИЙ В СРЕДНЕ- И НИЗКОЧАСТОТНОМ ДИАПАЗОНЕ ВОЛН ПО СЕЙСМИЧЕСКИМ ТРАССАМ, ПОДОБРАННЫМ ДЛЯ АНАЛИЗА СКОРОСТЕЙ (ИССЛЕДОВАНИЕ НА ДВУХМЕРНОЙ МОДЕЛИ)

Эрнест Ф. ПАЛ

Приуроченные к зоне малых скоростей аномалии могут повлиять на сейсмические данные разными путями. Они могут изменить или полностью устранить рельеф структур небольшого замыкания. Они могут искажать форму гиперболы отраженных волн на отобранных сейсмических трассах. Однако, самым явным эффектом является снижение отношения сигнал—шум, которое приводит к ухудшению разрешения отражений на накопленных сейсмических трассах.

Среди трех типов аномалий: длинных, средних и коротких — наиболее трудно определять аномалии со средними и длинными волнами. Аномалия со средней длиной волн искажает форму годографов отраженных волн на отобранных сейсмических трассах, в связи с чем последующий анализ скоростей, при котором гиперболически обследуются эти искаженные кривые высокого порядка, дает ошибочно определяемые скорости с пониженными значениями когерентности. Исследование на двухмерной модели показывает искажение вступлений отраженных волн, имеющих в нормальном случае гиперболическую форму, аномалиями волн средних длин. Для решения проблемы в работе приводится процедура итерактивной обработки, в которой необходимы комбинированные эффекты длиноволновой статической поправки с применением преломленных волн и коротковолновой статической поправки с применением отраженных волн. Устранение составляющей со средними длинами волн требуется прежде всего для точного определения скорости не столько в интересах получения хороших кинематических поправок, как с целью получения правильных скоростей миграции, и что еще более важно, для получения надежных интервальных скоростей Дикса для преобразования времени в глубину.

GEOPHYSICAL TRANSACTIONS 1987
Vol. 32. No. 4. pp. 307–312

HOW VIBRATOR BEHAVIOUR INFLUENCES SEISMIC RESULTS

Hans A. K. EDELMANN*

The paper describes empirically the phenomenon of a viscous layer under the base-plate of a *P*-wave vibrator as a pre-requisite for coupling on different types of ground. The effect of this viscous layer can be derived from the phase behaviour of the ground force and from the active power transmitted into the ground by a *P*-wave vibrator. The consequences of the vibrator behaviour for the discrimination of phase and amplitude anomalies of seismic reflections are discussed.

Keywords: seismic sources, reflection methods, *P*-wave vibrator, VIBROSEIS*, amplitude, phase, anomalies, vibrator–ground coupling

1. Introduction

It has been well known since the beginning of VIBROSEIS® applications that many of the non-linear effects related to VIBROSEIS® operation are introduced by the non-linear behaviour of the ground. Under unfavourable circumstances more energy is transformed into the range of harmonic frequencies than is available in the fundamental frequency range [EDELMANN 1982]. Nevertheless, many interesting investigations have been made which ignore non-linear effects in a first approach. These investigations foster the impression that the behaviour of the vibrator in the field could be understood and controlled on the basis of a linear model. In the following I have tried to describe a phenomenon which has been observed in many areas and which strongly contributes to the non-linear behaviour of the ground. This effect can be described from measurement results.

2. Some remarks about the theories of the servohydraulic vibrator

Several theories have been developed to describe the behaviour of a servohydraulic vibrator on different types of ground [LERWILL 1981, SAFAR 1984]. To make numerical calculations on the basis of such a model, some assumptions have to be made. Lerwill, for example, assumes that the so-called driving force of the vibrator is constant, i.e. independent of frequency. Another assumption is that the coupling between base-plate and underlying soil is constant. Detailed

* PRAKLA-SEISMOS AG, POB 510530, D 3000 Hannover 51
* Conoco trademark
Paper presented at the 31st International Geophysical Symposium, 29 September–4 October, 1986, Gdańsk, Poland

investigations from different vibrators show that both assumptions are valid only to a limited extent. Under certain conditions these assumptions are not valid at all and therefore conclusions, with respect to vibrator design, should not be drawn from this theory. In practice today, therefore, we build servohydraulic vibrators which are mainly based on modern rules of machine technology, but are not a product of strictly followed theoretical models.

The approach made by SALLAS [1984] which is based on the measurement of different physical parameters of a vibrator, has a far better chance of gaining practical application. The reaction of the ground to the operating vibrator cannot normally be predicted. In this situation the reaction must be measured and the result of this measurement must be fed back to correct the input values of the vibrator. This means that the output of the vibrator can be controlled in such a way that geophysical parameters are kept within certain limits and, at the same time, the vibrator is not destroyed by overload.

Today there still are many vibrator manufacturers who mislead their clients by giving them peak force values which can be transformed into seismic energy only under very rare specific circumstances. And still today, geophysicists cannot say precisely which parameter can be regarded as the main parameter of a vibrator — to be controlled and guaranteed by the manufacturer. Many manufacturers would feel far better if they knew more about this. The problem has been solved by some manufacturers by providing a toggle switch in the vibrator control unit so that the customer can make his own choice out of base-plate acceleration, base-plate velocity, and base-plate displacement.

3. Source characteristic

Discussions about vibrator output were re-opened when VIBROSEIS® records were required to be linked meticulously with dynamite records [BROETZ et al. 1985]. None of the parameters mentioned above proved to be comparable to the impulse emitted from a dynamite shot. Initially some people believed that the problems could be solved by a polarity decision until they noticed that there existed a frequency dependent phase shift between dynamite records and VIBROSEIS records, both measured in the far-field range or in routine seismic records [WAGENBRETH et al. 1985]. Some investigations indicate that the phase characteristic of the ground force of the vibrator comes closer to the phase characteristic of a dynamite shot and to a certain extent is phase-wise less sensitive to variations introduced by changing surface conditions [MARTINEZ 1985].

As long as it is only the determination of travel times that is the main objective of seismic measurements, we have to worry only about the phase-characteristic of what we regard as vibrator output. But as soon as we want to separate variations in phase and amplitude caused by surface effects from variations caused by the exploration target, we cannot any longer rely upon a constant phase characteristic of the vibrator output, but also have to keep an eye on the amplitude characteristic.

4. A reproducible source characteristic

To distinguish anomalies due to transmission and reflection properties of the target zone, the amplitude and phase characteristic as well as the transmission effects of near-surface layers must be taken into account. This is normally done by equalizing CMP traces to an average characteristic using an adequate time window. This method works well as long as the variability of the target-zone effect is larger than the variability of the other factors, i.e. source characteristic and near-surface layer characteristic. Inevitable noise introduces additional problems for the inherent wavelet processing step.

To improve the capabilities of the seismic method with respect to resolution, the reproducibility of the source characteristic should be as good as possible. It is therefore not so important to find out a specific parameter such as base-plate acceleration, reaction mass acceleration, ground force or any other as long as the parameter we select can be used to control the reproducibility of the seismic source characteristic. To come closer to the solution of this problem, it is very helpful to investigate what is going on under a vibrator base-plate.

5. The viscous zone

The vertical movement of the base-plate leads to high shear stress values in the ground at the outer rim of the plate [TAN 1985]. This again leads to a reduction of the shear modulus in this area which results in a radial viscous zone. By this the stress is released in the outer part and increases in the centre part under the base-plate. Dependent upon the force amplitude, the frequency and the preload, a radial flow begins, and then continues or comes to a standstill during the sweep period. Compaction of the material under the base-plate may take place; this compaction is determined by the grain size distribution and water saturation. The compaction which has been achieved at higher frequency and lower amplitudes may be destroyed at lower frequencies and higher amplitudes. At higher preloads, higher amplitudes can be applied without destroying this compaction. Size and properties of the viscous zone under the vibrator base-plate very much depend upon the local properties of the soil. Deeply frozen ground, e.g., ground which is frozen down to the zone of higher compaction, provides excellent coupling conditions for vibrators, also at high force amplitudes, whereas in dry and loose sand large force amplitudes may lead to a permanent radial viscous flow under the base-plate during the sweep operation. In the same survey area, therefore, coupling on compacted soil and coupling through a viscous zone is possible. In many cases, coupling through a viscous zone takes place at low frequencies whereas at high frequencies coupling on compacted ground takes place. Therefore the elastic properties of the soil are frequency dependent and dependent upon the process of the preceding period; this dependence leads to a rather complex phase characteristic of the ground force when compared with base-plate acceleration.

6. The coupling of the base-plate at its worst

A great difference exists between the impedances of vibrator and soil in view of which efficient coupling can only be achieved in a very limited frequency range. Large forces therefore must inevitably lead to a continuous break-up of the soil and thus to a viscous coupling as described above. Only in this way are larger displacement amplitudes of the base-plate made possible, and only through this viscous zone is the base-plate thoroughly coupled to the ground.

Base-plates are not ideally rigid. When being operated on the viscous flow pillow, they change their shape at specific resonance frequencies. At higher frequencies which still lie within the range of the transmitted frequency band, amplitudes at different points of the base-plate are out of phase so that the pressure amplitude which acts on the ground can appreciably be reduced by destructive interference. Hard material under the base-plate such as outcropping rock may worsen the coupling, so that a viscous flow pillow cannot be formed.

7. The phase characteristic of the ground force

If we regard the ground force as the decisive output parameter which controls the phase and amplitude of the outgoing seismic signal and at the same time compensates for the base-plate acceleration signal to be inphase with the vibrator input sweep, it is instructive to analyse the phase deviation between these two parameters. When using the ground model taking into account ground compliance, radiation resistance, and radiation mass [SAFAR 1984] this phase angle can vary between 0° lag for zero frequency approaching 180° lag for very high frequencies. The amount of phase lag depends upon the character of the soil. For soft soil (mud) larger phase lags are possible at high frequencies than for hard soil (chalk). Because of the fact that a viscous flow zone forms under the base-plate at low frequencies, in practice the phase shift can be far larger for low frequencies than is predicted by the linear theory. Phase-shifts of 90° are not anomalous, which are reduced at higher frequencies to a level comparable with the theoretical values. A large phase-shift is a strong indication for the elastic properties of the soil drastically changing as a function of frequency.

8. The active power generated by a vibrator

The difference between the theoretical model and practice comes out very clearly when comparing the active power radiated by a vibrator. From the theoretical model the active power can be calculated as the square of the base-plate velocity multiplied by the radiation resistance. This leads to the rather smooth curve (curve *A*) in *Fig. 1*. The curve was derived from the model

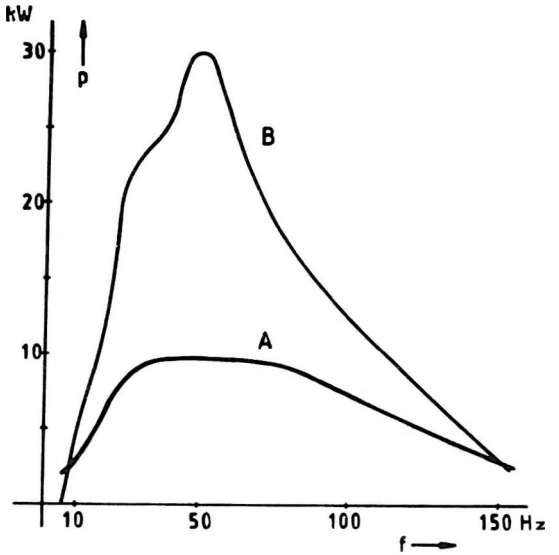

Fig. 1. Emitted active power of a vibrator on sand as a function of frequency
A — calculated from [LERWILL 1981];
B — measured

1. ábra. A vibrátor leadott aktív teljesítménye homokon, a frekvencia függvényében
A — LERWILL [1981] adataiból számítva; B — mért értékek

Рис. 1. Выпускаемая вибратором активная мощность на песке в зависимости от частоты
A — расчетная по Лервил[1981];
B — замеренная

given by LERWILL [1981]. For a radiation resistance for sand $R_r = 2 \cdot 10^6$ Ns/m, curve *A* reaches a maximum at about 35 Hz and then drops slowly towards high frequencies. This calculated result differs strongly from the results achieved from measurements on sandy soil. As the system becomes non-linear, the product of ground force and base-plate velocity has to be determined by measurement and is shown as curve *B* for comparison. It can be seen that an appreciable amount of energy is transformed into soil flow which is a dominating process in seismic energy generation.

9. Conclusions

From measurements it can be shown that a vibrator generates an appreciable amount of active power. This supports the assumption that the base-plate is underlain by a visco-elastic pillow which is necessary to couple the plate to the ground and to generate seismic elastic energy for seismic purposes.

Acknowledgement

The author thanks H.-P. Müller for his patience in helping to evaluate the measurement results by providing adequate computer programs. The project was partly funded by the Bundesministerium für Forschung und Technologie under 03A-6172-A. The permission of PRAKLA-SEISMOS AG to publish this paper deserves grateful acknowledgement.

REFERENCES

BROETZ, R., MARSCHALL R., KNECHT M. 1985: A unified processing approach for Vibroseis and jetted-hole source data. Paper presented at the 47th European Assoc. of Exploration Geophysicists Meeting, Budapest, Hungary, 3–6 June

EDELMANN H. A. K. 1982: A contribution to the investigation of amplitude characteristics of vibrator signals. Geophysical Prospecting **30,** 6, pp. 774–785

LERWILL W. E. 1981: The amplitude and phase response of a seismic vibrator. Geophysical Prospecting **29,** 4, pp. 503–528

MARTINEZ D. R. 1985: A case history comparing vibrator phase-locking techniques. Paper presented at the 55th SEG-Meeting, Washington, 7–11 October, 1985

SAFAR M. H. 1984: On the determination of the downgoing P-waves radiated by the vertical seismic vibrator. Geophysical Prospecting **32,** 3, p. 392–405

SALLAS J. J. 1984: Seismic vibrator control and the downgoing P-wave. Geophysics **49,** 6, pp. 732–740

TAN T. H. 1985: The elastodynamic field of N interacting vibrators (two-dimensional theory). Geophysics **50,** 8, pp. 1229–1252

WAGENBRETH G., MARSCHALL R., BODEMANN W. 1985: Polung und Anpassung. Prakla-Seismos AG Auftraggeber-Seminar, Dezember

HOGYAN BEFOLYÁSOLJÁK A VIBRÁTOR TULAJDONSÁGAI A SZEIZMIKUS EREDMÉNYEKET

Hans A. K. EDELMANN

A tanulmány tapasztalati alapon ismerteti a P-hullám vibrátor alaplemeze alatt kialakuló viszkózus réteget, amely — bizonyos talajtipusokon — a csatolás előfeltétele. A viszkózus réteg hatása levezethető a talajban fellépő erőhatás fázisviszonyaiból és a P-hullám vibrátornak a talajba juttatott aktív teljesítményéből. A tanulmány megvizsgálja, hogy milyen következményekkel járnak a vibrátor tulajdonságai a reflektált hullámok fázis- és amplitúdó-anomáliáinak megkülönböztetése szempontjából.

КАК ВЛИЯЮТ ТЕХНИЧЕСКИЕ ХАРАКТЕРИСТИКИ ВИБРАТОРА НА СЕЙСМИЧЕСКИЕ РЕЗУЛЬТАТЫ

Ганс А. К. ЭДЕЛЬМАН

В работе дается эмпирическое описание вязкого пласта под опорной плитой вибратора волн сжатия в качестве предпосылки связи при разных типах почв. Влияние такого вязкого пласта выводится из фазового поведения силы, действующей на грунт, и активной мощности, передаваемой в почву вибратором волн сжатия. Обсуждаются последствия поведения вибратора для выделения фазовых и амплитудных аномалий в сейсмических отражениях.

GEOPHYSICAL TRANSACTIONS 1987
Vol. 32. No. 4. pp.313–318

ERROR PROPAGATION FOR POTENTIAL FIELD DATA PROCESSING IN THE FREQUENCY DOMAIN

Marian IVAN*

The accuracy of gravity/magnetic data processing in the frequency domain is studied by assuming each observed value to be subject to a random error of standard deviation E. For a certain filter characteristic, the standard deviation of the final results is derived as a function of E, of the sampling interval and the number of field values used for computation. The accuracy of the upward continuation in the frequency domain at great elevations above the datum plane is also discussed. A magnetic model is used to illustrate the theoretical results.

Keywords: gravity field, magnetic field, frequency domain analysis, errors, standard deviation, upward continuation

1. Spectral algorithm

Classical formulae for data processing in the space domain allow direct evaluation of the accuracy of the final results as a function of the random errors added to the observed values [ROSENBACH 1953]. This paper presents similar results when the computations are based on filtering performed in the frequency domain.

A given pair of DFTs (discrete Fourier transforms) is defined [MESKÓ 1984] as

$$G_n = \sum_{k=0}^{N-1} g_k \exp(-ju_{kn}) \qquad k, n = 0, 1, \ldots, N-1 \qquad (1)$$

$$g_k = 1/N \sum_{n=0}^{N-1} G_n \exp(ju_{kn})$$

with

$$j = \sqrt{-1}, \qquad u_{kn} = 2\pi kn/N.$$

G denotes the direct DFT of the sampled field g at an interval s, N is the number of field values used for computation. Both direct and inverse DFTs can be computed with fast routines, their input and output include complex quantities with real (r_k, R_n) and imaginary (a_k, A_n) sets of coefficients.

* Geoph. Labs., University of Bucharest, Str. Traian Vuia 6, 70138 Bucharest 37, Romania
Manuscript received: 6 August, 1986

At the beginning, the input sets are initialized as

$$\begin{aligned} r_k &= g_k \\ a_k &= 0 \end{aligned} \qquad k = 0, 1, \ldots, N-1 \tag{2}$$

and the direct DFT is performed. The output of the routine is

$$R_n = \sum_{k=0}^{N-1} r_k \cos u_{kn}$$

and $$n = 0, 1, \ldots, N-1 \tag{3}$$

$$A_n = -\sum_{k=0}^{N-1} r_k \sin u_{kn}$$

Generally, a filter of characteristic coefficients

$$H_n + jI_n \qquad n = 0, 1, \ldots, N-1 \tag{4}$$

multiplies the complex signal represented by Eq. (3). The real and the imaginary part of the new signal are consequently

$$R_n^* = H_n R_n - I_n A_n$$

and $$n = 0, 1, \ldots, N-1 \tag{5}$$

$$A_n^* = H_n A_n + I_n R_n$$

respectively.

The inverse DFT is performed and the output gives the result of the filtering

$$r_k^* = 1/N \sum_{n=0}^{N-1} (R_n^* \cos u_{kn} - A_n^* \sin u_{kn}) \qquad k = 0, 1, \ldots, N-1 \tag{6}$$

By using Eqs. (2), (3) and (5), Eq. (6) becomes finally

$$r_k^* = 1/N \sum_{p=0}^{N-1} g_p \sum_{n=0}^{N-1} (H_n \cos v_{pnk} + I_n \sin v_{pnk}) \qquad k = 0, 1, \ldots, N-1 \tag{7}$$

where

$$v_{pnk} = 2\pi(p-k)n/N$$

2. Random errors

Let us suppose that each field value g_k is subject to a random error of standard deviation E. The Gaussian law of error propagation gives the standard deviation of Eq. (7) as

$$E_k^* = \sqrt{\sum_{p=0}^{N-1} (\partial r_k^*/\partial g_p)^2}\, E \qquad k = 0, 1, \ldots, N-1 \tag{8}$$

Differentiating Eq. (7) and taking into account the orthogonality of the

trigonometric functions involved, a final formula (which is independent of k) is obtained as

$$E^* = \sqrt{H_0^2 + 0.5 \sum_{k=1}^{N-1} (H_k^2 + I_k^2 + H_k H_{N-k} - I_k I_{N-k})}\, E/\sqrt{N} \tag{9}$$

In the case of some classical filters, the last formula can be simplified. For the analytical continuation to a level h above/under the datum plane, the filter coefficients in Eq. (4) are

$$H_n = \exp(-2\pi n h/s/N), \qquad I_n = 0 \qquad n = 0, 1, \ldots, N-1 \tag{10}$$

Here, negative values of h correspond to downward continuation. Then Eq. (9) becomes

$$E^* = \sqrt{1 + 0.5(N-1)\exp(Na/2) + 0.5[\exp(Na) - \exp(a)]/[\exp(a) - 1]}\, E/\sqrt{N} \tag{11}$$

with

$$a = -4\pi h/s/N \qquad h \neq 0$$

The formula corresponding to the horizontal derivative of the field is

$$E^* = \pi E/s/N \sqrt{(N-1)(N-2)/3} \tag{12}$$

Similar formulae can be derived in the cases of the first and second vertical derivative of the field. They are

$$E^* = \pi E/s \sqrt{(N-1)/N} \tag{13}$$

and

$$E^* = 2\pi^2 E/s^2 \sqrt{(N-1)(7N^3 - 8N^2 + 2N + 2)/15/N^2} \tag{14}$$

respectively.

Formula (9) can be extended to surface data processing (an $M \times N$ field values matrix) as

$$E^* = E/\sqrt{2MN} \times$$

$$\times \sqrt{H_{0,0}^2 - I_{0,0}^2 + \sum_{l=0}^{M-1} \sum_{k=0}^{N-1} (H_{l,k}^2 + I_{l,k}^2) + \sum_{l=0}^{M-1} \sum_{k=0}^{N-1} (H_{l,k} H_{M-l,N-k} - I_{l,k} I_{M-l,N-k})} \tag{15}$$

3. Numerical application

A magnetic noise was simulated with the aid of 64 values, (pseudo) randomly distributed in the range of -100 to 100 nT at a sampling interval of 20 m. The arithmetic mean of those values was rigorously set to zero because h approaching infinity in Eq. (10) makes all the filter coefficients vanish except H_0. From Eq. (7) one can conclude that the upward continued field in the frequency

domain does not vanish at great elevations above the datum plane. All its values approach the arithmetic mean of the input data *(Fig. 1)*.

The above noise was analytically continued in the frequency domain. *Figure 2* shows the good agreement of the results of that continuation with the values predicted by Eq. (11). High values of noise (in the range of − 11,500 to 12,900 nT) are obtained when the downward continuation is performed at 20 m below the datum plane (the predicted value is ± 10,300 nT). The necessity of using a smoothing filter is obvious in this case. Numerical tests have indicated the validity of Eqs. (12), (13) and (14).

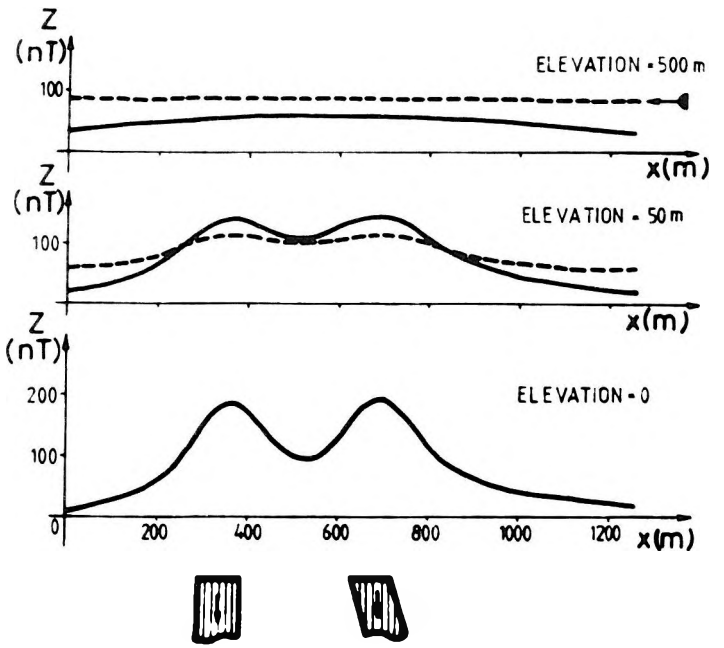

Fig. 1. Z component of the magnetic field (solid line) of two semi-infinite vertical magnetized dykes at different elevations above the datum plane. Dashed lines show the values obtained with the spectral algorithm. The arrow shows the arithmetic mean of the processed data. Sampling interval is 20 m, magnetization is 100 nT

1. ábra. Két félig-végtelen, függőleges mágnesezett telér mágneses terének *Z* komponense (folytonos vonal) a vonatkozási szint felett különböző magasságokban. A szaggatott vonal a spektrális algoritmussal kapott értékeket mutatja. A nyíl a feldolgozott adatok számtani középértékét jelzi. Mintavételi köz 20 m, a mágnesezettség 100 nT

Рис. 1. Вертикальная составляющая магнитного поля (сплошная линия) двух полу-бесконечных вертикальных намагниченных жил на разных высотах над основной плоскостью. Пунктиром показаны значения, полученные при помощи спектрального алгоритма. Стрелкой показана аритметическая средняя обработанных данных. Шаг квантования — 20 м, намагниченность — 100 нТ

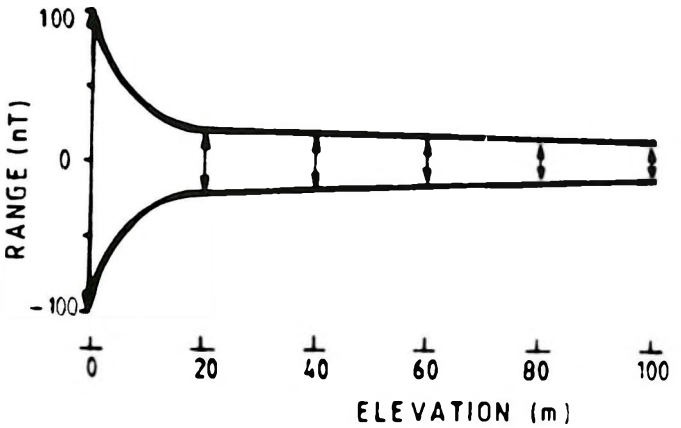

Fig. 2. Range of the upward continued noise at various elevations above the datum plane. Solid lines show the theoretical predicted values

2. ábra. A felső féltérbe folytatott zaj tartománya a vonatkozási szint felett különböző magasságokban. Folytonos vonalakkal jeleztük az elméletileg előre jelzett értékeket

Рис. 2. Диапазон продолженного вверх шума на разных высотах над основной плоскостью. Сплошной линией показаны теоретически предсказанные значения

4. Conclusions

It is possible to predict quantitatively the impact of random errors on the final results of potential field data processing in the frequency domain. In some cases, smoothing filters are necessary to obtain stable results [BULLARD and COOPER 1948, GRANT and WEST 1965, IANĂŞ and MOLDOVEANU 1974, MESKÓ 1984]. The transfer function for such filters depends generally on an unknown parameter. Equation (9) suggests a possibility for choosing that value by keeping the errors within a certain range.

Erroneous results are obtained when the upward continuation is performed in the frequency domain at great elevations above the datum plane. It is useful to compare the continued values with arithmetic mean of the processed data as a means of estimating the accuracy of the results. A number of techniques designed to minimize the edge effects and the finite number of observation points are expected to improve that accuracy [CORDELL and GRAUCH 1982, IVAN 1986].

REFERENCES

Bullard E. C., Cooper R. I. B. 1948: Determination of the masses necessary to produce a given gravitational field. Proc. Roy. Soc. A 194, pp. 332–347

Cordell L., Grauch V. J. S. 1982: Reconciliation of the discrete and integral Fourier transforms. Geophysics **47**, 2. pp. 237–243

Grant F. S., West G. F. 1965: Interpretation theory in applied geophysics. McGraw-Hill, New York

Ianăș M., Moldoveanu N. 1974: The stability of the solutions of the potential field transformations. Geophys. Prosp. **22**, 1. pp. 143–152

Ivan M. 1986: On the upward continuation of potential field data between irregular surfaces. Geophys. Prosp. **34**, 5. pp. 735–742

Mesko A. 1984: Digital Filtering: Applications in Geophysical Exploration for Oil. Akadémiai Kiadó, Budapest, 636 p.

Rosenbach O. 1953: A contribution to the computation of the "Second derivative" from gravity data. Geophysics **18**, 4. pp. 894–912

HIBATERJEDÉS POTENCIÁLTÉR-ADATOK FREKVENCIATARTOMÁNYBELI FELDOLGOZÁSÁNÁL

Marian IVAN

Gravitációs és mágneses adatok frekvenciatartományban végzett feldolgozásának pontosságát úgy vizsgáltuk, hogy minden észlelt értéket a normál eltérés E véletlenszerű hibájával terheltnek tekintettünk. Egy bizonyos szűrőkarakterisztikára vonatkozóan a végleges eredmények normál eltérése az E, a mintavételi köz és a számításhoz felhasznált tér-értékek száma függvényeként vezethető le. Példaként tárgyaljuk frekvenciatartományban a felső féltérbe való folytatás pontosságát, a vonatkozási szint feletti nagy magasságokon. Az elméleti eredményeket mágneses modellen szemléltetjük.

ОЦЕНКА ОШИБОК ПРИ ОБРАБОТКЕ ДАННЫХ ПО ПОЛЯМ ПОТЕНЦИАЛОВ В ЧАСТОТНОЙ ОБЛАСТИ

Мариан ИВАН

Точность обработки в частотной области гравиразведки и магниторазведки данных изучается при предположении, что каждое наблюденное значение несет случайную ошибку E нормального отклонения. Для некоторой характеристики фильтра нормальное отклонение окончательных результатов может быть выведено как функция E, шага квантования и количества использованных для расчета значений поля. Кроме того, обсуждается точность продолжения в верхнее полупространство в частотной области на больших высотах над основной плоскостью. Приводится магнитная модель для иллюстрации теоретических результатов.

GEOPHYSICAL TRANSACTIONS 1987
Vol. 32. No. 4. pp.319–332

THE INTERPRETATION OF RESISTIVITY SOUNDING OVER WEATHERED ROCKS

L. ZIMA*

Exponentially increasing resistivity with depth is supposed for a layer of weathered rocks (transitional layer). For this case a simple recursive formula has been developed for computing the resistivity transform function. The resistivity transform function for sections containing transitional layers and layers of constant resistivity can easily be calculated by combining the formula in question with the well-known recursive formula for layers of constant resistivity. Resistivity sounding curves can be obtained by digital convolution of the resistivity transform function with a set of filter coefficients. Interpretation of field curves is difficult and has to be based on a certain model of a resistivity section. A combination of numerical and graphical methods in resistivity transform domain is suggested for the interpretation. Examples of the interpretation from a metamorphic rock area are given. Obtained results are discussed and compared with drilling and seismic data.

Keywords: resistivity sounding, weathered rocks, transitional layer, interpretation

1. Introduction

When one interprets resistivity sounding measurements, one supposes horizontally stratified earth. The layers have different but constant resistivity and they can be considered as resistivity uniform or homogeneous layers. However, in some cases the resistivity varies, more or less continuously, in a certain direction in the layer. Such layers may be regarded as transitional layers.

Many authors have presented theoretical solutions for the potential of direct current source in the case of continuously varying conductivity or resistivity with depth. The solutions of SLICHTER [1933] and SUNDE [1949] belong to the oldest works. A three-layer model where the second layer has a linear variation of conductivity with depth was considered by MALLICK and ROY [1968] and by JAIN [1972]. Various other models with linear, exponential, power law or more complicated dependences of resistivity or conductivity with depth have been studied, for example, by LAL [1970], PAUL and BANERJEE [1970], STOYER and WAIT [1977], MALLICK and JAIN [1979], BANERJEE et al. [1980a, b]. KOEFOED [1979a] derived a recursive formula for the resistivity transform function in layers in which resistivity varies linearly with depth. Some practical results in the interpretation of sections containing transitional layers were obtained by PATELLA [1977, 1978] and especially by MUNDRY and ZSCHAU [1983].

* GEOFYZIKA n. p. Brno, Geologická 2, 152 00 Prague 5, Czechoslovakia
Paper presented at the 47th meeting of the EAEG, 4–7 June, 1985, Budapest, Hungary

The zone of weathered rock is a characteristic example of a transitional layer. Weathered rock in situ often exhibits a typical transition from quite decomposed rock through partly weathered and jointed rock to unweathered rock [OLLIER 1969]. Because the resistivity of rock depends on the intensity of weathering, we may observe a continuous increase of resistivity with depth [DORTMAN 1976, MALLICK and ROY 1968, STÖTZNER 1975]. This fact has to be taken into account when interpreting the resistivity sounding measurements over weathered rocks. The exact quantitative expression for the resistivity/depth relationship is very difficult to find. The most suitable approximations are in the form of a linear or exponential function; the latter is used in this study.

2. Theory

The differential equation for the electric potential V of a direct current source in a medium with conductivity σ may be written as [GRANT and WEST 1965]

$$\nabla \cdot (\sigma \nabla V) = 0 \tag{1}$$

If the resistivity $\varrho = \frac{1}{\sigma}$ varies with depth, i.e. $\varrho = \varrho(z)$, we obtain

$$\nabla^2 V - \frac{1}{\varrho(z)} \frac{\partial \varrho(z)}{\partial z} \frac{\partial V}{\partial z} = 0 \tag{2}$$

The current source is placed at the origin of the coordinate system. In cylindrical coordinates according to the symmetry with respect to the z-axis, equation (2) becomes

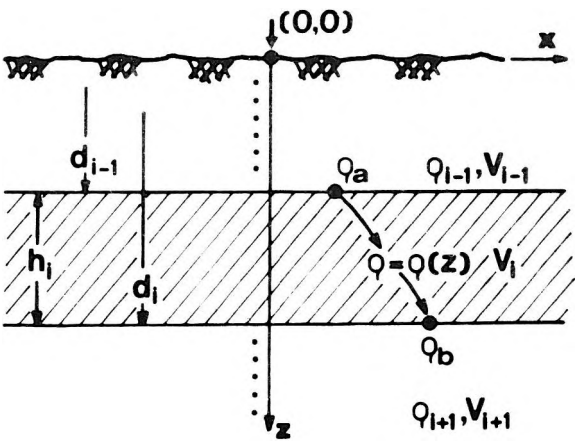

Fig. 1. Model of transitional layer

1. ábra. Az átmeneti réteg modellje

Рис. 1. Модель переходного слоя

$$\frac{\partial^2 V}{\partial r^2} + \frac{1}{r}\frac{\partial V}{\partial r} + \frac{\partial^2 V}{\partial z^2} - \frac{1}{\varrho(z)}\frac{\partial \varrho(z)}{\partial z}\frac{\partial V}{\partial z} = 0 \tag{3}$$

For horizontally stratified earth with layers each having constant resistivity, equation (3) is reduced to Laplace's equation. Its solution by separation of variables gives us an expression for the potential in the i-th homogeneous layer

$$V_i(r, z) = \int_0^\infty [A_i(\lambda)\mathrm{e}^{-\lambda z} + B_i(\lambda)\mathrm{e}^{\lambda z}]J_0(\lambda r)\,\mathrm{d}\lambda \tag{4}$$

where $J_0(\lambda r)$ is a Bessel function of the first kind and zero order, λ is the separation constant, and $A_i(\lambda)$, $B_i(\lambda)$ are functions to be determined from the boundary conditions for the potential.

Potential in the transitional layer

Let us consider that in the i-th layer (*Fig. 1*) resistivity exponentially varies with depth

$$\varrho(z) = \varrho_a \mathrm{e}^{\alpha(z - d_{i-1})}, \qquad d_{i-1} \le z \le d_i \tag{5}$$

On the upper boundary of this layer ($z = d_{i-1}$) $\varrho(z) = \varrho_a$; on the lower boundary of the i-th layer $\varrho(z) = \varrho_b$ and then α from (5) becomes

$$\alpha = \frac{\ln \dfrac{\varrho_b}{\varrho_a}}{d_i - d_{i-1}} = \frac{\ln \dfrac{\varrho_b}{\varrho_a}}{h_i} \tag{6}$$

where h_i is the thickness of the layer. In our case resistivity increases with depth in this transitional layer ($\varrho_b > \varrho_a$) and thus $\alpha > 0$. Substituting (5) into (3) we obtain

$$\frac{\partial^2 V}{\partial r^2} + \frac{1}{r}\frac{\partial^2 V}{\partial r^2} + \frac{\partial^2 V}{\partial z^2} - \alpha\frac{\partial V}{\partial z} = 0 \tag{7}$$

This equation may be solved by separation of variables $V(r, z) = R(z)Z(z)$. Then (7) results in two equations

$$\frac{\mathrm{d}^2 R}{\mathrm{d}r^2} + \frac{1}{r}\frac{\mathrm{d}R}{\mathrm{d}r} + \lambda^2 R = 0 \tag{8}$$

and

$$\frac{\mathrm{d}^2 Z}{\mathrm{d}z^2} - \alpha\frac{\mathrm{d}Z}{\mathrm{d}z} - \lambda^2 Z = 0 \tag{9}$$

The solution of (8) satisfying the far-source condition for the potential is $J_0(\lambda r)$. Equation (9) is a linear differential equation the solution of which is

$$Z(z) = E(\lambda)e^{vz} + F(\lambda)e^{wz} \tag{10}$$

where

$$v = \frac{\alpha + \sqrt{\alpha^2 + 4\lambda^2}}{2}; \qquad w = \frac{\alpha - \sqrt{\alpha^2 + 4\lambda^2}}{2} \tag{11}$$

A general solution of (7) can be written in the form

$$V_i(r, z) = \int_0^{\infty} [E_i(\lambda)e^{vz} + F_i(\lambda)e^{wz}]J_0(\lambda r)\,d\lambda \tag{12}$$

where $V_i(r, z)$ is the potential in the i-th transitional layer.

Boundary conditions

Let us suppose that the transitional layer is embedded between two homogeneous layers. The potential in the homogeneous layer is equal to the potential in the transitional layer at the boundary between them; the same applies to normal components of current density. On the upper boundary of the transitional layer at $z = d_{i-1}$ according to (4) and (12) we obtain

$$A_{i-1}(\lambda)e^{-\lambda d_{i-1}} + B_{i-1}(\lambda)e^{\lambda d_{i-1}} = E_i(\lambda)e^{vd_{i-1}} + F_i(\lambda)e^{wd_{i-1}} \tag{13}$$

$$\frac{1}{\varrho_{i-1}}[-\lambda A_{i-1}(\lambda)e^{-\lambda d_{i-1}} + \lambda B_{i-1}(\lambda)e^{\lambda d_{i-1}}] = \frac{1}{\varrho_a}[vE_i(\lambda)e^{vd_{i-1}} + wF_i(\lambda)e^{wd_{i-1}}] \tag{14}$$

On the lower boundary of the transitional layer ($z = d_i$), under the same conditions it holds that

$$E_i(\lambda)e^{vd_i} + F_i(\lambda)e^{wd_i} = A_{i+1}(\lambda)e^{-\lambda d_i} + B_{i+1}(\lambda)e^{\lambda d_i} \tag{15}$$

$$\frac{1}{\varrho_b}[vE_i(\lambda)e^{vd_i} + wF_i(\lambda)e^{wd_i}] = \frac{1}{\varrho_{i+1}}[-\lambda A_{i+1}(\lambda)e^{-\lambda d_i} + \lambda B_{i+1}(\lambda)e^{\lambda d_i}] \tag{16}$$

We divide both sides of (13) and (15) by the corresponding sides of (14) and (16). The following equations are the result

$$\varrho_{i-1}\frac{A_{i-1}(\lambda) + B_{i-1}(\lambda)e^{2\lambda d_{i-1}}}{A_{i-1}(\lambda) - B_{i-1}(\lambda)e^{2\lambda d_{i-1}}} = \lambda\varrho_a\frac{-E_i(\lambda) - F_i(\lambda)e^{d_{i-1}(w-v)}}{vE_i(\lambda) + wF_i(\lambda)e^{d_{i-1}(w-v)}} \tag{17}$$

$$\lambda\varrho_b\frac{-E_i(\lambda) - F_i(\lambda)e^{d_i(w-v)}}{vE_i(\lambda) + wF_i(\lambda)e^{d_i(w-v)}} = \varrho_{i+1}\frac{A_{i+1}(\lambda) + B_{i+1}(\lambda)e^{2\lambda d_i}}{A_{i+1}(\lambda) - B_{i+1}(\lambda)e^{2\lambda d_i}} \tag{18}$$

Now we introduce the function $T_{i+1}(\lambda)$ which is equal to the right-hand side of (18). This function represents the ratio of the potential to the normal component of current density and it is called the resistivity transform function [MATVEEV 1974, KOEFOED 1979b]. Following KOEFOED's [1979a] logical deduction it is possible to equate the right-hand side of (17) with $T_i(\lambda)$. Through solving (17)

for the ratio $E_i(\lambda)/F_i(\lambda)$ and substituting this into the left-hand side of (18) we obtain the relation between $T_i(\lambda)$ and $T_{i+1}(\lambda)$ for the transitional layer. It follows from (11) that $vw = -\lambda^2$ and after some manipulations we obtain

$$T_{i+1}(\lambda) = \varrho_b \frac{T_i(\lambda)\,[v - we^{-h_i(w-v)}] + \lambda\varrho_a[1 - e^{-h_i(w-v)}]}{\lambda T_i(\lambda)\,[1 - e^{-h_i(w-v)}] - \varrho_a[w - ve^{-h_i(w-v)}]} \tag{19}$$

The solution of this equation for $T_i(\lambda)$ can be written as

$$T_i(\lambda) = \varrho_a \frac{T_{i+1}(\lambda)\,[w - ve^{-h_i(w-v)}] + \lambda\varrho_b[1 - e^{-h_i(w-v)}]}{\lambda T_{i+1}(\lambda)\,[1 - e^{-h_i(w-v)}] - \varrho_b[v - we^{-h_i(w-v)}]} \tag{20}$$

If $\varrho_a = \varrho_b = \varrho_i$ then after substitution $v = -\lambda$ and $w = +\lambda$ (choice after (11)) we obtain

$$T_{i+1}(\lambda) = \varrho_i \frac{T_i(\lambda)\,[1 + e^{-2\lambda h_i}] - \varrho_i[1 - e^{-2\lambda h_i}]}{\varrho_i[1 + e^{-2\lambda h_i}] - T_i(\lambda)\,[1 - e^{-2\lambda h_i}]} \tag{21}$$

and

$$T_i(\lambda) = \varrho_i \frac{T_{i+1}(\lambda)\,[1 + e^{-2\lambda h_i}] + \varrho_i[1 - e^{-2\lambda h_i}]}{\varrho_i[1 + e^{-2\lambda h_i}] + T_{i+1}(\lambda)\,[1 - e^{-2\lambda h_i}]} \tag{22}$$

which are known recursive relations for the resistivity transform function in the case of a homogeneous layer [KOEFOED 1979b].

Calculation and transformation of sounding curves

The relation for the apparent resistivity $\varrho_a(r)$ can be derived from the expression for the potential on the earth's surface. For Schlumberger array we have [GHOSH 1971a]

$$\varrho_a(r) = r^2 \int_0^\infty T_1(\lambda) J_1(\lambda r)\lambda\,\mathrm{d}\lambda \tag{23}$$

The resistivity transform $T_1(\lambda)$ can easily be calculated by means of recursive relations which were presented above. For the homogeneous layer we use relation (22) and for the transitional layer equation (20). Calculation starts from last layer ($T_n(\lambda) = \varrho_n$) and proceeds through individual layers upwards using the values of $1/\lambda = AB/2 = r$. Thus the resistivity section composed from homogeneous and transitional layers can be calculated in this way. Calculation of $\varrho_a(r)$ presents no problem because (23) can be converted into digital convolution [GHOSH 1971b]

$$\varrho_a^{(m)}(r) = \sum_j d^{(j)} T_1^{(m-j)}(\lambda); \qquad m = 0, 1, 2, \ldots \tag{24}$$

where $d^{(j)}$ are inverse filter coefficients.

Further it is possible to express the resistivity transform function $T_1(\lambda)$ from (23) by Hankel transformation. Again in digital form it becomes

$$T_1^{(m)}(\lambda) = \sum_j c^{(j)} \varrho_a^{(m-j)}(r); \qquad m = 0, 1, 2, \ldots \tag{25}$$

where $c^{(j)}$ are forward filter coefficients. Applying (25) to the measured field values $\varrho_a(r)$ we obtain resistivity transform curve $T_1(\lambda)$. Recursive relations (19) and (21) may be used for reduction to a lower boundary plane [KOEFOED 1979b]. It means that we "remove" the upper layer the parameters of which are known. In this manner we may go down to the last layer $(T_n(\lambda) = \varrho_n)$.

Although it could be of great interest to examine in details the transfer of errors of the measured $\varrho_a(r)$ curve to the $T_1(\lambda)$ curve, this is beyond the scope of this paper.

Recursive relations (19), (20), (21) and (22) can easily be programmed on a pocket calculator (e.g. HP 67). Such a calculator could also be used to calculate the $\varrho_a(r)$ curve and to transform the resistivity curve. As a suitable set of coefficients, that of NYMAN and LANDISMAN [1977] may be used; it consists of 13 coefficients with an optimum sampling rate of 4.438 points per decade. The calculation time needed for interpreting one sounding curve is about 15–30 minutes using a HP 67.

3. Interpretation of sounding curves over weathered rocks

It is obvious from the preceding part that there is no problem in calculating the resistivity sounding curve for sections with homogeneous and transitional layers. In contrast, it is not so easy to interpret the measured field curve. The first important step in the interpretation procedure is to introduce the geological model. In our case the model has three main parts: surface layer of homogeneous resistivity (or layers), weathered rock (transitional layer) and unweathered rock with constant resistivity. The necessity for this geological–geophysical approach is illustrated in *Fig. 2*. The measured curve may be interpreted (within given limits of accuracy) in terms of at least three equivalent models with different geological meanings. If we suppose the existence of weathered rock, then model 3 is most acceptable. We use this model to interpret similar sounding curves in the given area.

At present, many interpretation techniques exist. One of them is the interpretation in the resistivity transform domain, which utilizes recursive relation for the succesive "removal" of upper layers [KOEFOED 1979b]. This method is particularly important in our case because it enables us to reduce the measured curve on the surface of the transitional. A combined graphical and numerical method of interpretation has been elaborated consisting of the following.

The measured curve $\varrho_a(r)$ is first transformed into curve $T_1(\lambda)$ by means of relation (25). The resistivity and thickness of the first layer are determined graphically by two-layer master curves (in the $\varrho_a(r)$ or $T_1(\lambda)$ domain). The curve

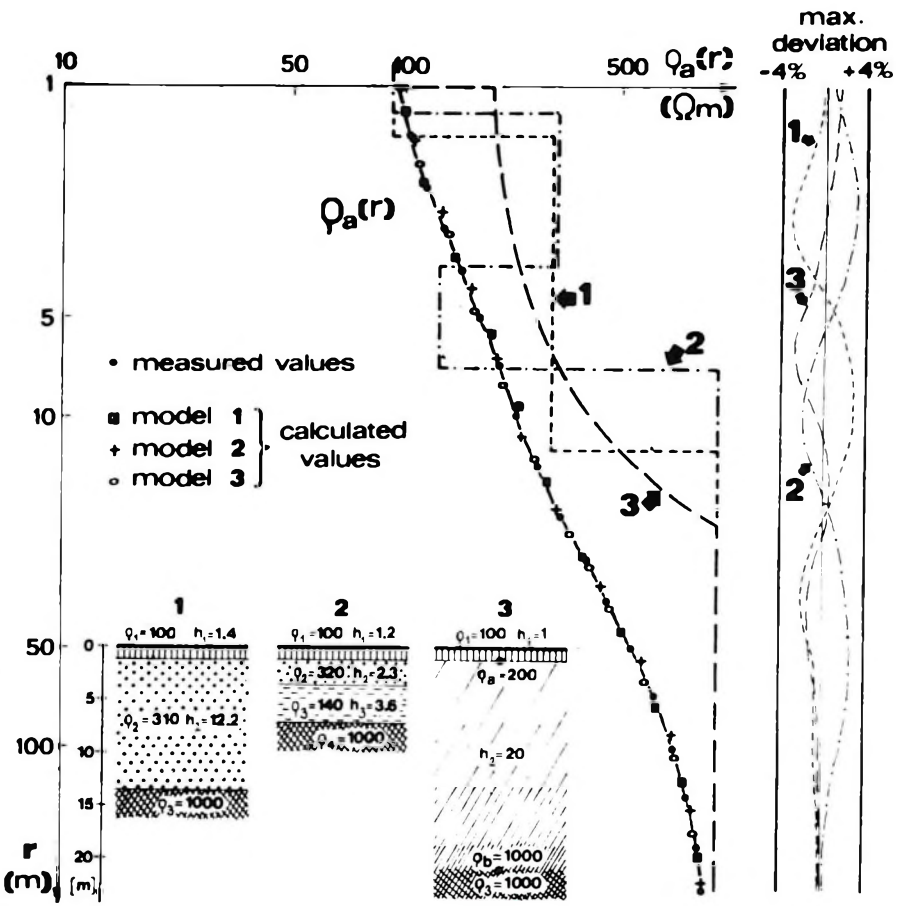

Fig. 2. Equivalent models with different geological approach of interpretation

2. ábra. Ekvivalens modellek az értelmezésre vonatkozó különböző földtani elképzelésekkel

Рис. 2. Эквивалентные модели с разными геологическими подходами к интерпретации

is then reduced downwards (21), i.e. we "remove" the first layer. If the overburden is composed of more homogeneous layers we repeat this procedure until we reach the surface of weathered rock. This moment may be recognized, for example, from seismic measurements, drilling data, or from characteristic features of the curve. Thus we have obtained a sounding curve "measured" directly on the surface of weathered rock. The asymptotic behaviour of the curve determines resistivities ϱ_a and ϱ_b. Exponentially increasing resistivity with depth is supposed between these two values. In order to determine the thickness of the transitional layer it is possible to use a precalculated set of master curves $T_1(\lambda)$ for the three-layer model with a transitional second layer (variable ϱ_b/ϱ_a and

constant h_2/h_1). There may be several such sets for suitable ratios h_2/h_1 and on comparing the reduced curve with these we obtain h_2.

Another method for the approximate determination of the thickness of the transitional layer uses longitudinal conductance S. The decrease in conductance S_g with depth in the transitional layer may be expressed as

$$dS_g = \frac{dz}{\varrho(z)} \tag{26}$$

After substituting relation (5) for $\varrho(z)$ and in consequence of (6), integrating (26) from d_{i-1} to d_i gives

$$S_g = \frac{h_i}{\varrho_a \varrho_b} \frac{\varrho_b - \varrho_a}{\ln \frac{\varrho_b}{\varrho_a}} \tag{27}$$

The resistivities ϱ_a, ϱ_b are known and S_g may be determined by subtracting the longitudinal conductances $S_1 = h_1/\varrho_1$, $S_2 = h_2/\varrho_2$, ... from the total conductance S. The total conductance can be defined graphically by means of two-layer master curves [KELLER and FRISCHKNECHT 1970, MATVEEV 1974]. Thus

$$h_i = \varrho_a \varrho_b \frac{\ln \frac{\varrho_b}{\varrho_a}}{\varrho_b - \varrho_a} [S - (S_1 + S_2 + \ldots)] \tag{28}$$

The final step is to calculate the sounding curve ($T_1(\lambda)$ or $\varrho_a(r)$) for interpreted parameters of the whole section, comparing the calculated curve with the measured curve. Interpretation is complete when the calculated and measured curves coincide. If there is some discrepancy, interpretation should be repeated after modifying the resistivities and thicknesses.

4. Practical examples

Some results obtained from interpreting sounding curves from metamorphic rock area in SE Bohemia are presented. Biotite paragneiss is the dominating rock in this area; it is mostly covered with unconsolidated sediments (sand, gravel, clay) of small thickness. Fractured zones and deeply weathered parts of gneiss are suitable places for migration and accumulation of ground water. Resistivity sounding (Schlumberger array) in combination with shallow refraction seismics were used for determining depth and intensity of weathering and the VLF method was used for searching for linear zones of fractured rocks.

An example of the interpretation of a resistivity sounding curve near a well is shown in *Fig. 3*. Sands and gravel-sands with resistivity of 460 Ωm are deposited under the surface soil. The upper part of the bedrock consists of quite decomposed weathered gneiss (sand-clay eluvium) which has a resistivity of

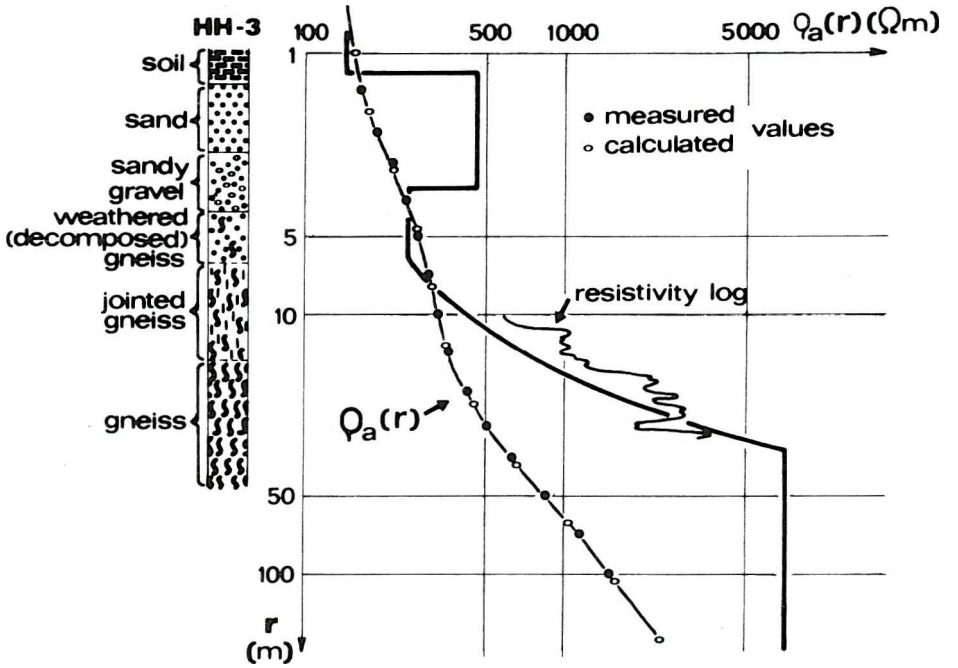

Fig. 3. Example of interpretation of resistivity sounding curve near a well and comparison with resistivity log

3. ábra. Példa fúrólyuk közelében nyert ellenállás-szondázási görbe kiértékelésére és az eredmény összehasonlítása a lyukban felvett ellenállás-szelvénnyel

Рис. 3. Пример интерпретации кривой зондирования по методу сопротивления вблизи скважины и ее сопоставление с каротажной диаграммой сопротивления

about 250 Ωm. Successive transition through strongly jointed weathered parts into slightly jointed and compact gneiss appears lower. It is characterized by increasing resistivity with depth. The interpretation of weathered rock as a transitional layer corresponds well with the resistivity log curve.

It is known that in weathered rock the seismic velocity is lower than in compact rock. Thus the weathered rock zone may be regarded as a velocity transitional layer too [DORTMAN 1976]. This problem was studied by SKOPEC and HRÁCH [1976]. They elaborated a special interpretation procedure for determining the distribution of velocities of seismic waves at various depths. *Figure 4* demonstrates a comparison of their results with the interpretation of resistivity sounding measurements. The unconsolidated overburden with a thickness of 2.4 m has a velocity of 300 m/s and a resistivity of 330 Ωm. Strongly weathered gneiss has a surface velocity of 1400 m/s and a resistivity of 460 Ωm. In the downgoing direction both resistivity and seismic velocity increase. Even at depths of 5–7 m gneiss may still be considered as weathered rock (2000 m/s, 500–600 Ωm).

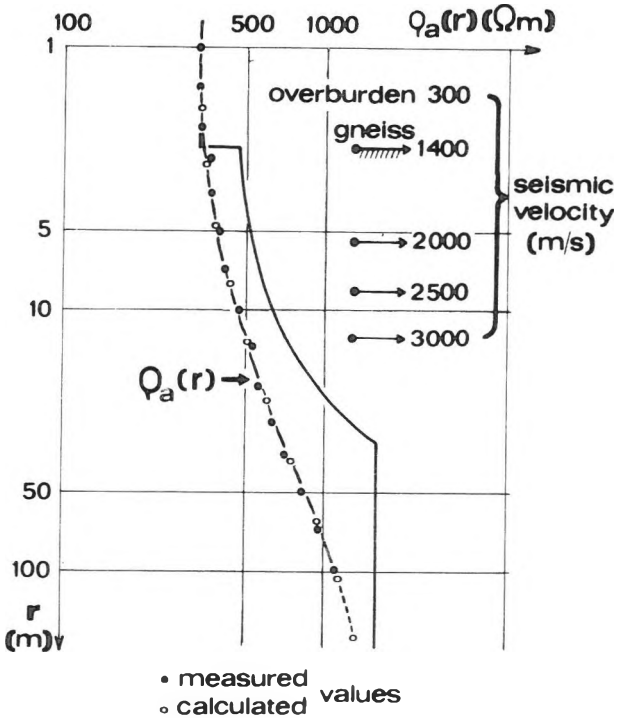

Fig. 4. The results of interpretation of resistivity and seismic measurements

4. ábra. Az ellenállásmérések és a szeizmikus mérések kiértékelésének eredménye

Рис. 4. Результаты интерпретации кривых сопротивления и данных сейсморазведки

Joint interpretation of resistivity and seismic measurements was carried out at many places in the given area. Comparison of interpreted resistivities and seismic velocities in weathered gneiss with respect to drilling results is summarized in *Fig. 5*. This figure enables one to approximate by estimate the weathering intensity on the basis of resistivities and seismic velocities.

In the lower part of *Fig. 6* an interpretation of resistivity sounding measurements along profile A–A′ is shown. High resistivities at small depth were found at sounding points Nos. 9–13. From Fig. 5 we may deduce the occurrence of compact or only slightly jointed gneiss under the overburden.

Another situation is at soundings Nos. 7 and 8 in the western part of the profile. Low resistivities on the surface of gneiss and relatively slow increase in their values with depth offers evidence of the presence of strongly weathered gneiss. The conductivity anomaly of the VLF method is also situated in this part of the profile (see upper part of Fig. 6). The anomalous VLF zone can be followed on several profiles and it is caused by fractured and weathered gneiss. It is also obvious that the ground-water well situated in this zone has five times higher specific yield than the other well localized outside this zone.

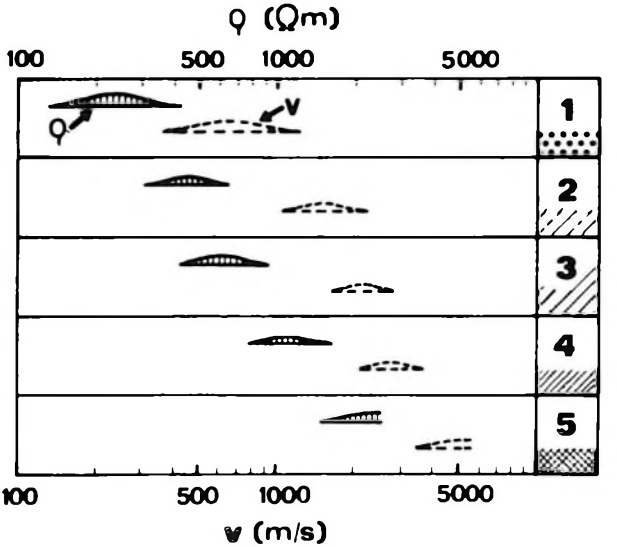

Fig. 5. Approximate estimation of gneiss weathering on the basis of resistivities and velocities
1 — decomposed gneiss (sand–clay eluvium); 2 — weathered gneiss; 3 — slightly weathered, strongly jointed gneiss; 4 — slightly jointed gneiss; 5 — compact gneiss

5. ábra. A gneisz mállottságának becslése, fajlagos ellenállások és sebességek alapján:
1 — teljesen bontott gneisz (homokos–agyagos eluvium); 2 — mállott gneisz; 3 — gyengén mállott, erősen repedezett gneisz; 4 — gyengén repedezett gneisz; 5 — tömör gneisz

Рис. 5. Приблизительная оценка выветривания гнейсов на основании сопротивлений и скоростей
1 — совершенно разложенные гнейсы (песчано–глинистый элювий); 2 — выветрелые гнейсы; 3 — слабо выветрелые, сильно трещиноватые гнейсы; 4 — слабо трещиноватые гнейсы; 5 — массивные гнейсы

5. Conclusions

A simple recursive formula for computing the resistivity transform function has been developed for transitional layers with exponential increase in resistivity with depth. A graphical–numerical method for interpreting resistivity soundig curves has been suggested. The method is based on interpreting the resistivity transform domain which opens the way to reducing the resistivity transform curve towards the surface of weathered rock. As has been demonstrated by practical examples, the assumption that the weathered rock may be approximated by a transitional layer corresponds better to reality.

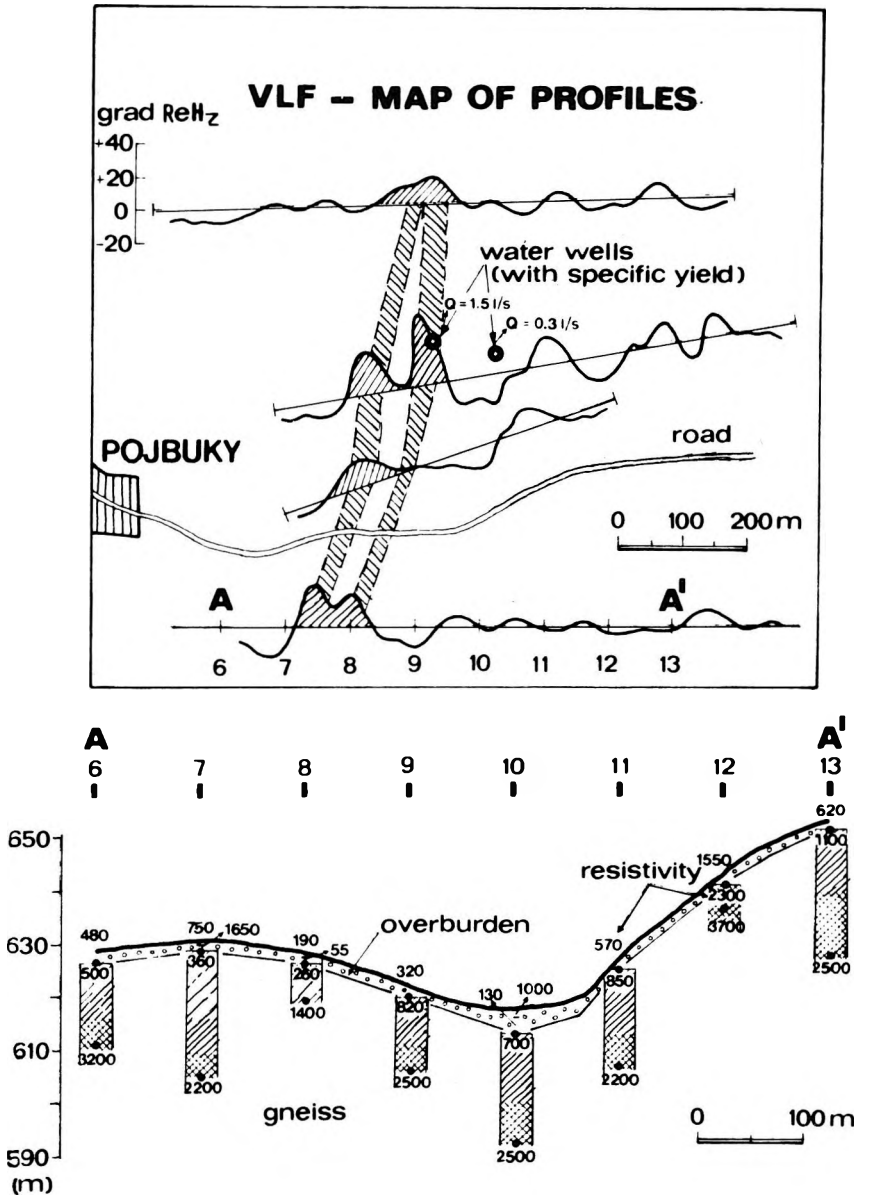

Fig. 6. Results of resistivity sounding (lower part) and VLF measurements (upper part) at Pojbuky locality. North is at the top of the map

6. ábra. Az ellenállás-szondázások (alul) és VLF mérések (felül) eredménye Pojbuky közelében. A térkép É-felé van tájolva

Рис. 6. Результаты зондирований методом сопротивления (внизу) и измерений методом СДВР (вверху) — участок Пойбуки. Север — вверх по карте

REFERENCES

BANERJEE B., SENGUPTA B. J. and PAL B. P. 1980a: Apparent resistivity of a multilayered earth with a layer having exponentiality varying conductivity. Geophysical Prospecting **28**, 3, pp. 435–452

BANERJEE B., SENGUPTA B. J. and PAL B. P. 1980b: Resistivity sounding on a multilayered earth containing transition layers. Geophysical Prospecting **28**, 5, pp. 750–758

DORTMAN N. B. 1976: Physical Properties of Rocks (in Russian). Nedra, Moscow

GHOSH D. P. 1971a: The application of linear filter theory to the direct interpretation of geoelectrical resistivity sounding measurements. Geophysical Prospecting **19**, 2, pp. 192–217

GHOSH D. P. 1971b: Inverse filter coefficients for the computation of apparent resistivity standard curves for a horizontally stratified earth. Geophysical Prospecting **19**, 4, pp. 769–775

GRANT F. S. and WEST G. F. 1965: Interpretation Theory in Applied Geophysics. McGraw-Hill Book Co., New York, 583 p.

JAIN S. C. 1972: Resistivity sounding on a three-layer transitional model. Geophysical Prospecting **20**, 2, pp. 283–292

KELLER G. V. and FRISCHKNECHT F. C. 1970: Electrical Methods in Geophysical Prospecting. Pergamon, Oxford, 519 p.

KOEFOED O. 1979a: Resistivity sounding on an earth model containing transition layers with linear change of resistivity with depth. Geophysical Prospecting **27**, 4, pp. 862–868

KOEFOED O. 1979b: Geosounding Principles, 1. Resistivity Sounding Measurements. Elsevier, Amsterdam, 276 p.

LAL T. 1970: Apparent resistivity over a three-layer earth with an inhomogeneous interstratum. Pure and Applied Geophysics **82**, pp. 259–269

MALLICK K. and ROY A. 1968: Resistivity sounding on a two-layer earth with transitional boundary. Geophysical Prospecting **16**, 4, pp. 436–446

MALLICK K. and JAIN S. 1979: Resistivity sounding on a layered transitional earth. Geophysical Prospecting **27**, 4, pp. 869–875

MATVEEV B. K. 1974: Interpretation of Electromagnetic Soundings (in Russian). Nedra, Moscow

MUNDRY E. and ZSCHAU H.-J. 1983: Geoelectrical models involving layers with a linear change in resistivity and their use in the investigation of clay deposits. Geophysical Prospecting **31**, 5, pp. 810–828

NYMAN D. C. and LANDISMAN M. 1977: VES dipole-dipole filter coefficients. Geophysics **42**, 5, pp. 1037–1044

OLLIER C. 1969: Weathering. Edinburgh

PATELLA D. 1977: Resistivity sounding on a multi-layered earth with transitional layers. Part I: Theory. Geophysical Prospecting **25**, 4, pp. 699–729

PATELLA D. 1978: Resistivity sounding on a multi-layered earth with transitional layers. Part II: Theoretical and field examples. Geophysical Prospecting **26**, 1, pp. 130–156

PAUL M. K. and BANERJEE B. 1970: Electrical potentials due to a point source upon models of continuously varying conductivity. Pure and Applied Geophysics **80**, pp. 218–237

SKOPEC J. and HRÁCH S. 1976: Interpretation of a medium with vertical velocity gradient by means of difference curves (in Czech). Acta Universitatis Carolinae, Geologica **4**, pp. 295–308

SLICHTER L. B. 1933: The interpretation of the resistivity prospecting method for horizontal structures. Physics **4**, pp. 307–322

STÖTZNER U. 1975: Ingenieurgeophysikalische Untersuchungsmethodik und Komplexinterpretation zur Lösung felsmechanischer Aufgaben. Freiberger Forschungshefte C-307, Leipzig, 114 p.

STOYER C. H. and WAIT J. R. 1977: Resistivity probing of an "exponential" earth with a homogeneous overburden. Geoexploration **15**, 1, pp. 11–18

SUNDE E. D. 1949: Earth Conduction Effects in Transmission Systems. D. Van Nostrand Co., New York

MÁLLOTT KŐZETEKEN VÉGZETT ELLENÁLLÁS-SZONDÁZÁS KIÉRTÉKELÉSE

L. ZIMA

A mélységgel exponenciálisan növekvő ellenállásról feltételezzük, hogy az mállott kőzeteken álló (átmeneti) réteget jelez. Erre az esetre egy egyszerű rekurzív képletet vezettünk le, a fajlagos ellenállás transzformációs függvényének kiszámításához. Ez a függvény könnyen kiszámítható változó és állandó ellenállású rétegeket tartalmazó szelvényre, a tárgyalt képlet és az állandó fajlagos ellenállású rétegekre kidolgozott, ismert rekurzív képlet összekapcsolása útján. Az ellenállás-szondázási görbe megkapható az ellenállás transzformációs függvény és szűrőegyüttható digitális konvolúciójával. A terepi görbék kiértékelése nehéz és egy feltételezett fajlagos ellenállás-modellen kell alapulnia. A kiértékeléshez numerikus és grafikus módszerek kombinációját javasoljuk, a fajlagos ellenállás transzformációs tartományában. Kiértékelési példát mutatunk be metamorf kőzetek területéről. Ismertetjük az eredményeket és összehasonlítjuk ezeket a fúrási és szeizmikus adatokkal.

ИНТЕРПРЕТАЦИЯ КРИВЫХ ЗОНДИРОВАНИЯ МЕТОДОМ СОПРОТИВЛЕНИЯ В ВЫВЕТРЕЛЫХ ПОРОДАХ

Л. ЗИМА

Сопротивление, возрастающее с глубиной по экспоненциальному закону, предположительно является признаком наличия (переходной) зоны выветрелых пород. Для этого случая была разработана простая рекурсивная формула с целью вычисления функции преобразования сопротивления. Функция преобразования сопротивления может быть легко вычислена для разрезов, состоящих их переходных слоев и слоев постоянного удельного сопротивления, путем сочетания обсуждаемой формулы с известной рекурсивной формулой для слоев постоянного удельного сопротивления. Кривая зондирования по методу сопротивления может быть получена путем цифровой конволюции функции преобразования сопротивления и фильтровых коэффициентов. Интерпретация полевых кривых трудоемка и должна базироваться на предполагаемой модели разреза удельных сопротивлений. Рекомендуется комбинация цифровых и графических методов в области преобразования сопротивлений для интерпретации. Приводятся примеры интерпретации из района распространения метаморфических пород. Полученные результаты обсуждаются и сопоставляются с данными бурения и сейсморазведки.

GEOPHYSICAL TRANSACTIONS 1987
Vol. 32. No. 4. pp. 333–353

AUTOMATIC RELATIVE DEPTH MATCHING OF BOREHOLE INFORMATION I. THEORETICAL REVIEW

Dénes SZENDRŐ*

One of the prerequisites for interpreting borehole information is that data of the given well should be correct according to depth. In order to obtain a common depth point it is assumed that the $\Delta(X)$ relative depth deviations changing from point to point can be approximated by a polynomial. Developing in a series the $Y(X)$ log or logs to be matched according to depth, the $\Delta(X)$ depth deviations in the Taylor's series agree with the substitution values of the polynomial. Minimizing the error function which can be formed from the data to be matched, the coefficients of the polynomial can be calculated and the corrected data obtained. If the process is repeated several times the calculated values converge. The method is suitable not only for correcting linear slips but, depending on the degree of the polynomial, also for eliminating deviations of varying sign. If the order of the polynomial describing the depth deviation is zero, i.e. it is a constant slip, the result obtained by the method is as good as that of the conventional cross correlation method. It is, however, substantially faster than the conventional one because of calculating the slip. The method is suitable for correcting depth deviations between well logs, between core data and well logs, and between the lithological column and well logs.

Keywords: well logging, depth deviation, borehole information, computer programs, algorithm, matching

1. Introduction

Similarly to every measurement, borehole information has its uncertainties characterizing the method, viz. the conditions, the instrument and the physical parameters of measurement. Both the method and the measured quantities may considerably differ from each other, but when determining their characteristics common features can be found as well. In the case of borehole information this common feature is their being recorded as a function of depth. Since measurements generally follow each other, measured values of geophysical and geological parameters corresponding to the same depth will not appear at the same place on the records, depth differences may occur. The causes of depth deviations will be discussed later.

In order to decrease the depth differences either the methodology should be modified or the logs should be corrected afterwards. In the first case the application of sonde trains would be necessary but even then there would not

* Eötvös Loránd Geophysical Institute of Hungary, POB 35, Budapest, H-1440
Manuscript received: 4 November, 1986

be any possibility to perform all the measurements simultaneously because of the great number of geophysical parameters. In the second case, in the conventional manual evaluation, the characteristic points of the curves (maximum, minimum, inflexion point, etc.) are taken into consideration when fitting the logs, i.e. matching relative depth. Using this method the experience of the expert and visual examination of the curves yield good results, but in the field of computer aided processing there is limited reference in the literature to depth matching.

In recent years attempts have been made to shift the curves to an extent determined by the operator, after reproducing the logs on a graphic display connected to a computer. It seems that this interactive method is suitable only for correcting very great deviations. The method mostly applied automatically corrects the constant slip of the logs. A reference log is selected, it is recorded for each run together with the geophysical parameters to be measured. The repeatedly measured log is considered as the base log. For depth matching cross correlation is computed between the base logs. Maxima of the correlation coefficient mark out the corresponding values. If this method is employed for the complete log, it only eliminates the constant deviation, although not only the extent but even the direction of the depth differences may vary from point to point. If cross correlation is performed for short intervals, then the problem arises in smoothing the differences at the boundaries of the intervals.

In this paper the mathematical phrasing of the possibilities of depth matching is presented, and a computer aided method is described which eliminates the above mentioned difficulty. A further advantage of the method to be described is that it is not necessary to measure the base log for each run.

2. Mathematical phrasing of depth differences

In order to describe mathematically the relative depth differences of well logs one has to start by examining the measurements. For well logging the sonde is lowered into the borehole by a cable. The signals emitted by the sonde are transmitted to galvanometers or to the magnetic tape recorder through cable-conductors. The camera is controlled by the movement of the cable through a transmission system whereas when using magnetic tape recording two independent depth determinations are used, viz. magnetic depth marks on the cable and the sampling interval controlled by the logging speed. Deviations from the correct depth values may originate from the following causes: differences in the reference points of the sondes; stretching of the cable caused by the interaction of the cable, the sonde and the borhole; inaccuracy of the transmission system between the camera and the cable; deviations from the set logging speed when recording on magnetic tape.

Dealing with the causes of the $\Delta(X)$ depth discrepancies in increasing order of the powers of the recorded X depth of the sonde, leads to the following grouping:

a) The constant term (of zero order) comes from the difference between the reference points of the sondes:

$$\Delta(X)_0 = C \tag{2.1}$$

b) The linear term is obtained from cable stretching caused by:
— cable stretching due to sonde weight. This can be calculated on the basis of Hooke's and Archimedes' laws supposing elastic deformation and including the buoyant force of the mud:

$$\Delta(X)_1 = k \cdot Q\left(1 - \frac{\gamma_m}{\gamma_s}\right) \cdot X \tag{2.2}$$

where k is the elastic module of the cable,
Q is the weight of the sonde in air,
γ_s is the specific weight of the sonde,
γ_m is the specific weight of the mud;

— cable stretching due to the friction of the sonde on the wall of the borehole and/or to the pressing of it against the wall:

$$\Delta(X)_2 = k\mu N \cdot X \tag{2.3}$$

where μ is the friction coefficient between the sonde and the sidewall,
N is the pressure force against the sidewall;

— the changing of the actual size of the film or paper, when digitizing analog logs:

$$\Delta(X)_3 = k_1 X \tag{2.4}$$

c) The second order term is obtained by means of the following:
— the weight of the cable lowered in the borehole is in linear ratio with the length of the cable thus if cable stretching obtained by Hooke's and Archimedes' laws is integrated according to depth, a relation is obtained which is a depth function of second order:

$$\Delta(X)_4 = \frac{1}{2} kq\left(1 - \frac{\gamma_m}{\gamma_c}\right) \cdot X^2 \tag{2.5}$$

where q is the weight of the cable for unit length,
γ_c is the specific weight of the cable;

— the hydrostatic compression on the surface of the cable in the mud is proportional to its length. Thus the relation obtained by integrating the frictional force—proportional to the hydrostatic compression—is also a depth function of second order:

$$\Delta(X)_5 = \frac{1}{2} k\gamma_m(W + j)X^2 \tag{2.6}$$

where W is the friction of rest between cable and mud,
$j = j(v)$ is a quantity depending on logging speed;

— the force due to the friction of the cable on the wall of deviated boreholes is proportional to the component, perpendicular to the wall of the borehole, of the weight proportional to the length of the cable. Integrating this effect according to depth gives a quadratic relationship:

$$\Delta(X)_6 = \frac{1}{2} kq\mu_1 \left(1 - \frac{\gamma_m}{\gamma_k}\right) \sin\varphi \cdot X^2 \tag{2.7}$$

where μ_1 is the friction coefficient between cable and sidewall,
φ is the angle between the axis of the borehole and the vertical;

— integrating the effect of the temperature increasing quasi-linearly in depth, again a quadratic relation is obtained:

$$\Delta(X)_7 = \frac{1}{2} \alpha g_t X^2 \tag{2.8}$$

where α is the linear thermal expansion coefficient of the cable,
g_t is the geothermic gradient.

d) Added to the former terms, the following can be approximated with those of higher order:
— the effect of sticking and restarting of the sonde,
— the effect of harmonic vibration of the sonde during the run,
— the "depth correction" of the operator or, with digital recording, that of the special electronic unit.

If logs of different runs are matched then the relative depth deviations are obtained as the difference of the two polynomials — which is also a polynomial. The coefficients of the terms describing the relative depth difference are obtained from the changing of the parameters in relations (2.1)—(2.8) between two runs.

In the case of sidewall coring the same reasoning can be applied since the depth difference is caused by cable stretching here too. For conventional coring, deformation of the drill pipe should be taken into consideration instead of that of the cable. During well logging, tensile load affects the cable whereas in coring compressive forces are acting on the drill pipe, thus the depth differences owing to elastic strain are supposed to sum up.

3. Relative depth matching of well logs

For the mathematical phrasing let us consider *Fig. 1*. As a first approach let us suppose that curves $Y_2(X)$, $Y_3(X)$, ..., $Y_N(X)$ are related to each other correct in depth and we should like to match function $Y_1(X)$ to them. At depth point X_i, $(i = 1, 2, ..., L)$, to function values $Y_2(X_i)$, $Y_3(X_i)$, ..., $Y_N(X_i)$ belongs the value $Y_1[X_i + \Delta(X_i)]$ of the function to be matched. For the sake of clarity the function values belonging to each other are marked in the figure and the deviation function $\Delta(X)$ is plotted at the bottom.

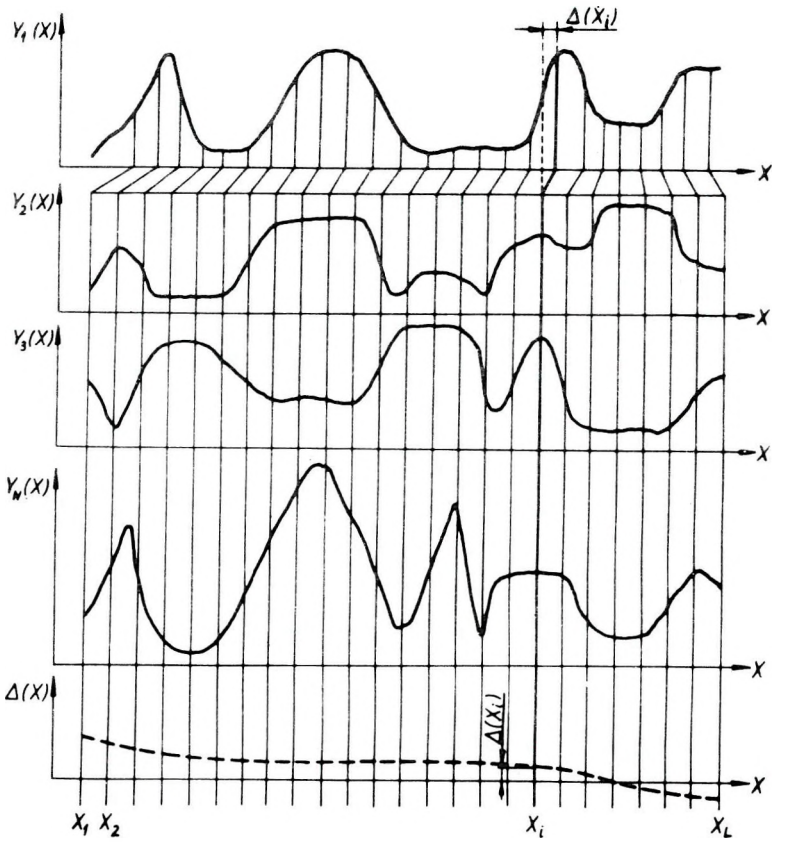

Fig. 1. Illustration of depth deviations of well logging curves
$Y_1(X)$ — curve to be matched; $Y_2(X)$, $Y_3(X)$, ..., $Y_N(X)$ — curves considered to be correct in depth; $\Delta(X)$ — function of depth deviation

1. ábra. Karotázsgörbék mélységeltéréseinek szemléltetése
$Y_1(X)$ — egyeztetni kívánt görbe; $Y_2(X)$, $Y_3(X)$, ..., $Y_N(X)$ — mélységileg helyesnek tekintett görbék; $\Delta(X)$ — a mélységeltérést leíró függvény

Рис. 1. Демонстрация расхождений между каротажными кривыми по глубине
$Y_1(X)$ — кривая, подлежащая согласованию по глубине; $Y_2(X)$, $Y_3(X)$, ..., $Y_N(X)$ — кривые, считающиеся правильными по глубине; $\Delta(X)$ — функция, описывающая расхождения по глубине

Our aim is to determine $\Delta(X)$ since in the knowledge of this, depth correction means substituting the respective $Y_1[X_i + \Delta(X_i)]$ function value into $Y_1(X_i)$ at the $i = 1, 2, ..., L$ sampling points.

To perform the calculation we assume that the values belonging to each other are related; this relationship can be defined by an operator F since each log provides certain geophysical information about the same place:

$$Y_1^{corr}(X_i) = Y_1[X_i + \Delta(X_i)] = F[Y_2(X_i),\ Y_3(X_i),\ \ldots,\ Y_N(X_i)]$$
$$i = 1, 2, \ldots, L \tag{3.1}$$

If the operator were precisely known, then the system of equations (3.1) would theoretically be solvable because it contains L unknowns in the values at the $i = 1, 2, \ldots, L$ sampling points of the $\Delta(X_i)$ function of depth deviation and it consists of altogether L equations. Knowing the F operator, however, would give the impression of a contradiction since it would mean that the $Y_1(X)$ curve could be obtained from the other curves and so it would not be necessary to measure it. Naturally from geophysical aspects it cannot be true since the individual logging methods yield additional characteristic information related to the other measurements. Since our aim is, besides keeping the characteristic features of the curve $Y_1(X)$, to match its characteristic places with those of the other curves—and not produce it from the other curves—exact knowledge of operator F is not required. Between certain logs there is evident correlation, e.g. the resistivity logs correlate with each other and with the SP log. In practice, in the course of processing, the SP and the gamma-ray logs are replaced by each other many times because of their similar characteristics. The porosity indicator logs, the neutron-gamma, the neutron-neutron and the acoustic logs are necessarily correlated with each other.

With regard to quasi symmetrical logs it can be assumed that operator F can be approximated by their linear combination. The more curves there are in it, mathematically the more probable it is that with one of them the correlation is close. If the theoretical function-connection is not linear, it results in a decrease of the correlation coefficient; this, however, does not considerably influence the result of the subsequent calculations. (If a gradient curve is correlated then in the F operator the derivatives of the symmetrical curves should be used.)

From the above it can be assumed that operator F can be approximated by the linear combination of the $Y_2(X)$, $Y_3(X)$, ..., $Y_N(X)$ logs:

$$F[Y_2(X_i),\ Y_3(X_i),\ \ldots,\ Y_N(X_i)] \approx b_1 + b_2 Y_2(X_i) + b_3 Y_3(X_i) + \ldots + b_N Y_N(X_i)$$
$$i = 1, 2, \ldots, L \tag{3.2}$$

Here parameters $b_1, \ldots, b_N$ are further unknowns characterizing the correlation of the functions.

To determine the depth deviation varying from point to point, let us develop in a series the left side of relation (3.1) and to preserve the linearity in $\Delta(X_i)$, i.e. approximating it up to the first term, the following can be written:

$$Y_1[X_i + \Delta(X_i)] \approx Y_1(X_i) + \Delta(X_i) \cdot Y_1'(X_i) \qquad i = 1, 2, \ldots, L \tag{3.3}$$

Here the following notation was used:

$$Y_1'(X_i) \equiv \left.\frac{\mathrm{d}Y_1(X)}{\mathrm{d}x}\right|_{x = X_i} \tag{3.4}$$

The derivative (3.4) exists for all analog logs since, due to the continuous recording of a finite speed, the curve is continuous and always has a definite tangent not perpendicular to the abscissa. Thereby it satisfies the criterion concerning the existence of the derivative.

If the $Y_1(X_i)$ curve is known from sampling points, then using the function values in the two-two neighbouring digitization points, the derivative (3.4) can be approximated by the formula [OBÁDOVICS 1977]:

$$Y_1'(X_i) \approx \frac{1}{12h}[Y_1(X_{i+2}) - 8Y_1(X_{i+1}) + 8Y_1(X_{i-1}) - Y_1(X_{i-2})] \qquad (3.5)$$

$$i = 3, 4, \ldots, L-2$$

where h is the sampling interval. There are other approximations using fewer or more neighbouring function values than Eq. (3.5), but this was chosen because with fewer points, statistical noise would be increased whereas relations with more sampling points result in an increase in machine time. Naturally at both ends of the curves where there are no neighbouring points one has to be content with an approximation with the left or right derivatives [OBÁDOVICS 1977]:

$$\begin{aligned} Y_1'(X_i) &\approx \frac{1}{h}[Y_1(X_{i+1}) - Y_1(X_i)] \qquad i = 1, 2 \\ Y_1'(X_i) &\approx \frac{1}{h}[Y_1(X_i) - Y_1(X_{i-1})] \qquad i = (L-1), L \end{aligned} \qquad (3.6)$$

As we have seen in Section 2 relative depth deviations can be approximated by a polynomial:

$$\Delta(X_i) \approx a_0 + a_1 X_i + a_2 X_i^2 + \ldots + a_P X_i^P \qquad i = 1, 2, \ldots, L \qquad (3.7)$$

It should be noted that relation (3.7)—disregarding the physical meaning—is mathematically according to Weierstrass' theorem [OBÁDOVICS 1977] in the case of a continuous function, since—choosing a suitably great number of power P—any accuracy of the approximation can be achieved.

Substituting approximation (3.3)—using relation (3.7)—into the left side and, approximation (3.2) into the right side of equation system (3.1) the following is obtained:

$$\begin{aligned} &Y_1(X_i) + Y_1'(X_i) \cdot [a_0 + a_1 X_i + a_2 X_i^2 + \ldots + a_P X^P] \approx \\ &\approx b_1 + b_2 Y_2(X_i) + b_3 Y_3(X_i) + \ldots + b_N Y_N(X_i) \qquad i = 1, 2, \ldots, L \end{aligned} \qquad (3.8)$$

One can see that instead of the $\Delta(X_i)$, $i = 1, 2, \ldots, L$ unknowns of equation system (3.1), in relation (3.8) considerably fewer, only the a_p, $p = 0, 1, \ldots, P$ coefficients in the polynomial of the depth deviation and the b_n, $n = 1, 2, \ldots, N$ parameters in the linear combinations of the functions, should be determined.

Since in this way the number of unknowns in (3.1) could be made much smaller than the number of equations, relation (3.8) becomes overdetermined

and the unknowns can be determined, e.g. by the method of least squares [JÁNOSSY 1965]. Forming the difference of the left and right side of relation (3.8) and then the quadratic sum the following can be written:

$$\Theta = \sum_{i=1}^{L} \{Y_1(X_i) + Y_1'(X_i) \cdot [a_0 + a_1 X_i + \ldots + a_P X_i^P] - b_1 - b_2 Y_2(X_i) - \ldots - b_N Y_N(X_i)\}^2 \tag{3.9}$$

The unknowns are determined so that Θ should be minimal, i.e. the derivatives according to the wanted parameters should be zero:

$$\frac{\partial \Theta}{\partial a_p} = 0, \quad p = 0, 1, \ldots, P$$
$$\frac{\partial \Theta}{\partial b_n} = 0, \quad n = 1, 2, \ldots, N \tag{3.10}$$

The normal equation system obtained after performing the derivations (3.10) includes $(N + P + 1)$ linear equations and as many unknowns. It should be noted that coefficients b_n, $n = 1, 2, \ldots, N$ will not be necessary further on: these are the so called surplus parameters needed only to establish the system of equations.

By introducing matrices the solution of (3.8) will be clearer using the method of least squares. Let:

$$\mathbf{M} = \begin{bmatrix} 1 & Y_2(X_1) & Y_3(X_1) & \ldots & Y_N(X_1) & -Y_1'(X_1) & -Y_1'(X_1)X_1 & \ldots & -Y_1'(X_1)X_1^P \\ 1 & Y_2(X_2) & Y_3(X_2) & \ldots & Y_N(X_2) & -Y_1'(X_2) & -Y_1'(X_2)X_2 & \ldots & -Y_1'(X_2)X_2^P \\ \vdots & & & & & & & & \\ 1 & Y_2(X_L) & Y_3(X_L) & \ldots & Y_N(X_L) & -Y_1'(X_L) & -Y_1'(X_L)X_L & \ldots & -Y_1'(X_L)X_L^P \end{bmatrix}$$

and

$$\mathbf{Y}_1 = \begin{bmatrix} Y_1(X_1) \\ Y_1(X_2) \\ \vdots \\ Y_1(X_L) \end{bmatrix} \qquad \mathbf{I} = \begin{bmatrix} b_1 \\ b_2 \\ \vdots \\ b_N \\ a_0 \\ a_1 \\ \vdots \\ a_P \end{bmatrix} \tag{3.11}$$

In matrix form (3.8) is:

$$\mathbf{M} \cdot \mathbf{I} \approx \mathbf{Y}_1 \tag{3.12}$$

The matrix equation obtained from (3.9) and (3.10) using the method of least squares is:

$$(\mathbf{M}^T \cdot \mathbf{M}) \cdot \mathbf{I} = \mathbf{M}^T \cdot \mathbf{Y}_1 \tag{3.13}$$

where $\mathbf{M}^T$ is the transposed matrix of $\mathbf{M}$. The solution of (3.13) is:

$$\mathbf{I} = (\mathbf{M}^T \cdot \mathbf{M})^{-1} \cdot (\mathbf{M}^T \cdot \mathbf{Y}_1) \tag{3.14}$$

One can see that the overdetermined linear system of equations (3.8) can be solved relatively easily in a suitably ordered form by means of transposition, multiplication and inversion of the matrix.

Knowing the polynomial coefficients $a_0, a_1, \ldots, a_p$ determined by (3.14) the depth deviation curve $\Delta(X_i)$ varying from point to point can numerically be given for every $i = 1, 2, \ldots, L$ sampling point by relation (3.7). After calculating deviations $\Delta(X_i)$ the corrected curve values are determined as follows: knowing the values of $\Delta(X_i)$ and the sampling interval h, sampling point X_k nearest to the corrected depth value can be determined. The distance $d(X_k)$ from this can be written as follows:

$$d(X_k) = \Delta(X_i) - (X_k - X_i) \tag{3.15}$$

where:

$$|d(X_k)| < h$$

Knowing X_k and $d(X_k)$ the interpolated value of the corrected function value is:

$$Y_1^{corr}(X_i) = Y_1[X_i + \Delta(X_i)] \approx Y_1(X_k) + d(X_k) \cdot Y_1'(X_k) \tag{3.16}$$

$$i = 1, 2, \ldots, L$$

where $Y_1'(X_k)$ can be calculated from (3.5).

Since in order to preserve the linearity in $\Delta(X_i)$ the series development of (3.3) went up to the first derivative only, (3.16) can be regarded as a first approximation only. Considering the corrected curve always as an initial value the iteration can be continued until the value of the quadratic deviation (3.9) no longer decreases to any great extent, i.e. the form of the corrected curve does not vary any more. It should be noted that because of assumption (3.2) the value of Θ given by (3.9) will not compulsorily approach zero with increasing number of iterations. This does not matter since, according to what was said at the beginning of the section, operator F in (3.1) cannot accurately be given. Moreover parameters $b_0, b_1, \ldots, b_N$ in the linear combination of Eq. (3.2) are not directly included in the values of the polynomial calculated from Eq. (3.7); thus, presumably the polynomial is not too sensitive to these parameters. As the results discussed later will also prove, the stipulation that from the good or less good Θ values the parameters belonging to the lowest possible Θ should be chosen seems acceptable even if this Θ is relatively still too high. (We do not intend to determine the function $Y_1(X)$ from the other curves, we only want to match it to them and, at the same time, retain its characteristic features.)

If there are K logs to be corrected and $(N-K)$ logs considered to be correct in depth, where K can be one of the 1, 2, ..., N values, then every iteration phase consists of K cyclically inverted iterations. Taking one of the logs to be corrected for Y_1, it is corrected in the way described above using the other $(N-1)$ curves.

Then the second, third, Kth log will be taken for Y_1 so that the $(N-1)$ curves to be used will include those corrected before. For depth matching, apart from giving the number of iterations, only the order number of the polynomial describing the relative depth deviation in (3.7) should be prescribed.

4. Relative depth matching of well logs and the quantities derived from coring

In the course of geological exploration, for the integrated interpretation of all information depth matching of data of different origin is required. Depth errors may lead to apparent contradiction between well logging and core data. Since the latter represent a small volume of rock, a small depth shift may cause great difference. The depth correction method described in Section 3 cannot directly be applied to this case since cores are not known at equidistant intervals, and — as generally the yield is not complete — the missing neighbouring points make derivation impossible even by approximation.

For phrasing the problem let us consider *Fig. 2*. The computed porosity logs $Y_1(X_i)$, $Y_2(X_i)$, ..., $Y_N(X_i)$, $i = 1, 2, \ldots, L$, are assumed to be correct in depth in relation to each other. (This can be obtained by the method described in Section 3.) Our aim is to match the quantities derived from the $\Phi(X_m)$, $m = 1, 2, \ldots, M$ core samples known at not equidistant sites to these logs. At depth point X_m $(m = 1, 2, \ldots, M)$, the $Y_1[X_m + \Delta(X_m)]$, ..., $Y_N[X_m + \Delta(X_m)]$ curve values, taken at the real depth point $(X_m + \Delta(X_m))$, belong to the $\Phi(X_m)$ quantity to be matched. The function describing the depth deviation is also illustrated in the figure. The task is to define the function $\Delta(X)$ since in the knowledge of this, depth correction means the transfer of the corresponding $\Phi(X_m)$ quantity from the X_m depth point to the $[X_m + \Delta(X_m)]$ point.

One can see that as opposed to the depth correction of the well logs, here not a new function value will be calculated in every sampling point but the corresponding quantity will be transferred to a new depth. The steps of the solution are similar to those in Section 3. We assume that the values belonging to each other are related; this relationship can be described by an operator F:

$$\Phi(X_m) = F[Y_1(X_m + \Delta(X_m)),\ Y_2(X_m + \Delta(X_m)),\ \ldots,\ Y_N(X_m + \Delta(X_m))]$$
$$m = 1, 2, \ldots, M \tag{4.1}$$

Operator F is approximated by a linear combination of the curves:

$$F[Y_1[X_m + \Delta(X_m)],\ \ldots,\ Y_N[X_m + \Delta(X_m)]] =$$
$$= b_0 + b_1 Y_1[X_m + \Delta(X_m)] + \ldots + b_N Y_N[X_m + \Delta(X_m)] \tag{4.2}$$
$$m = 1, 2, \ldots, M$$

Developing in a series the right side of Eq. (4.1), and — for the linearity in $\Delta(X_m)$ — approximating it up to the first term, we can write:

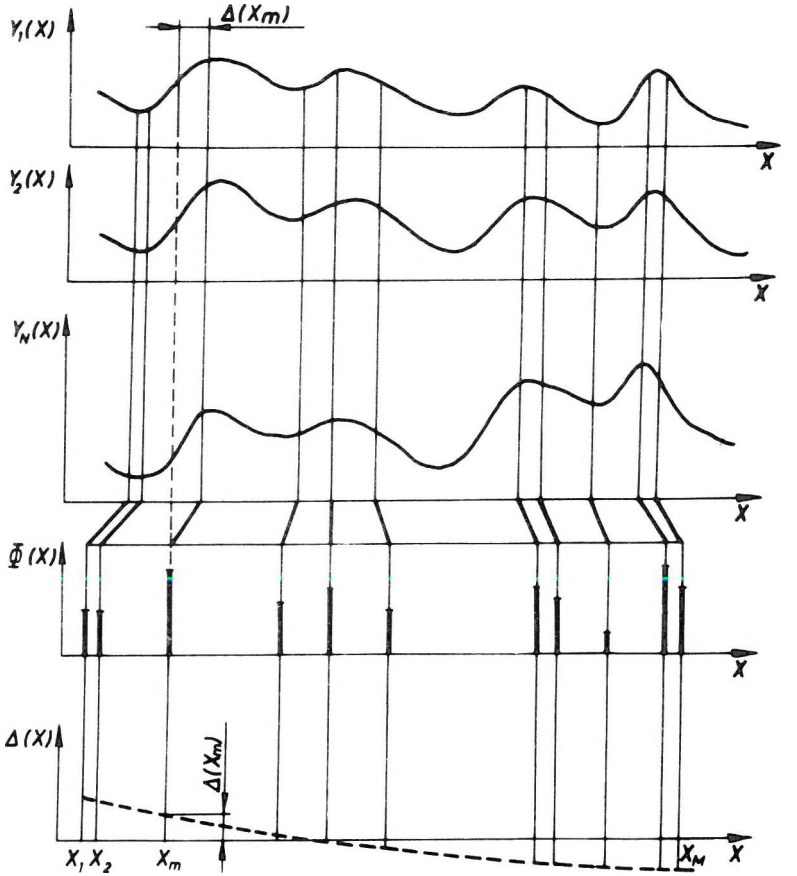

Fig. 2. Matching of core data to porosity–depth functions derived from well logging curves
$Y_1(X)$, $Y_2(X)$, ..., $Y_N(X)$ — porosity logs considered to be correct in depth; $\Phi(X)$ — porosity values of core samples; $\Delta(X)$ — function of depth deviation

2. ábra. Magadatok mélységének illesztése karotázs mérésekből származtatott porozitás görbékhez
$Y_1(X)$, $Y_2(X)$, ..., $Y_N(X)$ — mélységileg helyesnek tekintett porozitás szelvények;
Φ — a magadatokból számított, nem azonos közökként ismert porozitás értékek;
$\Delta(X)$ — a mélységeltérést leíró függvény

Рис. 2. Согласование глубины керна с кривой пористости, выведенной по скважинным измерениям
$Y_1(X)$, $Y_2(X)$, ..., $Y_N(X)$ — диаграммы пористости, считающиеся правильными по глубине;
Φ — вычисленные по керну значения пористости, полученные за неравные интервалы;
$\Delta(X)$ — функция, описывающая расхождения по глубине

$$Y_n[X_m + \Delta(X_m)] \approx Y_n(X_m) + \Delta(X_m) \cdot Y_n'(X_m) \tag{4.3}$$
$$n = 1, 2, \ldots, N \qquad m = 1, 2, \ldots, M$$

In Eq. (4.3) the notations of Eq. (3.4) were used and the derivative can numerically be approximated by formulae (3.5) and (3.6).

The $\Delta(X_m)$ depth deviation is approximated by a polynomial the same way as in Eq. (3.7):

$$\Delta(X_m) \approx a_0 + a_1 X_m + a_2 X_m^2 + \ldots + a_P X_m^P \qquad m = 1, 2, \ldots, M \tag{4.4}$$

Substituting the approximations (4.2), (4.3) and (4.4) into the system of equations (4.1) one gets:

$$\Phi(X_m) \approx b_0 + \sum_{n=1}^{N} b_n \left[Y_n(X_m) + Y_n'(X_m) \cdot \sum_{p=0}^{P} a_p X_m^p \right] \tag{4.5}$$
$$m = 1, 2, \ldots, M$$

This system of equations consists of M equations corresponding to the number of core samples and includes $(N+P+2)$ unknowns from which $(P+1)$ are the coefficients of the polynomial describing the depth deviation and $(N+1)$ are the parameters in the linear combination of the well logs. Since Eq. (4.5) contains the products of the parameters b_n $n = 0, 1, \ldots, N$ and a_p $p = 0, 1, \ldots, P$, the system of equations is not linear. If $M \geq N+P+2$ then the overdetermined system of equations of this type can be solved by iteration using the method of least squares. Because of series expansion (4.3) even the result obtained by the iteration can be considered only as a first approximation; thus, in order to avoid double iteration it is expedient to look for a perhaps less accurate but clearer and faster method for the solution of Eq. (4.5).

Let us write Eq. (4.5) in the form:

$$\Phi(X_m) \approx \left\{ b_0 + \sum_{n=1}^{N} b_n Y_n(X_m) \right\} + \left\{ \left[\sum_{n=1}^{N} b_n Y_n'(X_m) \right] \cdot \left[\sum_{p=0}^{P} a_p X_m^p \right] \right\} \tag{4.6}$$
$$m = 1, 2, \ldots, M$$

For the two terms in braces in equation system (4.6) let us introduce the notations

$$A(X_m) = b_0 + \sum_{n=1}^{N} b_n Y_n(X_m) \tag{4.7}$$

$$B(X_m) = \left[\sum_{n=1}^{N} b_n Y_n'(X_m) \right] \left[\sum_{p=0}^{P} a_p X_m^p \right] \qquad m = 1, 2, \ldots, M \tag{4.8}$$

Using (4.7) and (4.8), (4.6) can be written as follows:

$$\Phi(X_m) \approx A(X_m) + B(X_m) \qquad m = 1, 2, \ldots, M \tag{4.9}$$

Relation (4.9) expresses in an illustrative way that the quantity $\Phi(X_m)$ from the core sample can be composed of two terms. The first is a linear combination of the quantities obtained from the well log measurements and the second is the perturbation due to the depth deviation.

Since the $B(X_m)$ part describing the perturbation is probably much smaller than the $A(X_m)$ term, the system of equations (4.6) can be solved in two steps. First let us take the following quadratic sum:

$$\Theta_1 = \sum_{m=1}^{M} [\Phi(X_m) - A(X_m)]^2 \tag{4.10}$$

As one can see from (4.7), in (4.10) only the parameters b_n, $n = 0, 1, 2, \ldots, N$ are included. Their determination can be carried out by minimizing Θ_1:

$$\frac{\partial \Theta_1}{\partial b_n} = 0, \qquad n = 0, 1, 2, \ldots, N \tag{4.11}$$

The normal equation system obtained by derivation is linear thus the determination of the unknowns presents no problem.

After calculating the parameters b_n, $n = 0, 1, \ldots, N$ the following difference can be formed:

$$\Delta\Phi(X_m) = \Phi(X_m) - A(X_m) \qquad m = 1, 2, \ldots, M \tag{4.12}$$

This can be approximated by the perturbation term of Eq. (4.9):

$$\Delta\Phi(X_m) \approx B(X_m) \qquad m = 1, 2, \ldots, M \tag{4.13}$$

In the expression of $B(X_m)$ the polynomial coefficients a_p, $p = 0, 1, \ldots, P$ are the only unknowns (see Eq. 4.8) since coefficients b_n, $n = 0, 1, \ldots, N$ were calculated before. For the computation of a_p, let us produce the following quadratic sum:

$$\Theta_2 = \sum_{m=1}^{M} [\Delta\Phi(X_m) - B(X_m)]^2 \tag{4.14}$$

The value of Θ_2 is required to be minimal i.e. the derivatives according to a_p, $p = 0, 1, 2, \ldots, P$ should become zero:

$$\frac{\partial \Theta_2}{\partial a_p} = 0; \qquad p = 0, 1, \ldots, P \tag{4.15}$$

The normal equation system which is obtained after performing the derivation is also linear in the variables, thus the unknowns can easily be determined.

By introducing matrices, the algorithm of the solution is the following. Let:

$$\mathbf{M1} = \begin{bmatrix} 1 & Y_1(X_1) & Y_2(X_1) & \ldots & Y_N(X_1) \\ 1 & Y_1(X_2) & Y_2(X_2) & \ldots & Y_N(X_2) \\ \vdots & & & & \\ 1 & Y_1(X_M) & Y_2(X_M) & \ldots & Y_N(X_M) \end{bmatrix} \tag{4.16a}$$

$$\mathbf{\Phi} = \begin{bmatrix} \Phi(X_1) \\ \Phi(X_2) \\ \vdots \\ \Phi(X_M) \end{bmatrix} \qquad \mathbf{I1} = \begin{bmatrix} b_0 \\ b_1 \\ \vdots \\ b_N \end{bmatrix} \tag{4.16b}$$

The solution obtained by minimizing the quadratic sum (4.10) is

$$\mathbf{I1} = (\mathbf{M1}^{\mathrm{T}} \cdot \mathbf{M1})^{-1} \cdot (\mathbf{M1}^{\mathrm{T}} \cdot \mathbf{\Phi}) \tag{4.17}$$

The difference (4.12) in vector form is

$$\mathbf{\Delta\Phi} = \mathbf{\Phi} - \mathbf{M1} \cdot \mathbf{I1} \tag{4.18}$$

Knowing the coefficients b_n, $n = 1, 2, \ldots, N$ let us take

$$C(X_m) = \sum_{n=1}^{N} b_n Y_n'(X_m) \qquad m = 1, 2, \ldots, M$$

$$\mathbf{M2} = \begin{bmatrix} C(X_1) & X_1 C(X_1) & \ldots & X_1^p C(X_1) \\ C(X_2) & X_2 C(X_2) & \ldots & X_2^p C(X_2) \\ \vdots & & & \\ C(X_M) & X_M C(X_M) & \ldots & X_M^p C(X_M) \end{bmatrix} \qquad \mathbf{I2} = \begin{bmatrix} a_0 \\ a_1 \\ \vdots \\ a_P \end{bmatrix} \tag{4.19}$$

The solution obtained from the minimization of the quadratic sum (4.14) is:

$$\mathbf{I2} = (\mathbf{M2}^{\mathrm{T}} \cdot \mathbf{M2})^{-1} \cdot (\mathbf{M2}^{\mathrm{T}} \cdot \mathbf{\Delta\Phi}) \tag{4.20}$$

The non-linear, overdetermined equation system of (4.5) has been reduced to two linear systems of equations, to be solved one after the other, by the matrix algorithm of (4.16)–(4.20).

By means of solution (4.20) obtained for the coefficients of the polynomial describing the depth deviation the numerical value of the depth deviation ΔX_m can be computed for every core sample from relation (4.4). Depth correction means the transferring of the quantities $\Phi(X_m)$, $m = 1, 2, \ldots, M$ consecutively from depth X_m to depth $[X_m + \Delta(X_m)]$. Since the series expansion (4.3) was performed only up to the first derivative, the depth correction can be considered only as a first approximation. Considering the new depth values always as initial data, the method can be repeated till the values of the quadratic differences, (4.10) and (4.14), begin to decrease substantially. Note that core sampling point X_m should not necessarily coincide with one of the sampling points of well log curves since interpolated curves can be obtained, for example, by formula (4.3) as well.

In the algorithm it was assumed that the accuracy of the depth data of the well log measurements is much greater than that of coring because of the continuous measurement, thus the depth correction was performed only for the depth values of the core samples. The point of interest in the method is that the correlation coefficients often needed in practice are obtained together with the depth correction.

5. Relative depth matching of well logs and geological columns

In the course of industrial application it is often the case that the geological column obtained from coring or approximately known from neighbouring wells should be made accurate by means of the well logs of the given borehole. The $Y_1(X_j)$, $Y_2(X_j)$, ..., $Y_N(X_j)$, $j = 1, 2, ..., L$ well logs sampled and already corrected according to depth by the method described in Section 3 are illustrated in *Fig. 3*. The approximate knowledge of the geological column means that the lithological code representing the rock type cannot unconditionally be given even in a first approximation at every sampling point. (This may, for instance, be due to the insufficient core yield.) Moreover, where it is known, at that sampling point the indices $k = 1, 2, ..., K$ are introduced in order to differentiate the rock types. Thus $Y_n^{(k)}(X_j)$ means that the X_j sampling value of the nth well log can be assigned to the rock type denoted by the index k. Let the number of sampling points belonging to the rock types denoted by the indices $k = 1, 2, ..., K$ consecutively be $J_k = J_1, J_2, ..., J_K$. As in the previous Section, we consider that the well logs are correct in depth, thus the X_j place of the jth lithological code will be corrected at the sampling points for every j. We can assume that on the well logging curves some $[X_j + \Delta(X_j)]$ real depth value belongs to the X_j place to be corrected.

Approximating the function values taken at the real depth points the same way as was done for (3.3), we can write:

$$Y_n^{(k)}[X_j + \Delta(X_j)] \approx Y_n^{(k)}(X_j) + \Delta(X_j) \cdot Y_n(X_j)$$
$$j = 1, 2, ..., L \qquad n = 1, 2, ..., N \tag{5.1}$$

The depth deviation function $\Delta(X_j)$ is approximated by a polynomial, as in (3.7):

$$\Delta(X_j) \approx a_0 + a_1 X_j + ... + a_P X_j^P = \sum_{p=0}^{P} a_p X_j^p$$
$$j = 1, 2, ..., L \tag{5.2}$$

Substituting approximation (5.2) into relation (5.1) we get:

$$Y_n^{(k)}[X_j + \Delta(X_j)] \approx Y_n^{(k)}(X_j) + \left(\sum_{p=0}^{P} a_p X_j^p \right) Y_n'^{(k)}(X_j) \tag{5.3}$$

The average of the function values corrected by Eq. (5.3) can be calculated by rock types for every well logging curve:

$$A'_{nk} = \frac{1}{J_k} \sum_{j=1}^{L} Y_n^{(l)}[X_j + \Delta(X_j)] \cdot \delta_{kl}(X_j) =$$
$$= \frac{1}{J_k} \sum_{j=1}^{L} \left[Y_n^{(l)}(X_j) + Y_n'^{(l)}(X_j) \cdot \sum_{p=0}^{P} a_p X_j^p \right] \cdot \delta_{kl}(X_j) \tag{5.4}$$
$$n = 1, 2, ..., N \qquad k = 1, 2, ..., K$$

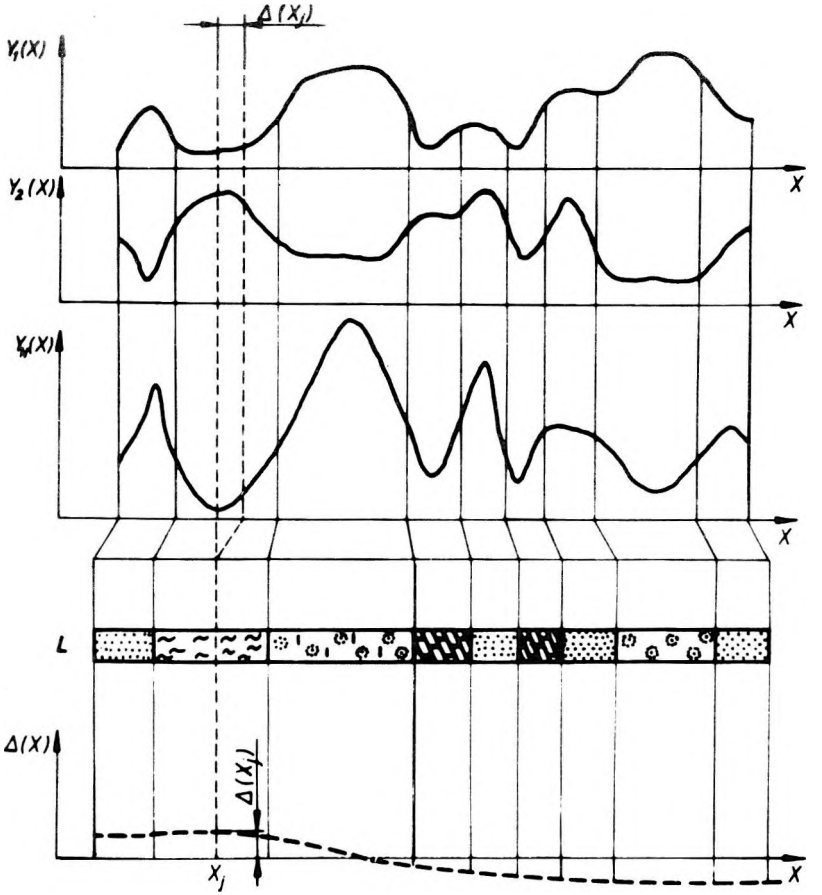

Fig. 3. Matching of geological column to well logging curves
$Y_1(X)$, $Y_2(X)$, ..., $Y_N(X)$ — well logs considered to be correct in depth; L — lithological column; $\Delta(X)$ — function of depth deviation

3. ábra. Geológiai rétegsor karotázs görbékhez történő igazítása
$Y_1(X)$, $Y_2(X)$, ..., $Y_N(X)$ — mélységileg helyesnek tekintett karotázs szelvények; L — litológiai rétegsor; $\Delta(X)$ — a mélységeltérést leíró függvény

Рис. 3. Согласование литологической колонки с каротажными кривыми
$Y_1(X)$, $Y_2(X)$, ..., $Y_N(X)$ — каротажные диаграммы, считающиеся правильными по глубине; L — литологическая колонка; $\Delta(X)$ — функция, описывающая расхождения по глубине

where $\delta_{kl}(X_j)$ is the Kronecker-delta:

$$\delta_{kl}(X_j) = \begin{cases} 1, & \text{if} \quad l = k \\ 0, & \text{if} \quad l \neq k \end{cases}$$

In formula (5.4) the summation should be performed log by log at places of the same k lithological code and the sum should be divided by the number of points in the sum. If there are N curves and K different lithological codes then a total of $N \cdot k$ different values of A'_{nk} will be obtained.

Let us introduce the following quantities that can numerically be calculated from the well logging curves:

$$A_{nk} \equiv \frac{1}{J_k} \sum_{j=1}^{L} Y_n^{(l)}(X_j) \cdot \delta_{kl}(X_j) \qquad n = 1, 2, \ldots, N \qquad k = 1, 2, \ldots, K \tag{5.5}$$

$$A_{nk}^{(p)} \equiv \frac{1}{J_k} \sum_{j=1}^{L} X_j^p \cdot Y_n'^{(l)}(X_j)\, \delta_{kl}(X_j) \tag{5.6}$$

$$n = 1, 2, \ldots, N, \qquad p = 0, 1, 2, \ldots, P, \qquad k = 1, 2, \ldots, K$$

Expression (5.5) means the average function value of the nth curve belonging to the kth lithological code. Expression (5.6) represents the mean of the derivative of the nth curve weighted by the corresponding power of the depth value belonging to the kth rock type.

Using expressions (5.5) and (5.6) the corrected mean value defined by relation (5.4) can be written — after some rearrangement — as follows:

$$A'_{nk} = A_{nk} + \sum_{p=0}^{P} a_p \cdot A_{nk}^{(p)} \qquad n = 1, 2, \ldots, N \qquad k = 1, 2, \ldots, K \tag{5.7}$$

The quadratic sum of the deviations from the average can be produced for every rock type and for every type of well logging:

$$\Theta'_{nk} = \sum_{j=1}^{L} \{Y_n^{(l)}[X_j + \Delta(X_j) - A'_{nk}]\}^2 \cdot \delta_{kl}(X_j) \tag{5.8}$$

$$n = 1, 2, \ldots, N \qquad k = 1, 2, \ldots, K$$

where the summation for j relates to places of the same rock type.

Substituting approximation (5.3) and relation (5.7) into the quadratic sum of (5.8), we get:

$$\Theta'_{nk} = \sum_{j=1}^{L} \left\{ Y_n^{(l)}(X_j) + \left(\sum_{p=0}^{P} a_p X_j^p \right) \cdot Y_n'^{(l)}(X_j) - A_{nk} - \sum_{p=0}^{P} a_p A_{nk}^{(p)} \right\}^2 \cdot \delta_{kl}(X_j) \tag{5.9}$$

$$n = 1, 2, \ldots, N \qquad k = 1, 2, \ldots, K$$

After rearranging expression (5.9) and summing by curves and by rock types we can write:

$$\Theta = \sum_{n=1}^{N} \sum_{k=1}^{K} \sum_{j=1}^{L} \left\{ [Y_n^{(l)} X_j - A_{nk}] + \left[\sum_{p=0}^{P} a_p (X_j^p \cdot Y_n'^{(l)}(X_j) - A_{nk}^{(p)}) \right] \right\}^2 \delta_{kl}(X_j) \tag{5.10}$$

The meaning of the terms in the first square brackets of the quadratic sum (5.10) is clear: the mean value belonging to the given rock and to the given curve and calculable by (5.5) should be subtracted from the respective curve value for every curve and every sampling point. The second square brackets contain the coefficients a_p, $p = 0, 1, \ldots, P$ of the polynomial describing the deviation which is to be determined. Furthermore, the derivatives of the logs weighted with the powers of the depth value and the respective mean derivatives weighted with the powers of the depth as defined by formula (5.6) can also be calculated numerically.

The coefficients of the polynomial describing depth deviations are determined so that (5.10) should be minimal, i.e. the derivatives according to the variables should be zero:

$$\frac{\partial \Theta}{\partial a_p} = 0, \qquad p = 0, 1, 2, \ldots, P \tag{5.11}$$

By performing the derivations of (5.11), a linear system of equations is obtained for the coefficient of the polynomial consisting of $(P+1)$ equations and including $(P+1)$ unknowns. The solution ensures that the quadratic sum of the deviations from the means characterizing the rock types will be minimal for each log. The solution using matrix formalism is the following. Let:

$$\mathbf{M} = \begin{bmatrix} \sum_{n=1}^{N} (Y_n'^{(k)}(X_1) - A_{nk}^{(0)}) & \sum_{n=1}^{N} (X_1 Y_n'^{(k)}(X_1) - A_{nk}^{(1)}) & \ldots & \sum_{n=1}^{N} (X_1^P Y_n'^{(k)}(X_1) - A_{nk}^{(P)}) \\ \sum_{n=1}^{N} (Y_n'^{(k)}(X_2) - A_{nk}^{(0)}) & \sum_{n=1}^{N} (X_2 Y_n'^{(k)}(X_2) - A_{nk}^{(1)}) & \ldots & \sum_{n=1}^{N} (X_2^P Y_n'^{(k)}(X_2) - A_{nk}^{(P)}) \\ \vdots & \vdots & & \vdots \\ \sum_{n=1}^{N} (Y_n'^{(k)}(X_L) - A_{nk}^{(0)}) & \sum_{n=1}^{N} (X_L Y_n'^{(k)}(X_L) - A_{nk}^{(1)}) & \ldots & \sum_{n=1}^{N} (X_L^P Y_n'^{(k)}(X_L) - A_{nk}^{(P)}) \end{bmatrix} \tag{5.12}$$

Matrix $\mathbf{M}$ consists of as many lines in as many sampling points the lithological code is known. The $A_{nk}^{(p)}$ weighted mean values of the derivatives previously calculated by formula (5.6) for the kth lithological code should be subtracted from the derivatives of each log multiplied by the powers of the depth. Further notations are:

$$\mathbf{Y} = \begin{bmatrix} \sum_{n=1}^{N} (A_{nk} - Y_n^{(k)}(X_1)) \\ \sum_{n=1}^{N} (A_{nk} - Y_n^{(k)}(X_2)) \\ \vdots \\ \sum_{n=1}^{N} (A_{nk} - Y_n^{(k)}(X_L)) \end{bmatrix} \qquad \mathbf{I} = \begin{bmatrix} a_0 \\ a_1 \\ \vdots \\ a_P \end{bmatrix} \tag{5.13}$$

The number of the lines of vector **Y** corresponds to the number of the columns of matrix **M**. Here, the curve values taken at the sampling points should be subtracted from the mean function value defined by formula (5.5) for the kth lithological code. The solution obtainable by minimizing (5.10) using matrices (5.12) and (5.13) is:

$$\mathbf{I} = (\mathbf{M}^{\mathrm{T}} \cdot \mathbf{M})^{-1} \cdot (\mathbf{M}^{\mathrm{T}} \cdot \mathbf{Y}) \tag{5.14}$$

Knowing the polynomial coefficients $a_0, a_1, \ldots, a_p$ determined by solution (5.14) the $\Delta(X_1)$ curve defining the depth deviation can be obtained by means of relation (5.2) for the sampling points $i = 1, 2, \ldots, L$.

The correction of the lithological column consists of transferring the places of lithological code jumps i.e. those of the layer boundaries from place X_j to the $[X_j + \Delta(X_j)]$ point by correction (5.2), and thus a new, corrected lithological column is obtained. Since the series expansion (5.1) was performed only up to the first term in order to preserve the linearity in $\Delta(X)$, the corrected geological column can be regarded as a first approximation. If averages (5.5), (5.6) and matrices (5.12), (5.13) are determined according to the new lithology, the iteration can be continued by solution (5.14) till the value of Θ defined by (5.10) substantially decreases.

To sum up, lithological columns are corrected by the above mathematical statistical method using the constraint describing depth deviations by a polynomial so that the quadratic sum of the differences between the measured values and the respective means should be minimal for the entirety of rock types with different mean values on different logs.

6. Conclusions

Relative depth matching of the information obtained from boreholes is an essential condition for interpretation purposes. The elaborated mathematical statistical method makes it possible for a computer to be used for the intermediate step between measurement and interpretation, i.e. for relative depth matching. It was illustrated that the measuring features enable the value of the depth deviation varying from point to point to be approximated by a polynomial. In this way the accordion-like depth correction is given a mathematical phrasing.

The method enables the simultaneous correction of all the given logs but it is possible that supposing certain curves to be correct in depth the others may be matched to them. It follows from the mathematics of the method that at the boundaries there are no missing values left thus the number of depth points will not change during correction. The method is suitable for dealing with the problems of matching core data and lithological columns to well logs as well. Depth deviations are determined by calculation — instead of trials — thus being

substantially faster even than the cross correlation method in spite of the fact that — depending on the order of the polynomial — higher order deviations are also considered.

The method induces hope that in production drillings the parameters of reservoir geology may be determined with sufficient accuracy without coring, merely from well logging, using the correlation coefficients from certain exploration drillings. To apply the method in practice a computer program was written [SZENDRŐ 1978, 1980]. Its description and the experience gained with its application as well as the results are due to be dealt with in a further paper.

REFERENCES

JÁNOSSY L. 1965: Theory and practice of the evaluation of measurements. Clarendon Press, Oxford

OBÁDOVICS J. GY. 1977: Numerical methods and their programming (in Hungarian). Tankönyvkiadó, Budapest, 304 p.

SZENDRŐ D. 1978: Computer aided relative depth matching of information from boreholes (in Hungarian). Post graduate thesis. Technical University for Heavy Industry, Miskolc, Hungary, 69 p.

SZENDRŐ D. 1980: Computerized relative depth correlation of well logging profiles (in Hungarian). Magyar Geofizika **21**, 2, pp. 51–56

A MÉLYFÚRÁSBÓL SZÁRMAZÓ INFORMÁCIÓK AUTOMATIKUS RELATÍV MÉLYSÉGEGYEZTETÉSE I. ELMÉLETI ÁTTEKINTÉS

SZENDRŐ Dénes

A mélyfúrásból származó információk alapján történő értelmezés előfeltétele, hogy az adott kútban levő adatok mélységhelyesek legyenek. A közös mélységpontra hozás céljából feltesszük, hogy a pontról pontra változó nagyságú $\Delta(X)$ relatív mélységeltérések polinommal közelíthetők. Sorba fejtve a mélységegyeztetésben részt vevő $Y(X)$ szelvényt a mélység szerint, a Taylor-sorban levő $\Delta(X)$ mélységeltérés éppen a polinom helyettesítési értékével egyezik meg. Minimalizálva az egyeztetésben részt vevő adatokból képezhető hibafüggvényt, a polinom együtthatói kiszámíthatók, s a korrigált adatok a sorfejtés alapján megkaphatók. Az eljárást néhányszor az összes mennyiségre megismételve, a számított értékek a mélységkorrigált adatokhoz konvergálnak. A módszer nem csak a lineáris elcsúszások korrigálására alkalmas, hanem a polinom fokszámától függően „harmonikázó" eltolódások kiküszöbölésére is. Ha a mélységeltérést leíró polinom fokszáma nulla, azaz konstans elcsúszásról van szó, akkor a módszer a hagyományos keresztkorrelációs eljárással megegyező eredményt szolgáltat. Mivel azonban az elcsúszást kiszámolja, a hagyományos eljárásnál lényegesen gyorsabb. Az eljárás alkalmas a karotázs szelvények közötti, a magadatok és a karotázs szelvények közötti, s a geológiai rétegsor és a karotázs szelvények közötti mélységeltérések korrigálására.

АВТОМАТИЧЕСКОЕ СОГЛАСОВАНИЕ ДАННЫХ СКВАЖИННОЙ ГЕОФИЗИКИ ПО ОТНОСИТЕЛЬНЫМ ГЛУБИНАМ I. ТЕОРЕТИЧЕСКОЕ ОБОСНОВАНИЕ

Денеш СЕНДРЁ

Предпосылкой интерпретации данных скважинной геофизики является правильное определение глубины, к которой относятся те или иные данные. Для приведения данных к общей глубинной точке предполагается, что относительные расхождения по глубине $\Delta(X)$, величина которых меняется от точки к точке, аппроксимируются полиномом. После разложения подвергнутой согласованию по глубине кривой $Y(X)$ в ряд, отклонение по глубине $\Delta(X)$ в ряду Тэйлора точно совпадает со значением подстановки полинома. После приведения к минимуму функции ошибок, образуемой из участвующих в согласовании данных, можно вычислить коэффициенты полинома и получить исправленные данные на основе разложения в ряд. Если такая процедура повторяется несколько раз для всех величин, вычисленные значения приблизятся к исправленным за расхождение по глубине данным. Метод пригоден не только для исправления линейных смещений, но также и для устранения отклонения с переменными знаками в зависимости от степени полинома. Если степень полинома, описывающего отклонение по глубине, равна нулю, т.е. имеет место постоянное смещение, метод дает результат, совпадающий с традиционным методом взаимной корреляции. Поскольку, однако, при этом вычисляется смещение, данный метод значительно быстрее традиционного, он также позволяет ввести поправки за расхождения по глубине между каротажными диаграммами, между керном и каротажными диаграммами, а также между литологической колонкой и каротажными диаграммами.